Viscosity, Density, and Surface Tension of Gasified Coal and Synthesized Slag Melts for Next-Generation IGCC

Arman

Viscosity, Density, and Surface Tension of Gasified Coal and Synthesized Slag Melts for Next-Generation IGCC

September, 2016

Arman

Department of Materials Science and Biotechnology,

Graduate School of Science and Engineering,

Ehime University, Japan

Viscosity, Density, and Surface Tension of Gasified Coal and Synthesized Slag Melts for Next-Generation IGCC

Written By:

Arman

Reg. Number 3862005K

Approved by:

Academic supervisor,

Prof. Dr. Hiromichi Takebe

Professor
Graduate School of Science and Engineering,
Ehime University
3 Bunkyo-cho, Matsuyama,
Ehime 790-8577, Japan
Email: takebe.hiromichi.mk@ehime-u.ac.jp

Ratification

Dissertation entitled **"Viscosity, Density, and Surface Tension of Gasified Coal and Synthesized Slag Melts for Next-Generation IGCC"** by Arman, Students Reg. Number 3862005K, has been tested in dissertation court at the Ehime University, Japan, on August 17th 2016.

This dissertation has been accepted as one of the requirements to obtain an Doctoral Engineering Degree (Dr. Eng.) at Department of Materials Science and Biotechnology, Graduate School of Science and Engineering, Ehime University, Japan.

Matsuyama, September 13th 2016

Viva voice

Chairman:	Prof. Dr. Hiromichi Takebe	Seal
Examiner:	1. Prof. Dr. Toshiro Tanaka	Seal
	2. Prof. Dr. Hiromichi Aono	Seal
	3. Prof. Dr. Akira Saitoh	Seal

Contents

Acknowledgment

First, and most of all, I would like to express my sincere gratitude and appreciation to my academic advisor Professor Dr. Hiromichi Takebe for guiding me to think scientifically, for inspiring me to design a good experiment, for helping me come to my own conclusions, and for constant support during the work of this doctoral thesis. I have learned many things through his conduct and leadership.

I also wish to thank Professor Toshiro Tanaka, Professor Hiromichi Aono and Professor Mitsuhiro Okayasu for their all lecturer, advice and guidance. It beneficially gave me knowledge and better understanding in dealing with physical, chemical, and mechanical properties of materials.

I would like to thank to Professor Dr. Akira Saitoh, for providing many ideas for this research, for his help with both technical and theoretical concerns during this project.

I thank to Dr. Satoshi Okano, and all staff in office, lab and field of Ehime University. Arata Tsuruda and Akiko Okada for measuring and support viscosity and surface tension data, and all the members of Materials Processing Engineering Laboratory (MPEL) many more unmentioned but not forgotten.

I acknowledge the New Energy and Industrial Technology Development Organization (NEDO) of Japan for sponsoring this research.

I am indebted to Directorate General of Human Resource for Science, Technology and Higher Education (DIKTI) of Indonesia to pursue a doctoral degree of financial support for author.

I would like to thank all the colleagues and friends at the State Polytechnic of Ujung Pandang as my institution.

I would also like to express my sincere appreciation to my family for their support: my parents, Kamaruddin Saleng and Sitti Khadijah for their never-ending support and encouragement, my brothers, Ardhy and Azwar for all their help and prayers, and my in-laws, Amir Siang and Rahmatiah Abdi for their endorsement.

Finally, I am especially grateful for my beloved wife, Airah Amir, my sons: Ammar Alfatih and Abizar Arrazi to keep my mind open even if my life situation was critical and always supporting me.

Chapter 1

General Introduction

1.1. Background of Present Study

1.1.1. Importance of IGCC and properties of coal slag melts

In this century, global electricity demand is increasing at about by over 40% in the next 20 years in worldwide operation due to high efficiency and environmental compliance to reduce CO_2 emissions because of global warming [1.1, 1.2]. There is a demand to improve the efficiency of energy use through changes in technology and to produce energy vectors such as H_2 with near zero emissions of greenhouse gases [1.3, 1.4]. One technology, integrated (coal) gasification in a combined cycle (IGCC), offered the promise of generating power from coal at high efficiency with low emissions and development activity intended at demonstrating and commercializing these plants [1.5]. This contributes to the improvement of power generation efficiency compared with conventional pulverized coal gasification plants as well as the reduction of emissions of greenhouse gases [1.6, 1.7]. Coal has been primarily used as a solid fuel in IGCC with different compositions depending on geographic origin [1.8, 1.9].

Coal is known as a very important energy resource that has the characteristics dispersed over a wide area and stable low price relatively, compared with other energy resources [1.10]. Coal shares will be about 25% in global primary energy demand and about 40%

in global power generation in 2035 as shown in **Figs. 1.1a and 1.1b** [1.11]. Japan is the second largest coal gasification power producer in the world. **Figs. 1.2a and 1.2b** show an increase of coal gasification power generation in Japan from 93 TWh in 1990 to 256 TWh in 2012 [1.12]. The operation of nuclear power plants in Japan has been suspended since the accident at the Fukushima Daiichi Nuclear Power Plant in 2011, making coal power within increased 25% for electricity supply in Japan [1.13].

Integrated Coal Gasification Combined Cycle (IGCC) is a high-efficiency power generation technology which gasifies coal to be used as the fuel for gas turbines. According to a NEDO report [1.14], compared with conventional pulverized coal-fired power plants, IGCC has many advantages as follows:

1. Improved power generation efficiency: Compared with conventional pulverized coal-fired power plants, IGCC can increase power generation efficiency by approximately 20% for commercial plants.
2. Lower environmental burden: Owing to the increase in power generation efficiency, the emissions of SO_x, NO_x, and dust per generated power unit are lower. In addition, CO_2 emissions are reduced to the level of the heavy-oil-fired power generation process.
3. Flexibility to use different grades of coal: IGCC can use coal with low ash melting points, which is difficult to use in conventional pulverized coal-fired power plants. As a result, IGCC broadens the variety of coal grades that can be used in coal-fired power plants.
4. Increase in fields that can utilize the ash: Since IGCC discharges coal ash in the form of glassy molten slag, the ash is expected to be effectively used as a component for civil engineering work.

5. Reduction of water consumption: Since the generated gas is desulfurized directly, IGCC does not need a flue gas desulfurization unit, which consumes large amounts of water. Accordingly, IGCC uses significantly less water than conventional pulverized coal-fired power plants.

Fig. 1.4a and 1.4b show the efficiency trend for coal gasification of electricity production for the period 1990–2012 [1.12]. Japan has achieved the world's highest efficiency levels for coal gasification power generation technology in the range of 39–41%.

The previous study reported [1.3] that gasification technologies can be classified into three groups of gasifier configurations according to their flow geometry:

1. Entrained-flow gasifiers, in which pulverized coal particles and gases flow concurrently at high speed. They are the most commonly used gasifiers for coal gasification.
2. Fluidized-bed gasifiers, in which coal particles are suspended in the gas flow; coal feed particles are mixed with the particles undergoing gasification.
3. Moving-bed (also called fixed bed) gasifiers, in which gases flow relatively slowly upward through the bed of coal feed.

Entrained flow gasifiers are the most widely used gasifiers with different gasification technologies based on entrained flow gasifiers presently used at industrial scale or under worldwide development [1.10].

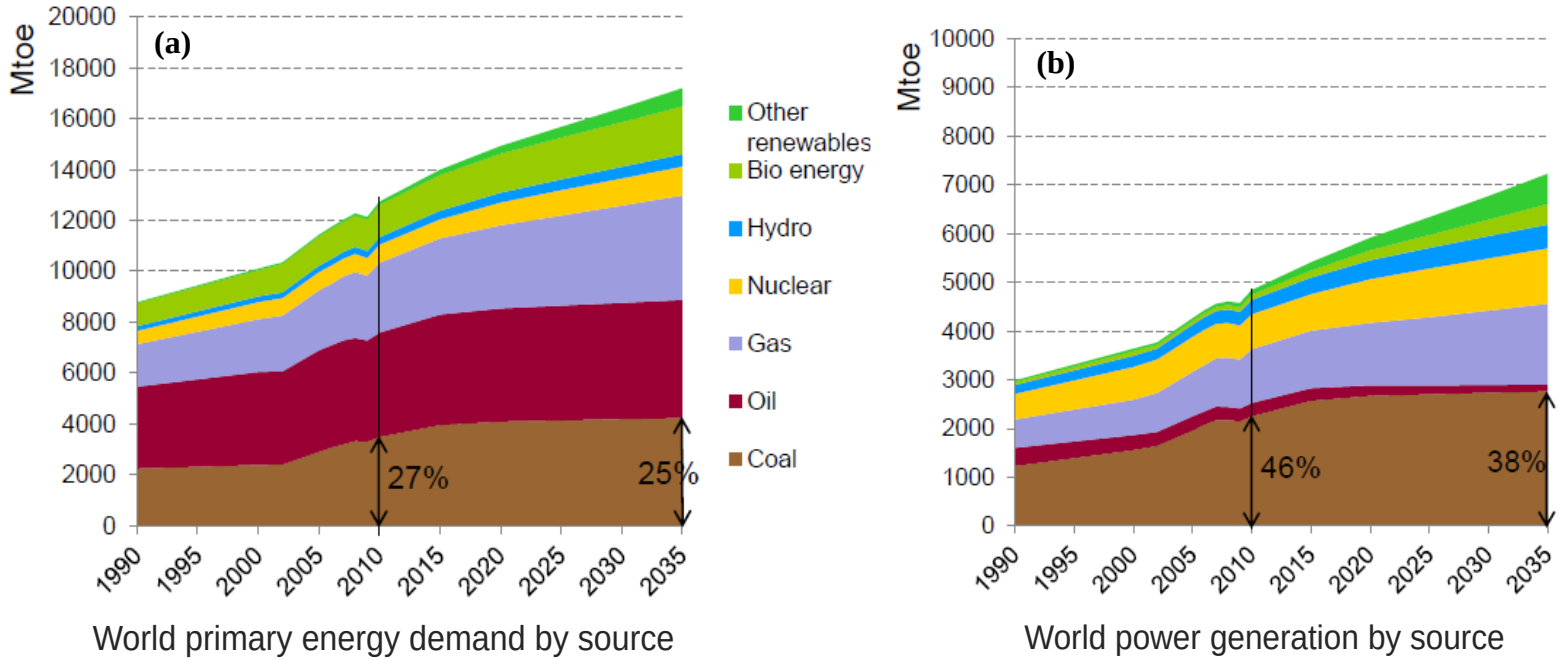

Fig. 1.1 (a) Coal shares in world primary energy demand and **(b)** world power generation by sources [1.11].

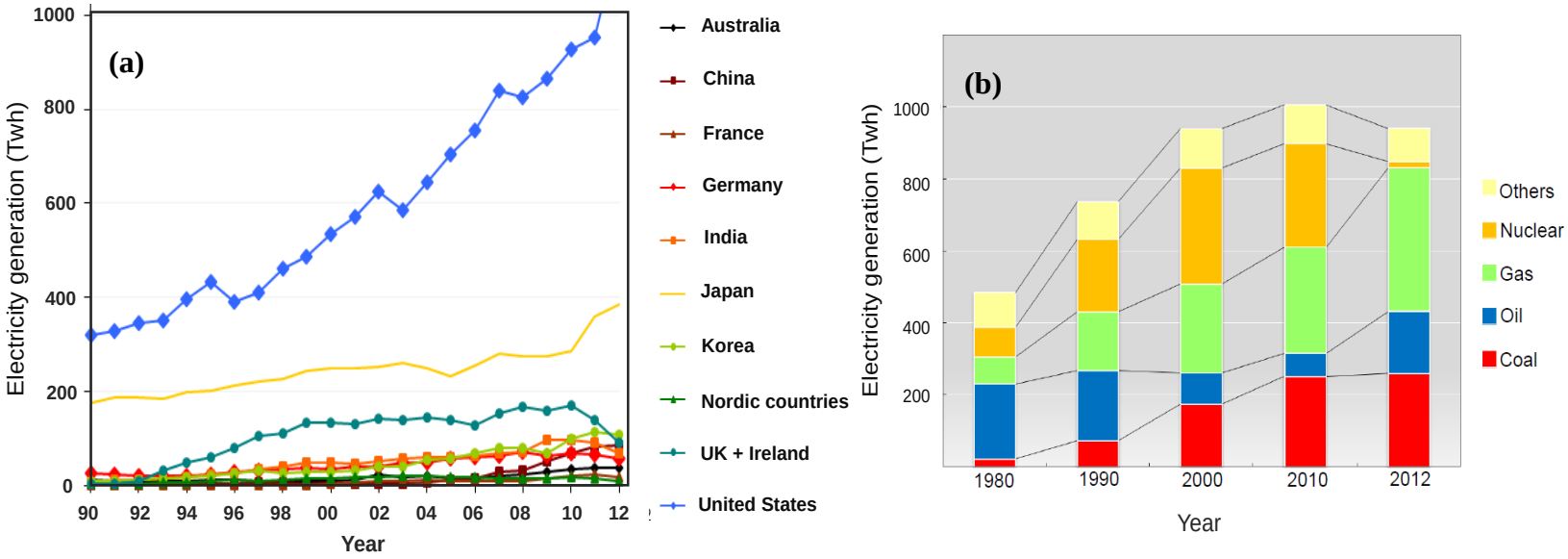

Fig. 1.2 (a) Coal gasification of power generation producer in the world and **(b)** Japan's power generation [1.12, 1.13].

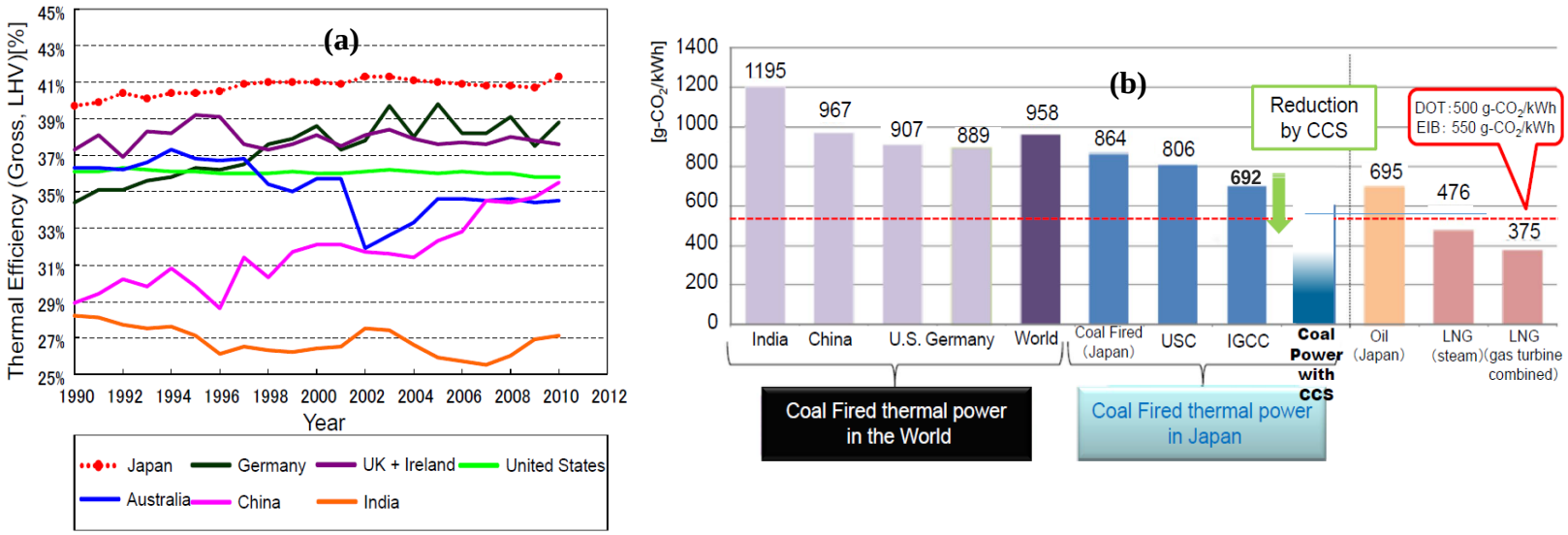

Fig. 1.3 (a) Average efficiency of coal gasification power production and **(b)** comparison CO_2 emission by some power generations [1.12].

In entrained-flow gasifiers, coal is typically gasified at high temperatures 1200 to 1600 °C [1.10] and high pressures 20–30 atm [1.15]. During gasification, organic material in coal is completely gasified and combusted under high-temperature and high-pressure conditions; the mineral matter in coal changes into ash during coal combustion; and the ash exposed to high-temperature conditions. The coal ash becomes liquid slag owing to the melting and reactions of its component mineral matter [1.16]. The coal is heated in the gasifier to convert the solid combustible mixture into the cleaned gases composed of CO, H_2 and CO_2 as a fuel to the gas-turbine [1.4, 1.17]. A schematic of a generalized design of an IGCC plant is shown in **Fig. 1.4** [1.17]. Meanwhile, the molten ash particles accumulate on the internal walls of the gasification chamber, then the wall is covered by a layer of solid slag [1.18]. The liquid slag flows under the force of gravity and out of the bottom of the gasifier into a water quenching system [1.19]. **Fig. 1.5** shows schematically the essential effect of viscosity, density, and surface tension of coal slag melts in the entrained-flow gasifier of IGCC [1.20]. Generally, the required slag viscosity at the tapping temperature should be 5–25 Pa s for entrained flow gasifier [1.21]. For instance, if the viscosity of coal slag is above 25 Pa·s, it will cause viscous, unpredictable slag flow from the gasifier, if the viscosity is below 5 Pa·s, it will result in rapid refractory wear of the gasifier [1.22]. Therefore, it is essential to understand the composition and temperature dependences of physical properties of coal slag melts, e.g., viscosity, density, surface tension, thermal conductivity, electric conductivity, heat capacity, and compressibility [1.23–1.27].

Among these properties, the viscosity, density, and surface tension are most fundamental properties of coal slag melts in the IGCC power plant [1.18, 1.28].

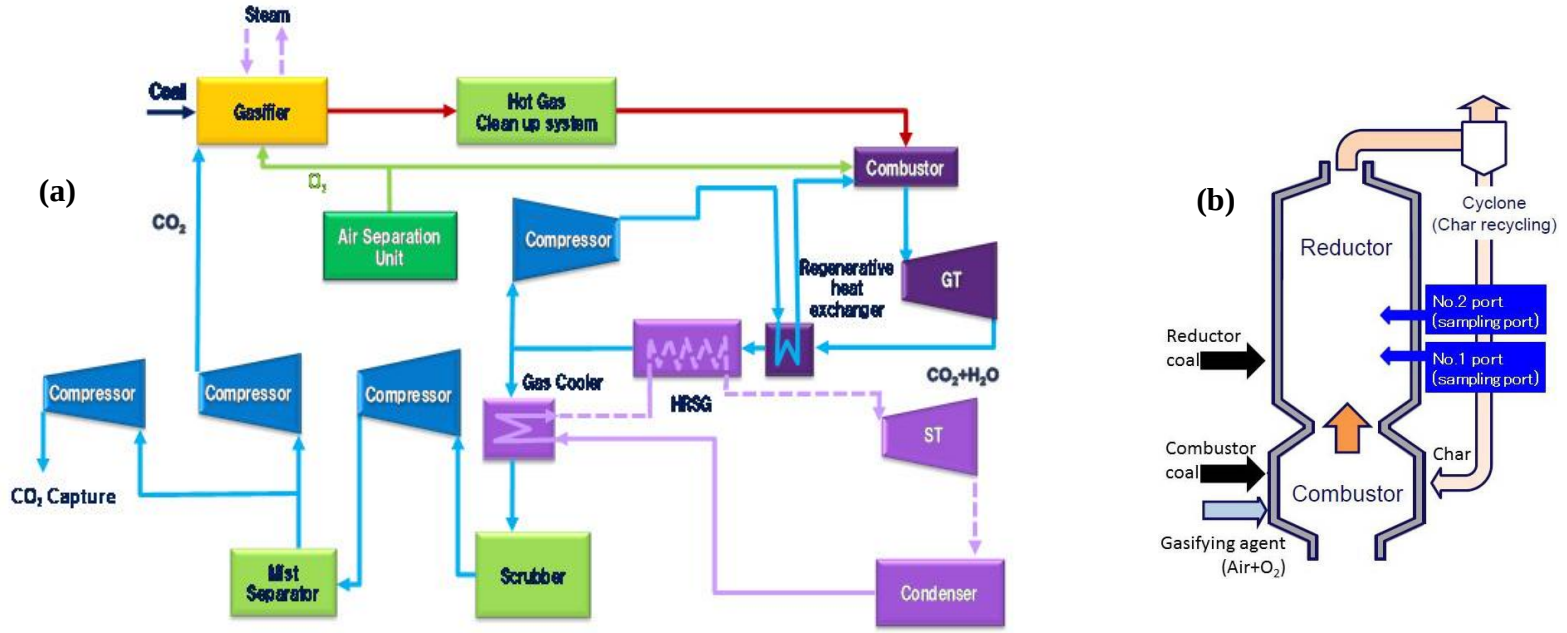

Fig. 1.4. (a) Detailed schematics of high-efficiency oxy-fuel IGCC (integrated (coal) gasification combine cycle) system, and **(b)** schematic of pressurized entrained flow of coal gasifier [1.17].

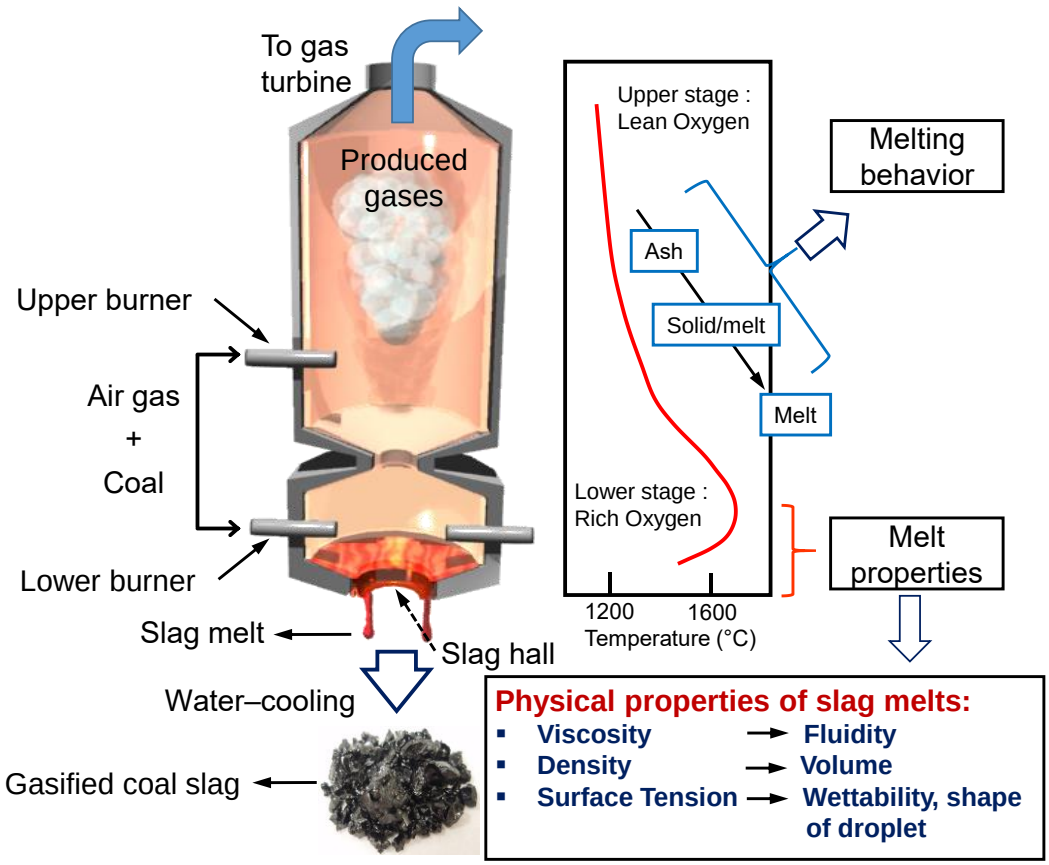

Fig. 1.5 The main physical properties of slag melts and schematic view of temperature distribution in the gasification furnace.

The operating temperature of the entrained-flow gasifiers is not necessary above the liquidus temperature of coal slags, the liquid coal slag tapped from the gasifier is possibly homogenous liquid slag or heterogeneous liquid slag containing crystallized particles [1.29]. It is important to understand that in the gasification process is not only the viscosity of fully liquid phase but also the viscosity of the liquid phase containing the partly crystallized solid particles for coal slag in the gasifier [1.20].

Viscosity (η) is a measure of the resistance of a liquid to shear deformation, and its SI unit is Pa·s. The viscosity is one of the key properties to determine the flow behaviors of slag melts. The flow behaviors influence the performance of continuous operation of the entrained-flow gasifier [1.30, 1.31]. It is widely considered that the viscosity of slag melts should be sufficiently low at the tapping temperature, typically less than 25 Pa.s at temperatures range 1300−1500 °C [1.18]. The viscosity of slag melts should have typically adequate values of 5−15 Pa·s with good flow [1.8, 1.32].

The density (ρ) is the mass per unit volume and its common unit is g/cm^3 (SI unit is 10^3 kg/m^3). The density of slag melts is important since it provides useful information about the glass melt structure. The density data is used to calculate molar volume and coefficient of volume expansion in order to discuss the molecular structure of slag melts [1.33–1.35]. The coefficient of volume expansion is one of important physical properties to control the melting process of slag melts [1.36, 1.37]. Furthermore, the temperature and composition dependences can be investigated with some methods of density measurements at high temperatures.

The surface tension (γ) in the coal gasification related with multicomponent slag melts is one of the most important parameters for controlling the various interfacial phenomena [1.38]. The surface tension defined as the energy required to increase the surface area of a liquid due to intermolecular forces is essential property of coal slag melts since its related to gasifier operating of IGCC [1.39]. The SI unit for surface tension is N/m and is identical dimensionally to the unit (J/m^2) for the surface energy; 1 J/m^2 = 1×10^3 erg/cm^3 = 1×10^3 dyne/cm = 1 N/m. The phenomena related to the surface tension of gasification are the process of coal slag melting. The surface tension plays a great role in controlling the homogeneity, bubble elimination from coal slag melts and gasifier corrosion. In addition, in the gasification process, surface tension is relevant to fluid flow of slags and slag ceramic interactions (wetting) [1.8, 1.36, 1.40]. Furthermore, the compositional and temperature dependences of surface tension provide us with important information on the glass melt structure [1.41, 1.42].

It is known that measurements of the viscosity, density, and surface tension of coal slag melts at high temperature are experimentally difficult to carry out, expensive, and time consuming [1.43]. In published literature, the physical properties of coal slag melts are limited. On the other hand, the importance of physical properties of gasified coal slag melts is primarily recognized to enable continuous operation. Therefore, the ability to measure and estimate viscosity, density, and surface tension for coal slag melts is useful for the practical gasification.

1.1.2. Significance of gasified coal slag melts

Coal has primarily been used as a solid fuel to produce electricity and heat through combustion such us in IGCC process. Coal is usually categorized and divided into several categories according to its properties, two major types are high–rank and low–rank coals [1.44]. Generally, classification of coals by rank and caloric values, bituminous coals, which are categorized as high–rank coals, are most commonly consumed in industrial sectors. In contrast, demand for low–rank coals such as sub–bituminous coal, lignite and brown coal are limited because of their lower heating values, compared with bituminous coal. Recently, efficient technologies to utilize low–rank coals have drawn attention [1.45], because there are limited reserves of the high–rank coals [1.14]. **Fig. 1.6** shows the proven recoverable of bituminous, sub-bituminous, and lignite coal in the world. Additionally, the **Fig. 1.7** shows the top coal producing countries.

Coal is a complex mixture of organic and inorganic compounds [1.44]. Due to the difficulty of quantitative analysis of the ash minerals, coal ash analysis is usually determined by chemical analysis for most elements produced by combustion. This means that ash and mineral matter are not the same material, physically or chemically although they are related [1.44]. Coal ash minerals encompass oxides, sulfides, and carbonates of silicon, aluminum, iron, calcium, magnesium [1.46]. While over 120 minerals have been identified in coal, only 8 are common constituents: quartz (SiO_2), kaolinite ($Al_2Si_2O_5(OH)_4$), illite ($(K, H_3O)(Al, Mg, Fe)_2(Si, Al)_4O_{10}[(OH)_2, (H_2O)]$), montmorillonite ($(Na, Ca)_{0.33}(Al, Mg)_2(Si_4O_{10})(OH)_2 \cdot nH_2O$), chlorite ($(Mg, Fe)_3(Si, Al)_4O_{10}(OH)_2 \cdot (Mg, Fe)_3(OH)_6$, pyrite ($FeS_2$), calcite ($CaCO_3$), and siderite ($FeCO_3$) [1.8].

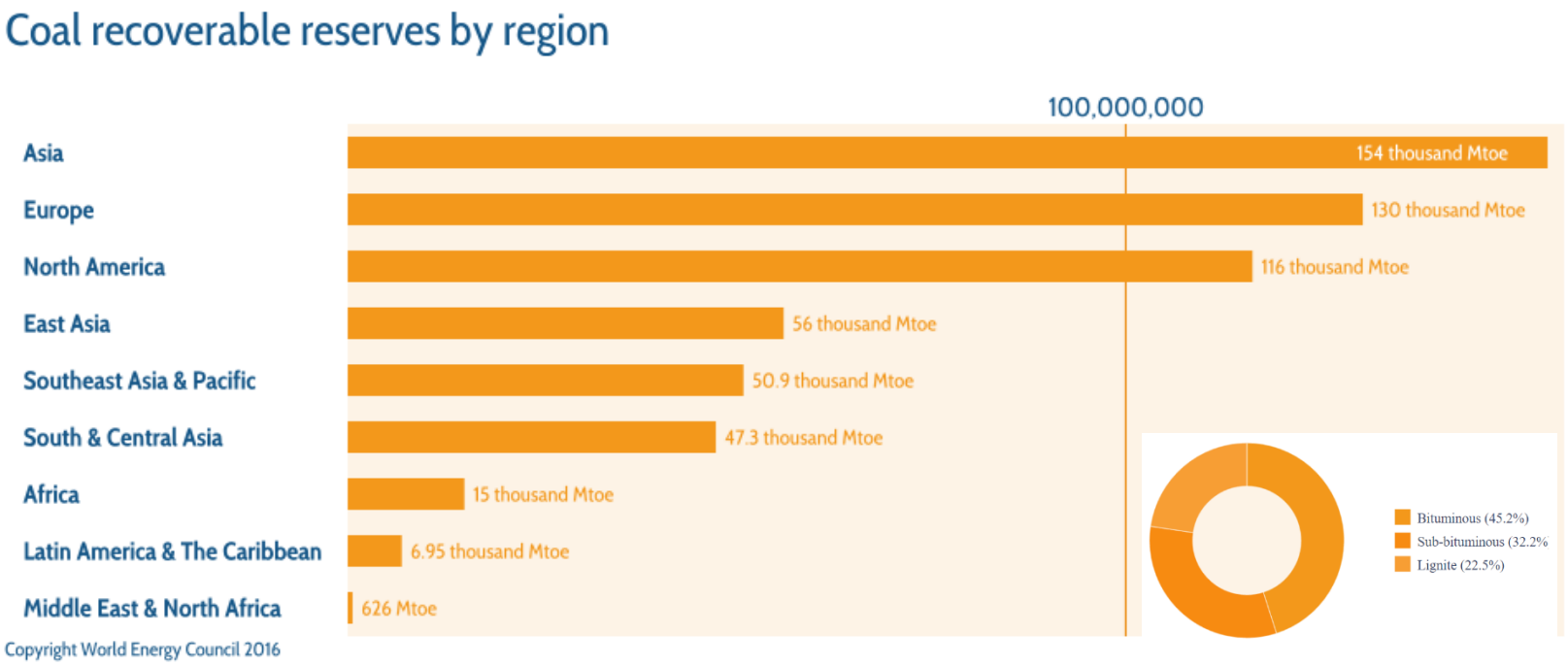

Fig. 1.6 The coal recoverable reserves by region of bituminous (high rank), sub-bituminous and lignite (high rank) [1.45] in the world by percentage (Source: https://www.worldenergy.org).

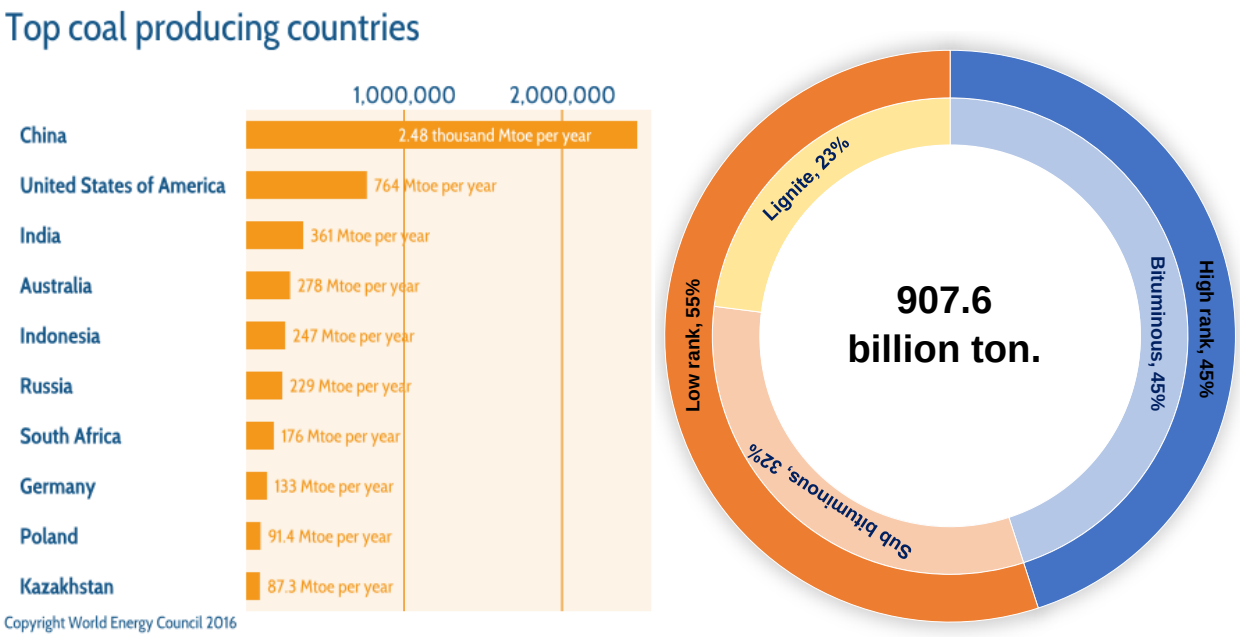

Fig. 1.7. The top coal producing countries and coal classification of bituminous (high rank), sub-bituminous and lignite (low rank) [1.45] in the world by percentage (Source: https://www.worldenergy.org).

The quantity of these mineral constituents differs considerably for coal ashes, depending on the geographic origin of the coal. The difference in coal ash causes substantial variability in their physical properties as a function of composition and temperature.

Coal slags formed during the gasification process mainly contain SiO_2, Al_2O_3, CaO, MgO, FeO, and Fe_2O_3 with small amounts of Na_2O, K_2O, TiO_2, P_2O_5, SrO, MnO, and other compounds [1.32, 1.34]. **Table 1.1** shows the major components of 45 coal slags from China using in the some IGCC power plants [1.20]. **Tables 1.2 and 1.3** show the major components of 52 and 32 coal slags analyses of low-iron and high iron from Australia, respectively [1.30, 1.32]. **Table 1.4** also shows the major components of 10 coal slag compositions used in the gasification system from Indonesia, USA, and Russia [1.47, 1.48]. **Table 1.5** summarizes 130 coal slags for IGCC process from China, Australia, Indonesia, USA, and Russia and their chemical compositions. **Table 1.5** shows that oxides of SiO_2, Al_2O_3, CaO, MgO, and Fe_2O_3 comprise more than 90% (mol) of mineral components. Minor components such as Na_2O, K_2O, TiO_2, P_2O_5, SrO, MnO, and other compounds account for about 10% (mol%) of the mineral components. A basicity composition parameter (base/acid ratio) (**Table 1.5**) without FeO_x components also covers the composition of these oxides mainly with $(CaO + MgO)/(Al_2O_3 + SiO_2)$ molar ratio in the range of 0.01 to 1.46.

Coal slags are similar in their compositions and properties to magmas, glasses, and slags [1.8]. Therefore, the study of molten silicates provides a useful first approximation to the behavior of coal slags derived under gasifier conditions. The gasified coal and synthesized slag melts with simplified silicate systems have been prepared here to understand the effect of the main components on viscosity. In this study, roles of Al_2O_3 and Fe_2O_3 on viscosity, density and surface tension as amphoteric oxides were mainly explored. Synthesized slag

melts for comparison are in the systems of $RO–Al_2O_3–SiO_2$ (R=Ca, Mg), $CaO–Fe_2O_3–SiO_2$ (CFS), and $CaO–Al_2O_3–Fe_2O_3–SiO_2$ (CAFS).

The roles of Al_2O_3 and Fe_2O_3 in silicate glasses, crystals and slag melts have been widely studied by various techniques such as Raman and Mössbaeur spectroscopies and several melt properties such as viscosity, surface tension and density at high temperatures [1.49–1.57]. Silicate slags consist of three-dimensional interconnected network of SiO_4 tetrahedra for SiO_2 as a network former (NWF) [1.33]. The basic oxides such as CaO, MgO break the silicate network to form non-bridging oxygen as network modifiers (NWM) [1.58]. The typical amphoteric oxides of Al_2O_3 and Fe_2O_3 play dual roles as NWF and NWM depending on slag composition [1.28].

From this point of view, a previous study [1.59] classified general oxides into four groups, based on the ionic radius and the electronegativity, as shown in **Fig. 1.8**. When the ionic radii and electro negativities of major component oxides of coal slag in **Fig. 1.8** are compared, it can be seen that the Si^{4+} is in group (A) as an acidic oxide for glass network. The Ca^{2+} and Mg^{2+} are in group (B) as basic oxides of alkali- and alkaline-earth oxides. The transition metal cations of Al^{3+}, Fe^{2+}, and Fe^{3+} are in group (D) functional cations (transition metal cations and amphoteric oxides). Transition metal cations have with d- or f-orbital valence electrons. Amphoteric oxides such as Al_2O_3 and Fe_2O_3 can behave as basic or acidic oxides, depending on slag composition.

Table 1.1 The major components of 45 coal slag samples from China [1.20].

Sample	Molar ratio (mass ratio)[a]											
	SiO_2		Al_2O_3		CaO		MgO		Fe_2O_3		Basicity parameter[b]	
LX	23.46	(18.92)	21.08	(28.85)	34.50	(25.97)	5.80	(3.14)	7.11	(15.24)	0.90	(0.61)
GJ	31.92	(23.55)	20.99	(26.28)	25.30	(17.42)	1.50	(0.74)	12.96	(25.42)	0.51	(0.36)
CL	41.30	(33.54)	22.70	(31.28)	9.16	(6.94)	13.07	(7.12)	6.28	(13.55)	0.35	(0.22)
HF	39.19	(32.08)	19.25	(26.74)	22.41	(17.12)	5.26	(2.89)	6.28	(13.66)	0.47	(0.34)
DT	44.26	(36.94)	21.73	(30.78)	20.81	(16.21)	5.57	(3.12)	4.11	(9.12)	0.40	(0.29)
PDS	44.72	(30.18)	21.36	(24.46)	9.56	(6.02)	2.30	(1.04)	20.59	(36.94)	0.18	(0.13)
GY	43.59	(37.32)	19.38	(28.15)	31.03	(24.79)	1.79	(1.03)	3.50	(7.96)	0.52	(0.39)
WL	53.48	(42.74)	23.44	(31.79)	8.76	(6.53)	3.47	(1.86)	5.54	(11.77)	0.16	(0.11)
AQ	51.53	(41.91)	22.44	(30.97)	17.44	(13.24)	0.51	(0.28)	4.23	(9.15)	0.24	(0.19)
XY	45.13	(36.88)	19.27	(26.73)	20.09	(15.32)	3.61	(1.98)	6.44	(13.98)	0.37	(0.27)
XLT	48.00	(41.57)	20.10	(29.54)	19.60	(15.84)	8.09	(4.70)	3.16	(7.28)	0.41	(0.29)
CC	61.66	(51.51)	25.20	(35.72)	6.31	(4.92)	2.89	(1.62)	1.70	(3.78)	0.11	(0.07)
GZ	52.22	(43.57)	21.07	(29.83)	18.10	(14.09)	2.14	(1.20)	3.87	(8.57)	0.28	(0.21)
SEK	48.13	(39.85)	19.11	(26.85)	19.54	(15.10)	5.65	(3.14)	6.50	(14.30)	0.37	(0.27)
YZ	38.44	(27.17)	14.16	(16.98)	23.29	(15.36)	2.45	(1.16)	20.35	(38.22)	0.49	(0.37)
SB	62.74	(54.33)	22.89	(33.64)	8.41	(6.80)	3.32	(1.93)	0.27	(0.61)	0.14	(0.10)
LEK	62.05	(52.18)	22.59	(32.24)	9.65	(7.57)	1.68	(0.95)	2.30	(5.14)	0.13	(0.10)
HM	49.17	(38.62)	17.79	(23.71)	12.44	(9.12)	5.50	(2.90)	9.98	(20.84)	0.27	(0.19)
SF2	53.67	(45.95)	18.73	(27.21)	19.02	(15.20)	2.70	(1.55)	2.98	(6.77)	0.30	(0.23)
CQ	58.16	(45.47)	20.15	(26.73)	9.24	(6.74)	0.84	(0.44)	8.16	(16.96)	0.13	(0.10)
GJW	62.01	(53.16)	20.84	(30.31)	7.00	(5.60)	5.22	(3.00)	1.94	(4.42)	0.15	(0.10)
JC	62.97	(54.46)	20.73	(30.42)	7.15	(5.77)	2.78	(1.61)	0.22	(0.50)	0.12	(0.09)
LW	53.12	(47.11)	17.49	(26.32)	21.87	(18.10)	1.04	(0.62)	0.99	(2.33)	0.32	(0.25)
YM	65.55	(56.15)	20.83	(30.28)	6.14	(4.91)	2.52	(1.45)	1.77	(4.02)	0.10	(0.07)
KL	41.80	(38.24)	12.97	(20.13)	33.93	(28.97)	5.41	(3.32)	1.77	(4.31)	0.72	(0.55)
DZ	53.64	(44.55)	16.64	(23.45)	19.27	(14.94)	2.08	(1.16)	5.92	(13.06)	0.30	(0.24)
HB	58.55	(46.32)	17.37	(23.32)	8.11	(5.99)	3.35	(1.78)	8.67	(18.22)	0.15	(0.11)
FH	62.21	(53.19)	18.06	(26.20)	10.98	(8.76)	2.67	(1.53)	2.92	(6.63)	0.17	(0.13)
HBL	30.98	(27.05)	8.63	(12.79)	47.18	(38.44)	3.01	(1.76)	7.26	(16.85)	1.27	(1.01)
ZZ	36.29	(32.84)	10.11	(15.52)	42.06	(35.52)	3.16	(1.92)	3.43	(8.25)	0.97	(0.77)
YB	61.37	(48.91)	16.94	(22.91)	8.31	(6.18)	2.34	(1.25)	8.55	(18.11)	0.14	(0.10)
HX	66.05	(57.78)	17.13	(25.43)	6.76	(5.52)	1.96	(1.15)	1.46	(3.40)	0.10	(0.08)
YC	61.01	(46.42)	15.60	(20.14)	6.00	(4.26)	1.43	(0.73)	12.62	(25.52)	0.10	(0.07)
XS	47.58	(42.51)	11.86	(17.99)	20.36	(16.98)	5.12	(3.07)	3.53	(8.38)	0.43	(0.33)
SF1	42.08	(37.38)	10.34	(15.58)	36.79	(30.50)	2.69	(1.60)	4.77	(11.26)	0.75	(0.61)
XZ	60.15	(50.77)	14.42	(20.65)	13.04	(10.27)	2.65	(1.50)	5.80	(13.02)	0.21	(0.16)
CJZ	52.98	(45.55)	12.49	(18.22)	19.47	(15.62)	5.20	(3.00)	6.29	(14.38)	0.38	(0.29)
DTU	54.64	(47.70)	12.88	(19.08)	18.25	(14.87)	3.62	(2.12)	3.93	(9.12)	0.32	(0.25)
FS	63.84	(53.13)	15.05	(21.25)	5.29	(4.11)	5.75	(3.21)	6.47	(14.32)	0.14	(0.10)
HX	46.84	(42.31)	10.94	(16.77)	23.94	(20.18)	11.69	(7.08)	4.91	(11.79)	0.62	(0.46)
SH	47.69	(41.45)	11.05	(16.30)	29.54	(23.96)	2.61	(1.52)	5.55	(12.82)	0.55	(0.44)
SM	37.06	(34.06)	8.58	(13.38)	42.55	(36.50)	3.13	(1.93)	3.75	(9.17)	1.00	(0.81)
ZLNE	39.60	(35.31)	8.91	(13.48)	37.97	(31.60)	4.06	(2.43)	5.69	(13.49)	0.87	(0.70)
LW	57.89	(47.54)	12.97	(18.08)	10.88	(8.34)	3.85	(2.12)	7.94	(17.32)	0.21	(0.16)
SX	58.73	(46.11)	12.95	(17.26)	12.45	(9.12)	1.27	(0.67)	11.53	(24.06)	0.19	(0.15)
Min.	23.46	(18.92)	8.58	(12.79)	5.29	(4.11)	0.51	(0.28)	0.22	(0.50)	0.10	(0.07)
Max.	66.05	(57.78)	25.20	(35.72)	47.18	(38.44)	13.07	(7.12)	20.59	(38.22)	1.27	(1.01)

Table 1.2 The major components of 52 coal slag of low-iron slag from Australia [1.30].

Sample	Molar ratio (mass ratio)[a]											
	SiO_2		Al_2O_3		CaO		MgO		Fe_2O_3		Basicity parameter[b]	
1	88.69	(79.50)	9.53	(14.50)	0.36	(0.30)	0.17	(0.10)	0.39	(0.94)	0.01	(0.01)
2	68.60	(59.10)	18.61	(27.20)	4.51	(3.63)	3.50	(2.02)	0.12	(0.28)	0.09	(0.07)
3	91.50	(85.40)	7.39	(11.70)	0.07	(0.06)	0.10	(0.06)	0.29	(0.71)	0.01	(0.01)
4	73.49	(60.00)	20.93	(29.00)	0.33	(0.25)	0.31	(0.17)	1.61	(3.49)	0.01	(0.00)
5	74.20	(60.20)	22.73	(31.30)	0.42	(0.32)	0.46	(0.25)	0.37	(0.80)	0.01	(0.01)
6	76.81	(61.90)	17.33	(23.70)	1.22	(0.92)	1.20	(0.65)	1.81	(3.87)	0.03	(0.02)
7	64.65	(51.50)	25.52	(34.50)	2.26	(1.68)	1.52	(0.81)	0.96	(2.04)	0.04	(0.03)
8	69.77	(58.70)	19.26	(27.50)	4.41	(3.46)	2.34	(1.32)	0.98	(2.19)	0.08	(0.06)
9	58.99	(47.20)	26.00	(35.30)	8.87	(6.62)	0.73	(0.39)	1.30	(2.76)	0.11	(0.08)
10	66.30	(54.60)	22.83	(31.90)	4.53	(3.48)	0.69	(0.38)	1.15	(2.52)	0.06	(0.04)
11	75.62	(65.90)	12.92	(19.10)	3.60	(2.93)	2.86	(1.67)	1.07	(2.47)	0.07	(0.05)
12	83.41	(75.20)	10.00	(15.30)	1.31	(1.10)	1.22	(0.74)	0.82	(1.97)	0.03	(0.02)
13	82.31	(73.90)	13.39	(20.40)	0.31	(0.26)	0.45	(0.27)	1.19	(2.85)	0.01	(0.01)
14	79.36	(67.30)	15.15	(21.80)	0.63	(0.50)	0.74	(0.42)	1.49	(3.35)	0.01	(0.01)
15	70.67	(59.00)	18.85	(26.70)	1.73	(1.35)	1.45	(0.81)	1.47	(3.26)	0.04	(0.03)
16	79.50	(69.00)	14.53	(21.40)	0.80	(0.65)	0.94	(0.55)	1.44	(3.32)	0.02	(0.01)
17	55.12	(45.50)	19.78	(27.70)	14.41	(11.10)	1.57	(0.87)	1.26	(2.76)	0.21	(0.16)
18	64.18	(51.60)	25.80	(35.20)	3.73	(2.80)	1.04	(0.56)	1.69	(3.61)	0.05	(0.04)
19	69.66	(56.70)	18.97	(26.20)	3.50	(2.66)	0.88	(0.48)	2.65	(5.73)	0.05	(0.04)
20	75.11	(62.10)	19.03	(26.70)	0.89	(0.69)	0.92	(0.51)	1.96	(4.31)	0.02	(0.01)
21	73.09	(61.00)	18.71	(26.50)	0.49	(0.38)	1.63	(0.91)	1.86	(4.12)	0.02	(0.01)
22	64.03	(49.90)	28.96	(38.30)	0.82	(0.60)	0.59	(0.31)	2.38	(4.93)	0.02	(0.01)
23	66.63	(55.10)	20.10	(28.20)	4.29	(3.31)	2.81	(1.56)	1.90	(4.18)	0.08	(0.06)
24	66.86	(54.60)	24.39	(33.80)	1.74	(1.33)	1.73	(0.95)	2.17	(4.70)	0.04	(0.03)
25	64.57	(53.10)	21.28	(29.70)	6.25	(4.80)	0.92	(0.51)	2.79	(6.10)	0.08	(0.06)
26	64.08	(49.80)	26.69	(35.20)	2.25	(1.63)	0.88	(0.46)	2.45	(5.06)	0.03	(0.02)
27	74.87	(62.30)	19.62	(27.70)	0.79	(0.61)	0.21	(0.12)	2.33	(5.15)	0.01	(0.01)
28	68.41	(56.80)	16.61	(23.40)	4.65	(3.60)	2.21	(1.23)	2.32	(5.13)	0.08	(0.06)
29	84.67	(74.80)	11.47	(17.20)	0.50	(0.41)	0.44	(0.26)	0.97	(2.28)	0.01	(0.01)
30	61.13	(49.80)	22.42	(31.00)	7.30	(5.55)	1.56	(0.85)	2.23	(4.82)	0.11	(0.08)
31	61.29	(53.80)	14.63	(21.80)	17.94	(14.70)	1.90	(1.12)	2.01	(4.69)	0.26	(0.21)
32	69.09	(54.70)	22.18	(29.80)	0.95	(0.70)	1.73	(0.92)	2.95	(6.21)	0.03	(0.02)
33	68.75	(57.60)	15.61	(22.20)	5.47	(4.28)	2.15	(1.21)	2.71	(6.03)	0.09	(0.07)
34	81.73	(70.70)	13.35	(19.60)	0.30	(0.24)	0.28	(0.16)	2.88	(6.61)	0.01	(0.00)
35	64.52	(53.00)	15.35	(21.40)	8.86	(6.79)	2.65	(1.46)	2.32	(5.06)	0.14	(0.11)
36	57.51	(50.20)	18.29	(27.10)	13.87	(11.30)	2.61	(1.53)	3.06	(7.11)	0.22	(0.17)
37	46.49	(38.70)	18.40	(26.00)	19.31	(15.00)	8.72	(4.87)	2.82	(6.25)	0.43	(0.31)
38	34.19	(28.00)	17.85	(24.80)	21.07	(16.10)	8.30	(4.56)	2.74	(5.97)	0.56	(0.39)
39	65.26	(52.90)	20.79	(28.60)	4.53	(3.43)	1.97	(1.07)	3.58	(7.72)	0.08	(0.06)
40	65.70	(53.10)	20.78	(28.50)	3.38	(2.55)	1.73	(0.94)	4.36	(9.37)	0.06	(0.04)
41	67.07	(56.60)	16.48	(23.60)	3.91	(3.08)	3.53	(2.00)	3.52	(7.90)	0.09	(0.06)
42	70.58	(56.60)	18.00	(24.50)	1.04	(0.78)	1.99	(1.07)	4.81	(10.25)	0.03	(0.02)
43	67.85	(57.20)	14.19	(20.30)	7.12	(5.60)	1.80	(1.02)	3.56	(7.97)	0.11	(0.09)
44	63.35	(49.40)	24.26	(32.10)	1.92	(1.40)	1.93	(1.01)	5.36	(11.10)	0.04	(0.03)
45	26.59	(21.70)	13.79	(19.10)	22.85	(17.40)	11.97	(6.55)	3.30	(7.15)	0.86	(0.59)
46	60.24	(47.70)	20.39	(27.40)	8.82	(6.52)	2.39	(1.27)	4.12	(8.67)	0.14	(0.10)
47	49.56	(40.10)	14.49	(19.90)	21.72	(16.40)	1.70	(0.92)	3.92	(8.43)	0.37	(0.29)
48	63.51	(50.80)	17.24	(23.40)	6.82	(5.09)	1.96	(1.05)	4.16	(8.84)	0.11	(0.08)

to be continued

49	34.48	(30.00)	10.57	(15.60)	39.04	(31.70)	6.48	(3.78)	3.69	(8.54)	1.01	(0.78)
50	70.56	(56.60)	18.00	(24.50)	1.04	(0.78)	1.99	(1.07)	4.83	(10.30)	0.03	(0.02)
51	83.06	(73.20)	3.61	(5.40)	2.63	(2.16)	1.23	(0.73)	5.29	(12.40)	0.04	(0.04)
52	58.66	(46.30)	19.93	(26.70)	10.07	(7.42)	2.49	(1.32)	4.58	(9.60)	0.16	(0.12)
Min.	26.59	(21.70)	3.61	(5.40)	0.07	(0.06)	0.10	(0.06)	0.12	(0.28)	0.01	(0.01)
Max.	91.50	(85.40)	28.96	(38.30)	39.04	(31.70)	11.97	(6.55)	5.36	(12.40)	1.01	(0.78)

Table 1.3 The major components of 23 coal slags of high-iron slag from Australia [1.32].

Coal slag	Molar ratio (mass ratio) [a]											
	SiO_2		Al_2O_3		CaO		MgO		Fe_2O_3		Basicity parameter[b]	
1	44.33	(35.20)	15.53	(20.93)	23.64	(17.52)	3.75	(2.00)	9.48	(20.00)	0.46	(0.35)
2	64.18	(50.42)	15.88	(21.17)	3.89	(2.85)	3.89	(2.05)	9.14	(19.09)	0.10	(0.07)
3	61.53	(49.61)	15.11	(20.68)	6.55	(4.93)	4.47	(2.42)	8.60	(18.42)	0.14	(0.10)
4	62.85	(50.73)	14.77	(20.23)	8.54	(6.43)	2.44	(1.32)	8.52	(18.28)	0.14	(0.11)
5	52.25	(38.42)	24.67	(30.78)	7.33	(5.03)	1.34	(0.66)	11.54	(22.55)	0.11	(0.08)
6	45.75	(33.81)	24.56	(30.80)	14.51	(10.01)	1.17	(0.58)	11.48	(22.54)	0.22	(0.16)
7	45.41	(34.03)	21.30	(27.09)	14.34	(10.03)	3.40	(1.71)	11.34	(22.59)	0.27	(0.19)
8	43.42	(32.17)	23.27	(29.26)	14.55	(10.06)	3.26	(1.62)	11.46	(22.57)	0.27	(0.19)
9	61.06	(47.39)	15.55	(20.48)	5.03	(3.64)	4.34	(2.26)	10.74	(22.16)	0.12	(0.09)
10	58.07	(46.80)	11.52	(15.75)	9.77	(7.35)	4.96	(2.68)	9.68	(20.73)	0.21	(0.16)
11	60.54	(47.64)	16.60	(22.17)	6.21	(4.56)	3.37	(1.78)	9.60	(20.07)	0.12	(0.09)
12	60.13	(47.44)	12.00	(16.07)	7.01	(5.16)	4.46	(2.36)	11.03	(23.12)	0.16	(0.12)
13	58.50	(45.44)	19.12	(25.20)	6.80	(4.93)	2.76	(1.44)	9.91	(20.45)	0.12	(0.09)
14	57.57	(44.43)	21.36	(27.97)	6.97	(5.02)	2.11	(1.09)	9.36	(19.20)	0.11	(0.08)
15	51.59	(40.46)	18.77	(24.98)	14.85	(10.87)	3.04	(1.60)	9.53	(19.87)	0.25	(0.19)
16	54.21	(43.24)	15.84	(21.44)	15.57	(11.59)	3.12	(1.67)	9.64	(20.44)	0.27	(0.21)
17	56.09	(45.63)	11.03	(15.22)	16.92	(12.85)	3.48	(1.90)	10.09	(21.82)	0.30	(0.24)
18	59.97	(48.80)	11.26	(15.55)	14.26	(10.83)	2.38	(1.30)	9.83	(21.26)	0.23	(0.19)
19	43.99	(34.32)	21.48	(28.44)	21.17	(15.41)	2.41	(1.26)	8.97	(18.60)	0.36	(0.27)
20	55.63	(42.26)	23.39	(30.16)	7.05	(5.00)	1.94	(0.99)	9.69	(19.57)	0.11	(0.08)
21	50.65	(41.05)	13.16	(18.10)	19.83	(15.00)	3.55	(1.93)	9.56	(20.60)	0.37	(0.29)
22	46.73	(37.34)	15.05	(20.41)	21.91	(16.34)	3.92	(2.10)	10.31	(21.89)	0.42	(0.32)
23	48.60	(36.93)	21.96	(28.31)	13.68	(9.70)	3.61	(1.84)	10.89	(21.99)	0.25	(0.18)
Min.	43.42	(32.17)	11.03	(15.22)	3.89	(2.85)	1.17	(0.58)	8.52	(18.28)	0.10	(0.07)
Max.	64.18	(50.73)	24.67	(30.80)	23.64	(17.52)	4.96	(2.68)	11.54	(23.12)	0.46	(0.32)

Table 1.4 The major components of 10 coal slags from Indonesia, USA, and Russia [1.47, 1.48].

Coal slag	Molar ratio (mass ratio)											
	SiO_2		Al_2O_3		CaO		MgO		Fe_2O_3		Basicity parameter[b]	
Baiduri[a]	38.44	(27.93)	12.73	(15.69)	25.54	(17.32)	11.63	(5.67)	4.91	(9.48)	0.73	(0.53)
Adaro[a]	51.92	(39.18)	14.66	(18.78)	15.97	(11.25)	5.12	(2.59)	8.26	(16.57)	0.32	(0.24)
Kideco[a]	51.82	(37.93)	12.20	(15.15)	17.60	(12.02)	5.23	(2.57)	11.04	(21.47)	0.36	(0.27)
Usibelli[b]	49.88	(42.73)	13.02	(18.93)	26.28	(21.01)	5.45	(3.13)	2.64	(6.00)	0.50	(0.39)
Cyprus[b]	62.74	(59.80)	10.03	(16.22)	9.00	(8.01)	3.24	(2.07)	2.73	(6.91)	0.17	(0.13)
SUFCo[b]	66.20	(60.21)	10.11	(15.60)	13.63	(11.57)	3.51	(2.14)	2.42	(5.85)	0.22	(0.18)
Pits. No 8[b]	59.57	(46.77)	18.52	(24.67)	7.51	(5.50)	2.03	(1.07)	8.27	(17.26)	0.12	(0.09)
PMA[b]	58.56	(43.79)	20.52	(26.04)	3.70	(2.58)	2.11	(1.06)	10.57	(21.01)	0.07	(0.05)
PMB[b]	57.03	(43.37)	22.69	(29.28)	4.95	(3.51)	2.33	(1.19)	8.20	(16.57)	0.09	(0.06)
Denisovsky[c]	65.48	(54.59)	18.64	(26.37)	5.64	(4.39)	3.38	(1.89)	3.74	(8.29)	0.11	(0.08)
Min.	38.44	(27.93)	10.03	(15.15)	3.70	(2.58)	2.03	(1.06)	2.42	(5.85)	0.07	(0.05)
Max.	66.20	(60.21)	22.69	(29.28)	26.28	(21.01)	11.63	(5.67)	11.04	(21.47)	0.73	(0.39)

[a, b, and c] The a, b, and c are the coal from Indonesia, USA and Russia, respectively.

Table 1.5. Range of major components and basicity ratios of coal from this study, China, Australia, Indonesia, USA, and Russia used to IGCC process.

Coal slag	Molar ratio (mass ratio)[a]											
	SiO_2		Al_2O_3		CaO		MgO		Fe_2O_3		Basicity parameter[b]	
This Study (4)	39–62	(34–55)	10–16	(15–23)	8–25	(6–20)	4–16	(2–10)	3–8	(6–19)	0.28–1.00	(0.26–0.99)
China (45)	24–66	(19–58)	8–25	(13–36)	5–47	(4–38)	0–13	(0–7)	0–21	(0–38)	0.10–1.27	(0.07–1.01)
Australia low-Fe_2O_3 (52)	27–92	(22–85)	4–29	(5–38)	0–39	(0–32)	0–12	(0–7)	0–5	(0–12)	0.01–1.01	(0.01– 0.78)
Australia high-Fe_2O_3 (23)	43–64	(32–51)	15–31	(15–31)	4–24	(3–18)	9–12	(18–23)	1–5	(1–3)	0.10–0.46	(0.07–0.32)
Indonesia (3)	38–52	(28–39)	12–15	(15–19)	16–26	(11–17)	5–12	(3–6)	5–11	(9–21)	0.24–0.73	(0.24–0.53)
USA (6)	38–52	(43–60)	12–15	(16–29)	16–26	(3–21)	5–11	(6–21)	5–2	(1–3)	0.07–0.50	(0.05–0.39)
Russia (1)	65	(55)	19	(26)	6	(4)	4	(8)	3	(2)	0.11	(0.08)

[a] Molar ratio (mass ratio) for gasified coal slags was obtained based on the contents of major components only.
[b] Basicity parameter (base/acid ratio) in Tables **1.1–1.5**: (CaO+MgO)/(Al_2O_3+SiO_2) in mass and molar ratios.

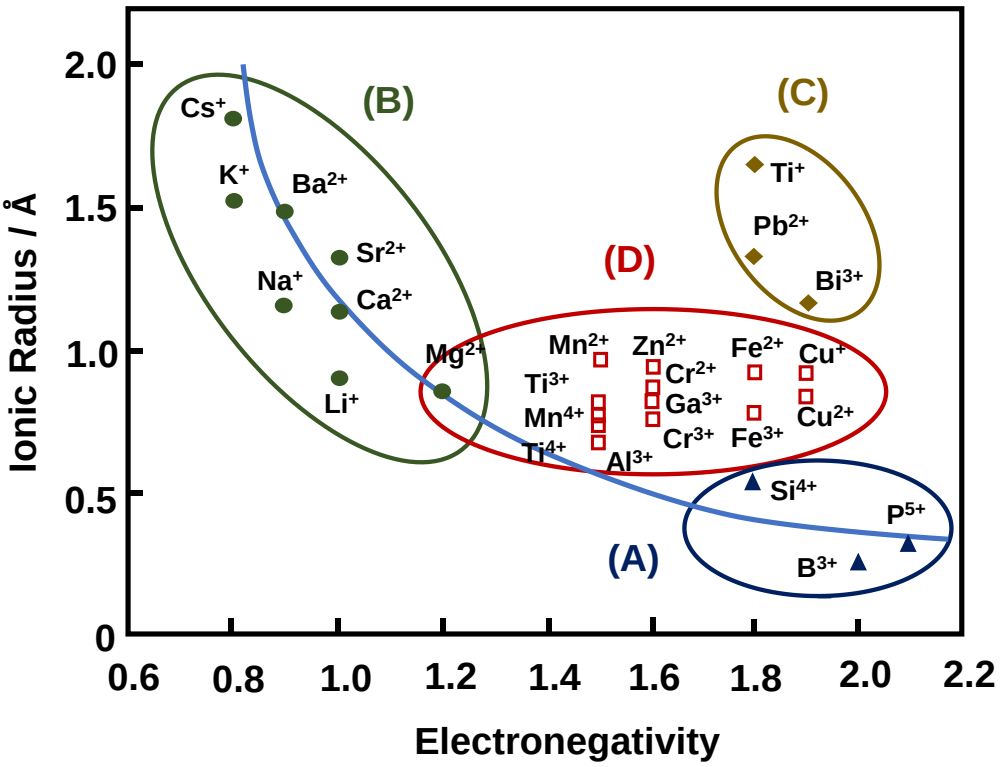

Fig. 1.8. Classification of general oxides with respect to their ionic radius and electronegativity [1.59].

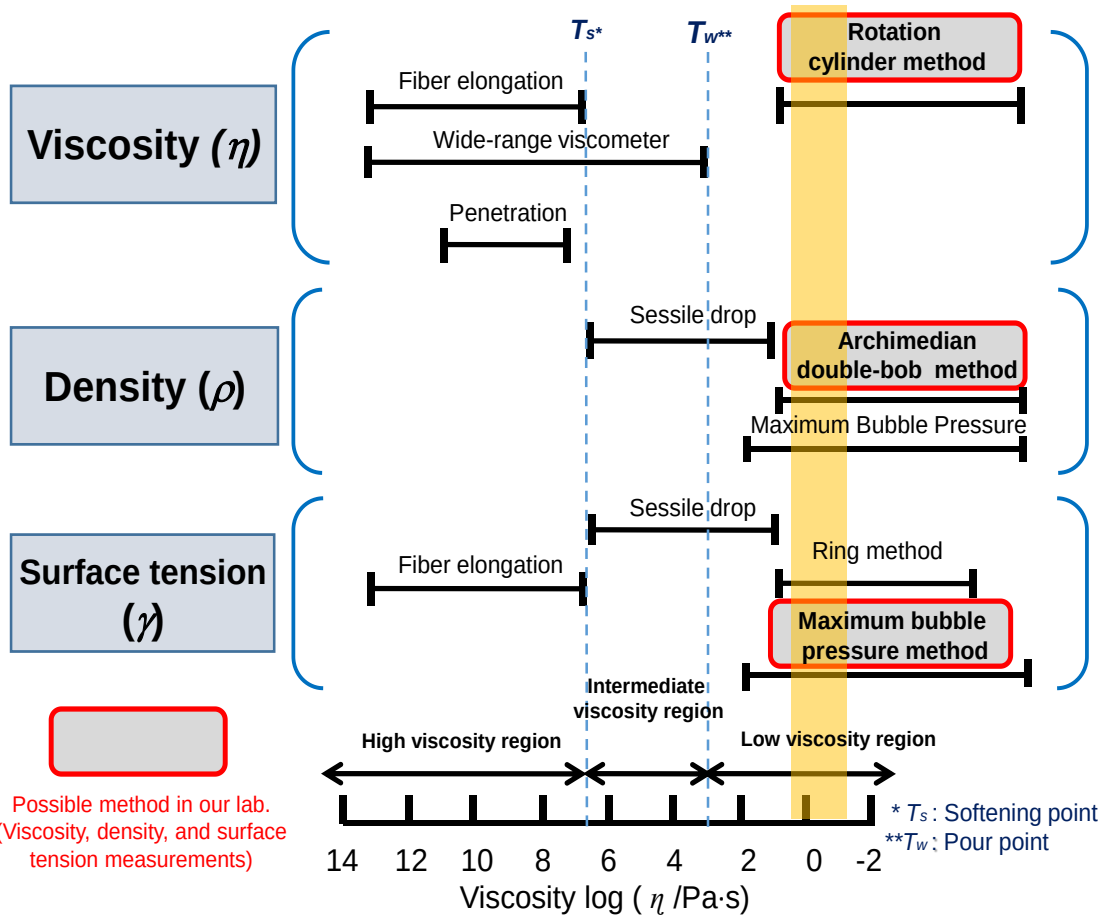

Fig. 1.9. General measurement methods of viscosity, density, and surface tension of slag melts [1.60].

From the above points of view, there is a great need to investigate the fundamental properties of gasified coal and synthesized coal slag melts. This is desirable for the IGCC process of coal in the gasifier and a better understanding of the problems that may be encountered in this practical applications. General measurements method of viscosity, density and surface tension of slag melts are classified in **Fig. 1.9** with respect to the viscosity range [1.60]. Among the measuring methods in **Fig. 1.9** the rotating cylinder method, the Archimedean double-bob method, and the maximum bubble method are used in this study for viscosity, density, and surface tension measurements, respectively.

1.2. Purposes of Present Study

The purposes of present study are as follows:

(i) to establish the viscosity, density, and surface tension measurements of gasified and synthesized coal slag melts,

(ii) to discuss the temperature and compositional dependences of viscosity, density, and surface tension of gasified coal and synthesized slag melts, and

(iii) to determine some empirical equations to predict viscosity, density, and surface tension from the corresponding composition of slags.

This dissertation consists of the following five chapters:

In chapter 1, the background, previous study, and purposes of the present study were summarized.

In chapter 2, the viscosities of gasified coal and synthesized slag melts were measured systematically using the rotation cylinder method. The temperature and compositional dependences of viscosity are discussed.

In chapter 3, the densities of gasified coal and synthesized slag melts obtained by systematic measurements using the Archimedean double-bob method are reported. The molar volume and coefficient of volume expansion were calculated from the density measurements. The temperature and compositional dependences of these properties are discussed.

In chapter 4, the surface tensions of synthesized slag melts were measured systematically using the maximum bubble pressure method. The temperature and compositional dependences of surface tension are discussed.

In chapter 5, the general conclusion and future direction of this dissertation are summarized.

References

[1.1] Song W, Dong Y, Wu Y, Zhu Z. Prediction of temperature of critical viscosity for coal ash slag. Am Inst Chem Eng 2011;57:2921–5. doi:10.1002/aic.12500.

[1.2] Cau G, Tola V, Deiana P. Comparative performance assessment of USC and IGCC power plants integrated with CO_2 capture systems. Fuel 2014;116:820–33. doi:10.1016/j.fuel.2013.06.005.

[1.3] Collot A-G. Matching gasification technologies to coal properties. Int J Coal Geol 2006;65:191–212. doi:10.1016/j.coal.2005.05.003.

[1.4] Franco A, Diaz AR. The future challenges for "clean coal technologies": Joining efficiency increase and pollutant emission control. Energy 2009;34:348–54. doi:10.1016/j.energy.2008.09.012.

[1.5] Electric Power development CO. L. Annual report: J-POWER 's cutting-edge coal-fired - thermal power plants and Innovative , next-generation coal-fired power technologies. 2010.

[1.6] Clayton SJ, Stiegel GJ, Wimer JG. Gasification Technologies: Gasification Markets and Technologies — Present and Future - An Industry Perspective. Energy 2002:100.

[1.7] Mondol JD, McIlveen-Wright D, Rezvani S, Huang Y, Hewitt N. Techno-economic evaluation of advanced IGCC lignite coal fuelled power plants with CO_2 capture. Fuel 2009;88:2495–506. doi:10.1016/j.fuel.2009.04.019.

[1.8] Hsieh PY, Kwong KS, Bennett J. Correlation between the critical viscosity and ash fusion temperatures of coal gasifier ashes. Fuel Process Technol 2016;142:13–26. doi:10.1016/j.fuproc.2015.09.019.

[1.9] Arman, Okada A, Takebe H. Density measurements of gasified coal and synthesized

slag melts for next-generation IGCC. Fuel 2016;182:304–13. doi:10.1016/j.fuel.2016.05.117.

[1.10] Minchener AJ. Coal gasification for advanced power generation. Fuel 2005;84:2222–35. doi:10.1016/j.fuel.2005.08.035.

[1.11] IEA. Energy and Climate Change. World Energy Outlook Spec Rep 2015:1–200. doi:10.1038/479267b.

[1.12] Final report: International comparison of fossil power efficiency and CO_2 intensity. 2015.

[1.13] J-POWER group annual report. 2015.

[1.14] New Energy and Industrial Technology Development Organisation (NEDO). Clean coal technologies in Japan: Technological innovation in the coal industry 2006:116.

[1.15] Buhre BJP, Browning GJ, Gupta RP, Wall TF. Measurement of the viscosity of coal-derived slag using thermomechanical analysis. Energy and Fuels 2005;19:1078–83. doi:10.1021/ef0497311.

[1.16] Ferreira LS, Trierweiler JO. Modeling and simulation of the polymeric nanocapsule formation process. IFAC Proc Vol 2009;7:405–10. doi:10.1002/aic.

[1.17] Oki Y, Hara S, Umemoto S, Kidoguchi K, Hamada H, Kobayashi M, Nakao Y. Development of high-efficiency oxy-fuel IGCC system. Energy Procedia 2014;63:471–5. doi:10.1016/j.egypro.2014.11.050.

[1.18] Kong L, Bai J, Li W, Wen X, Li X, Bai Z, Guo Z, Li H, The internal and external factor on coal ash slag viscosity at high temperatures, Part 1: Effect of cooling rate on slag viscosity, measured continuously. Fuel 2015;158:968–75. doi:10.1016/j.fuel.2015.02.055.

[1.19] Kong L, Bai J, Li W, Wen X, Liu X, Li X, Bai Z, Guo Z, Li H. The internal and external factor on coal ash slag viscosity at high temperatures, Part 2: Effect of residual carbon on slag viscosity. Fuel 2015;158:976–82. doi:10.1016/j.fuel.2015.06.055.

[1.20] Song W, Sun Y, Wu Y, Zhu Z, Koyama S. Measurement and simulation of flow properties of coal ash slag in coal gasification. Am Inst Chem Eng 2011;57:801–18. doi:10.1002/aic.

[1.21] Song W, Tang L, Zhu X, Wu Y, Rong Y, Zhu Z, Koyama S. Fusibility and flow properties of coal ash and slag. Fuel 2009;88:297–304. doi:10.1016/j.fuel.2008.09.015.

[1.22] Groen J, Brooker D, Welch P, Oh M. Gasification slag rheology and crystallization in titanium-rich, iron–calcium–aluminosilicate glasses. Fuel Process Technol 1998;56:103–27. doi:10.1016/S0378-3820(98)00063-0.

[1.23] Strezov V, Lucas JA, Wall TF. Effect of pressure on the swelling of density separated coal particles. Fuel 2005;84:1238–45. doi:10.1016/j.fuel.2004.06.035.

[1.24] Aineto M, Acosta A, Rincon J, Romero M. Thermal expansion of slag and fly ash from coal gasification in IGCC power plant. Fuel 2006;85:2352–8. doi:10.1016/j.fuel.2006.05.015.

[1.25] Shannon GN, Matsuura H, Rozelle P, Fruehan RJ, Pisupati S, Sridhar S. Effect of size and density on the thermodynamic predictions of coal particle phase formation during coal gasification. Fuel Process Technol 2009;90:1114–21. doi:10.1016/j.fuproc.2009.05.002.

[1.26] Lin X, Ideta K, Miyawaki J, Takebe H, Wang Y, Yoon S, Mochida I. Study on structural and compositional transitions of coal ash by using NMR. J Coal Sci Eng

2012;18:80–7.

[1.27] Lin X, Ideta K, Miyawaki J, Takebe H, Yoon SH, Mochida I. Correlation between fluidity properties and local structures of three typical Asian coal ashes. Energy and Fuels 2012;26:2136–44. doi:10.1021/ef201771f.

[1.28] Takebe H, Tsuruda A, Okada A, Ueda K. Viscosity characteristic of molten Slag for next-generation IGCC. J Japan Inst Energy 2015;94 (5):450–4.

[1.29] Bryers RW. Fireside slagging, fouling, and high-temperature corrosion of heat-transfer surface due to impurities in steam-raising fuels. Prog Energy Combust Sci 1996;22:29–120. doi:10.1016/0360-1285(95)00012-7.

[1.30] Hurst HJ, Novak F, Patterson JH. Viscosity measurements and empirical predictions for fluxed Australian bitumnous coal ashes. Fuel 1999;78:1831–40. doi:10.1016/S0016-2361(99)00094-0.

[1.31] Patterson JH, Hurst HJ. Ash and slag qualities of Australian bituminous coals for use in slagging gasifiers. Fuel 2000;79:1671–8. doi:10.1016/S0016-2361(00)00032-6.

[1.32] Ilyushechkin AY, Hla SS. Viscosity of high-iron slags from Australian coals. Energy and Fuels 2013;27:3736–42. doi:10.1021/ef400593k.

[1.33] Mysen BO, Virgo D, Seifert FA. The structure of silicate melts: Implications for chemical and physical properties of natural magma. Rev Geophys Sp Phys 1982;20:353–83. doi:10.1029/RG020i003p00353.

[1.34] Mills KC. Estimation of physicochemical properties of coal slag and ashes. Miner Mater Ash Coal, Am Chem Soc Washinton, DC 1986;301:195–214. doi:10.1021/bk-1986-0301.ch015.

[1.35] Hwang C, Fujino S, Morinaga K. Density of Bi_2O_3–B_2O_3 binary melts. J Am Ceram

Soc 2004;87:1677–82. doi:10.1111/j.1551-2916.2004.01677.x.

[1.36] Kuromitsu Y, Yoshida H, Takebe H, Morinaga K. Interaction between alumina and binary glasses. J Am Ceram Soc 1997;80 (6):1583–7. doi:10.1111/j.1151-2916.1997.tb03020.x.

[1.37] Toyoda S, Fujino S, Morinaga K. Density, viscosity and surface tension of 50RO–$50P_2O_5$ (R: Mg, Ca, Sr, Ba, and Zn) glass melts. J Non Cryst Solids 2003;321:169–74. doi:10.1016/S0022-3093(03)00174-1.

[1.38] Hanao M, Tanaka T, Kawamoto M, Takatani K. Evaluation of surface tension of molten slag in multi-component systems. ISIJ Int 2007;47:935–9.

[1.39] Miller S, Kalmanovitch D. Relation of slag viscosity and surface tension to sintering potential. Prepr Pap - Am Chem Soc Div Fuel Chem 1988;33:42–9.

[1.40] Melchior T, Pütz G, Müller M. Surface tension measurements of coal ash slags under reducing conditions at atmospheric pressure. Energy & Fuels 2009;23:4540–6.

[1.41] Weirauch DAJ, Ziegler DP. Surface tension of calcium aluminosilicate glass using computerized drop shape analysis. J Am Ceram Soc 1996;79:920–6.

[1.42] Fujino S, Hwang C, Moringa K. Density, Surface tension, and viscosity of PbO–B_2O_3–SiO_2 glass melts. J Am Ceram Soc 2004;87:10–6. doi:10.1111/j.1151-2916.2004.tb19937.x.

[1.43] Forsbacka L, Holappa L, Iida T, Kita Y, Toda Y. Experimental study of viscosities of selected CaO–MgO–Al_2O_3–SiO_2 slags and application of the Iida model. Scandanavian J Metall 2003;32:273–80. doi:10.1034/j.1600-0692.2003.00652.x.

[1.44] Edgar TF. Coal processing and pollution control. 1983.

[1.45] Frau C, Ferrara F, Orsini A, Pettinau A. Characterization of several kinds of coal and

biomass for pyrolysis and gasification. Fuel 2014;152:138–45. doi:10.1016/j.fuel.2014.09.054.

[1.46] Matjie RH, French D, Ward CR, Pistorius PC, Li Z. Behaviour of coal mineral matter in sintering and slagging of ash during the gasification process. Fuel Process Technol 2011;92:1426–33. doi:10.1016/j.fuproc.2011.03.002.

[1.47] Oh MS, Brooker DD, de Paz EF, Brady JJ, Decker TR. Effect of crystalline phase formation on coal slag viscosity. Fuel Process Technol 1995;44:191–9. doi:10.1016/0378-3820(95)00012-V.

[1.48] Yun Y, Yoo YD, Chung SW. Selection of IGCC candidate coals by pilot-scale gasifier operation. Fuel Process Technol 2007;88:107–16. doi:10.1016/j.fuproc.2004.08.009.

[1.49] Aksay I, Pask J, Davis R. Densities of SiO_2–Al_2O_3 Melts. J Am Ceram Soc 1973;62 (7-8):332–6. doi:10.1111/j.1151-2916.1979.tb19071.x.

[1.50] Morinaga K, Suginohara Y, Yanagase T. Density of CaO–SiO_2–Fe_2O_3, –Al_2O_3 melts. Tech Rep Kyushu Univ 1975;48 (6):859–65.

[1.51] Morinaga K, Suginohara Y, Yanagase T. Oxygen coordination number of Fe ions in CaO–SiO_2 and Na_2O–SiO_2 systems. J Japan Ints Met 1976;40 (05):480–6.

[1.52] Dingwell DB, Brearley M. Melt densities in the CaO–FeO–Fe_2O_3–SiO_2 system and the compositional dependence of the partial molar volume of ferric iron in silicate melts. Geochim Cosmochim Acta 1988;52:2815–25. doi:10.1016/0016-7037(88)90149-4.

[1.53] Mills KC, Jeffrey M. Rhine. The measurement and estimation of the physical properties of slags formed during coal gasification: 1. Properties relevant to fluid flow. Fuel 1989;68:193–200. doi:10.1017/CBO9781107415324.004.

[1.54] Nowok JW, Bieber JA, Benson SA, Jones ML. Physicochemical effects influencing the measurements of interfacial surface tension of coal ashes. Fuel 1991;70:951–6. doi:10.1016/0016-2361(91)90050-K.

[1.55] Neuville DR, Cormier L, Massiot D. Al coordination and speciation in calcium aluminosilicate glasses: Effects of composition determined by ^{27}Al MQ-MAS NMR and Raman spectroscopy. Chem Geol 2006;229:173–85. doi:10.1016/j.chemgeo.2006.01.019.

[1.56] Chevrel MO, Giordano D, Potuzak M, Courtial P, Dingwell DB. Physical properties of $CaAl_2Si_2O_8$–$CaMgSi_2O_6$–FeO–Fe_2O_3 melts: analogues for extra-terrestrial basalt. Chem Geol 2013;346:93–105. doi:10.1016/j.chemgeo.2012.09.004.

[1.57] Takahashi S, Neuville DR, Takebe H. Thermal properties, density and structure of percalcic and peraluminus CaO–Al_2O_3–SiO_2 glasses. J Non Cryst Solids 2015;411:5–12. doi:10.1016/j.jnoncrysol.2014.12.019.

[1.58] Mills KC. The influence of structure on the physico-chemical properties of slags. ISIJ Int 1993;33:148–55. doi:10.2355/isijinternational.33.148.

[1.59] Morinaga K. From slags to new glass –Introduction to basicity of oxide–. Shigen-to-Sozai 1995;111:696–973.

[1.60] Morinaga K, Fujino S. Research and development of Surface tension measurement of glass melts in high temperature range. New Glass 2002;17:3–6.

Chapter 2

Viscosity Measurements and Prediction of Gasified Coal and Synthesized Slag Melts

2.1. Introduction

The Integrated gasification combined cycle (IGCC) of the Central Research Institute of Electric Power Industry (CRIEPI) commissioned in a project of New Energy and Industrial Technology Development Organization (NEDO), Japan has been designed to produce electricity with CO_2 capture [2.1, 2.2]. The CRIEPI has used various coals with different compositions depending on geographic origin and has been set a goal to be applied a variety of coal grades in a next-generation IGCC project. The organic compounds of coals are converted to synthesis gas while the inorganic compounds become coal ash during gasification process. The slag melt due to the coal mineral matters is discharged through a hole under the entrained-gasifier by quenching in water as a gasified coal slag [2.3–2.5]. Thus physical properties of the slag melts play an important role in the IGCC [2.6]. The most fundamental physical properties of coal slag melts in the an IGCC power plant are the viscosity, density, and surface tension.

The previous study [2.7] reported that the entrained-flow gasification employs a high temperature, high pressure slagging gasifier, in which slag viscosity plays a key role in

determining operating conditions. The flow behavior affects the performance of continuous operation of the entrained-flow gasifier [2.8, 2.9].

The viscosity of slag melts should have typically adequate values of 5–15 Pa·s for entrained-flow gasifiers at tapping temperature with good flow [2.10, 2.11]. The influence of slag melt viscosity varies as a function of gasifier design, operating temperature and the chemical composition of coal ash slag [2.11]. Large numbers of researches have studied for the composition and temperature dependences of coal slag viscosity [2.12–2.14]. Various experimental results [2.15–2.20] and models [2.21–2.25] have been reported to estimate the viscosity of slag melts according to their chemical compositions. Some models were related to the main oxides frequently found in coal slags [2.26, 2.27].

The slags formed during the coal gasification process mainly contain SiO_2, Al_2O_3, CaO, MgO, FeO, and Fe_2O_3 with small amounts of Na_2O, K_2O, TiO_2, P_2O_5, SrO, MnO, and other compounds [2.10, 2.28, 2.29]. The gasified coal slags and synthesized ones containing the main components with systematic composition variations have been prepared here to understand the effects of the main components on viscosity. In the main components, roles of Al_2O_3 and Fe_2O_3 as amphoteric oxides depend on slag composition and melting conditions. The roles of Al_2O_3 and Fe_2O_3 on structure and properties in silicate melts, glasses, and crystals have been widely studied by various techniques such as Raman and Mössbaeur spectroscopies and several melt properties such as viscosity, surface tension and density at high temperatures [2.30–2.38]. In this study, roles of Al_2O_3 and Fe_2O_3 on viscosity as amphoteric oxides were mainly explored. Synthesized slag melts for comparison are in the systems of RO–Al_2O_3–SiO_2 (R=Ca, Mg), CaO–Fe_2O_3–SiO_2 (CFS), and CaO–Al_2O_3–Fe_2O_3–SiO_2 (CAFS).

According to these scientific and engineering backgrounds, the objectives of this research are (i) to establish a rotation cylinder method to measure viscosity of gasified and synthesized coal slag melts for homogeneous liquid state in silicate systems containing CaO or MgO and Al_2O_3 and/or FeO/Fe_2O_3, (ii) to study the composition and temperature dependences of viscosity, (iii) to discuss the effect of Al_2O_3 and Fe_2O_3 on viscosity, and (iv) to propose a composition parameter to optimize the viscosity of coal slag melts based on chemical composition for IGCC.

2.2 Materials and Methods

2.2.1 Sample preparation

2.2.1.1 Coal slag samples

Coal slag samples denoted as CH (Coal Valley), TH (Tanito Harum), MA (Malinau), and AD (Adaro) were provided by the CRIEPI of Japan. The samples were obtained after rapid quenching slag melts from a gasifier pilot plant into water. The samples were re-melted at 1650 °C in air for viscosity measurements in the temperature range 1300 to 1650 °C and then rapidly quenched to evaluate their chemical compositions. **Table 2.1** shows the chemical compositions determined by X-Ray fluorescence (XRF) analysis for coal slag samples. The valence state of iron oxide was evaluated using chelate titration method [2.39] in quenched samples. In the case of AD coal slag, the chelate titration method was not performed due to difficulty in dissolution of AD powder sample. Thus all the iron oxide in the AD coal slag was assumed to Fe_2O_3. A previous study [2.40] reported a similar result that all iron exists as ferric iron in a coal slag consisting mainly of CaO, MgO, Al_2O_3, and SiO_2 with 5 mol%Fe_2O_3 under the melting below 1400 ºC in air.

Table 2.1 Chemical composition of gasified coal slags for viscosity measurements.

Element	mol% (mass %)							
	Coal Valley (CV)		Tanito Harum (TH)		Malinau (MA)		Adaro (AD)	
Major component								
SiO_2	61.5	(54.8)	57.8	(49.8)	54.6	(46.2)	39.0	(34.3)
Al_2O_3	13.9	(21.1)	16.0	(23.4)	15.0	(21.6)	10.0	(14.9)
CaO	14.2	(11.9)	9.2	(7.4)	8.0	(6.3)	24.5	(20.1)
MgO	3.6	(2.1)	4.8	(2.8)	6.3	(3.6)	16.4	(9.7)
FeO	2.2	(2.3)	5.8	(6.0)	7.1	(7.2)	-	-
Fe_2O_3	1.4	(3.3)	2.6	(6.0)	3.9	(8.7)	8.0 [a]	(18.7) [a]
Minor component								
K_2O	1.1	(1.5)	1.4	(1.9)	1.3	(1.8)	0.9	(1.2)
TiO_2	0.6	(0.7)	1.0	(1.1)	1.0	(1.1)	0.8	(0.9)
P_2O_5	0.1	(0.4)	0.1	(0.4)	0.2	(0.8)	ND	(ND)
SrO	0.1	(0.2)	0.1	(0.2)	0.1	(0.1)	ND	(ND)
ZrO_2	0.1	(0.2)	ND[b]	(ND)	0.1	(0.2)	ND	(ND)
MnO	0.1	(0.1)	0.1	(0.1)	0.1	(0.1)	0.2	(0.2)
Cr_2O_3	0.1	(0.2)	ND	(ND)	0.1	(0.2)	ND	(ND)
BaO	0.2	(0.5)	ND	(ND)	0.1	(0.2)	ND	(ND)
Na_2O	0.8	(0.7)	1.1	(0.9)	2.1	(1.9)	ND	(ND)
Total	100	(100)	100	(100)	100	(100)	100	(100)

[a] All iron oxide was assumed to Fe_2O_3 in AD coal slag
[b] Not detected.

Table 2.2 Compositions of synthesized slags and major components of gasified coal slags.

Series	Sample	Fe^{3+}/Fe_{tot}[a]	Molar ratio (mass ratio) or mol% (mass%)[b]												T_L or T_{hm}[d] (°C)	Basicity parameter[e]
			SiO_2		Al_2O_3		CaO		MgO		FeO[c]		Fe_2O_3[c]			
Coal slag	Coal Valley (CV)	0.56	61.5	(54.8)	13.9	(21.1)	14.2	(11.9)	3.6	(2.1)	2.2	(2.3)	1.4	(3.3)	1,500	0.28
	Tanito Harum (TH)	0.47	57.8	(49.8)	16.0	(23.4)	9.2	(7.4)	4.8	(2.8)	5.8	(6.0)	2.6	(6.0)	1,450	0.30
	Malinau (MA)	0.52	54.6	(46.2)	15.0	(21.6)	8.0	(6.3)	6.3	(3.6)	7.1	(7.2)	3.9	(8.7)	1,450	0.36
	Adaro (AD)	-	39.0	(34.3)	10.0	(14.9)	24.5	(20.1)	16.4	(9.7)	0.0	(0.0)	8.0[f]	(18.7)	1,250	1.00
$(60-x)RO-xA_2O_3-40SiO_2$	CA10.40	-	40.0	(38.6)	10.0	(16.4)	50.0	(45.0)	0.0	(0.0)	0.0	(0.0)	0.0	(0.0)	1,351	1.00
(A=Al and/or Fe)	CA20.40	-	40.0	(35.9)	20.0	(30.5)	40.0	(33.6)	0.0	(0.0)	0.0	(0.0)	0.0	(0.0)	1,358	0.67
(R=Ca or Mg)	CA30.40	-	40.0	(33.6)	30.0	(42.8)	30.0	(23.5)	0.0	(0.0)	0.0	(0.0)	0.0	(0.0)	1,509	0.43
	CF08.39	0.80	39.2	(35.5)	0.0	(0.0)	49.0	(41.4)	0.0	(0.0)	4.0	(4.3)	7.8	(18.8)	1,362	0.55
	CAF15.11.39	0.76	38.6	(30.2)	14.5	(19.3)	29.0	(21.2)	0.0	(0.0)	6.9	(6.5)	11.0	(22.9)	1,428	1.55
$(50-x)RO-xA_2O_3-50SiO_2$	CA00.50	-	50.0	(51.7)	0.0	(0.0)	50.0	(48.3)	0.0	(0.0)	0.0	(0.0)	0.0	(0.0)	1,541	0.88
(A=Al or Fe)	CA12.50	-	50.0	(47.1)	12.5	(20.0)	37.5	(33.0)	0.0	(0.0)	0.0	(0.0)	0.0	(0.0)	1,295	1.00
(R=Ca or Mg)	CF07.49	0.69	48.5	(44.2)	0.0	(0.0)	38.8	(33.0)	0.0	(0.0)	6.1	(6.6)	6.7	(16.2)	1,202	0.60
$(40-x)RO-xA_2O_3-60SiO_2$	CA00.60	-	60.0	(61.6)	0.0	(0.0)	40.0	(38.4)	0.0	(0.0)	0.0	(0.0)	0.0	(0.0)	1,457	1.06
(A=Al or Fe)	CA10.60	-	60.0	(57.2)	10.0	(16.2)	30.0	(26.7)	0.0	(0.0)	0.0	(0.0)	0.0	(0.0)	1,317	0.70
(R=Ca or Mg)	MA10.60	-	60.0	(61.8)	10.0	(17.5)	0.0	(0.0)	30.0	(20.7)	0.0	(0.0)	0.0	(0.0)	1,363	0.43
	CF07.58	0.71	58.3	(52.7)	0.0	(0.0)	29.2	(24.6)	0.0	(0.0)	5.6	(6.1)	6.9	(16.6)	1,258	0.43
	CF14.57	0.74	57.1	(46.0)	0.0	(0.0)	19.0	(14.3)	0.0	(0.0)	9.8	(9.4)	14.1	(30.2)	1,308	0.72

[a] The fraction of Fe^{3+}/Fe_{tot} was analyzed two or three times for quenched samples using chelate titration method.

[b] Molar ratio (mass ratio) for gasified coal slags was obtained based on the contents of major components only. The total amount of minor components was less than 2.1 mol% (1.9 mass%). Synthesized slags consist of the major components only and their compositions are indicated.

[c] The contents of FeO and Fe_2O_3 were calculated from analyzed Fe^{3+}/Fe_{tot}.

[d] Liquidus temperatures T_L for synthesized slags were obtained using FactSage data bank. Homogeneous melting temperatures T_{hm} for gasified coal slags were determined experimentally by hot thermocouple (HTC) method.

[e] Basicity parameter (base/acid ratio) without including Fe_2O_3: $(CaO+MgO+FeO)/(Al_2O_3+SiO_2)$ in molar ratio.

[f] All iron oxide was assumed to Fe_2O_3 in Adaro coal slag.

2.2.1.2 Synthesized slag samples

Table 2.2 shows that the batches of synthesized slag samples were denoted into three composition series of (60-x)RO–xA_2O_3–40SiO_2, (50-x)RO–xA_2O_3–50SiO_2, and (40-x)RO–xA_2O_3–60SiO_2 in molar ratio, where R is Ca and Mg, A is Al and Fe without considering Fe valence state. The sample composition was selected for constant SiO_2 contents of 40, 50, and 60 mol% with various contents of CaO, MgO, Al_2O_3, and Fe_2O_3. The composition of synthesized slags was systematically varied by considering those of gasified coal slags for comparison (**Table 2.1**). The nominal contents used in this study are also shown in **Table 2.2.** The sample compositions are labeled by the type and molar fraction of components except for SiO_2, where C, A, and F mean respective oxides: CaO, Al_2O_3, and Fe_2O_3 and x and y are their molar fractions. The synthesized slag samples were prepared from a mixture of SiO_2, Al_2O_3, $CaCO_3$, MgO, and Fe_2O_3 powders with 99.99 % purity as raw materials. The mixture was melted at 1650 ºC for 2 hours in air using a Pt-30wt%Rh crucible placed in a $MoSi_2$ box furnace. The slag melt was poured onto a stainless steel mold, cooled to room temperature and then crushed for viscosity measurements. The valence state of iron was also determined experimentally in quenched samples after viscosity measurements using chelate titration method. The experimental results of Fe^{3+}/Fe_{tot} are presented in **Table 2.2.** The contents of FeO and Fe_2O_3 are calculated from Fe^{3+}/Fe_{tot} for determining sample composition.

2.2.2 Viscosity measurements of slag melts

The measuring temperature of viscosity was selected for homogeneous melting state. The temperature for homogeneous melting was confirmed by FactSage data bank [2.41] for

synthesized slags and experimentally by hot thermocouple (HTC) method [2.42] for coal ash slags. **Table 2.2** indicates the liquidus temperatures T_L of synthesized slags.

The HTC method [2.42] is an established experimental procedure combined the Pt-13%Rh/Pt thermocouple, a stereoscopic microscope, camera, and PC. The PC has an image capturing system to record the macroscopic change of coal slag melt samples. The monitor displays experimental conditions of morphologies and solidified fractions directly. **Fig. 2.1** shows the sequence photographs on the HTC measurements of the coal ash at different temperatures for selected homogeneous melting state. **Table 2.2** also shows homogeneous melting temperatures T_{hm} determined by the HTC method for four types of gasified coal slags.

The rotating cylinder method was established for viscosity measurements. The viscosity was determined from the torque measurement of the rotating cylinder viscometer. **Fig. 2.2** presents the schematic diagram of the measuring apparatus consisting of three main parts: an electric furnace, a furnace controller, and a set of rotation of cylinder method device. A Brookfield digital viscometer (Model DV-E) was used in this study. The viscometer was connected to the working cylinder by a Pt–30wt% Rh wire with 542 mm in length and with 2 mm in diameter. The crucible was made of Pt–30wt% Rh. The cylinder was suspended at the middle position upward the crucible before sample heating. The slag sample was re-melted at the highest measuring temperature and was kept for 2 hours before viscosity measurements. After temperature holding, the rotating cylinder was lowered and immersed into the slag melts. The optimized rotating speeds were selected for every measurement.

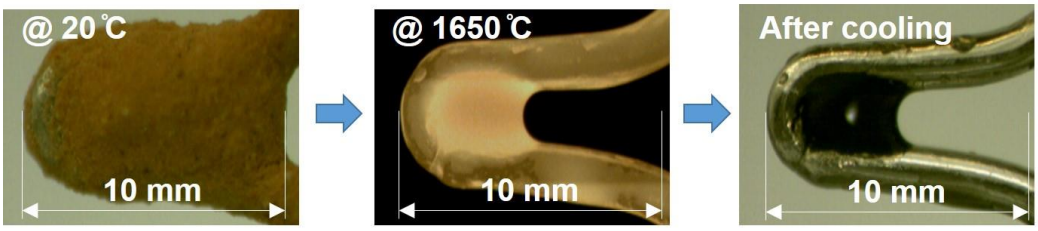

Fig. 2.1. The sequence photographs of the coal slag-ash on HTC measurements for determining homogeneous melting state.

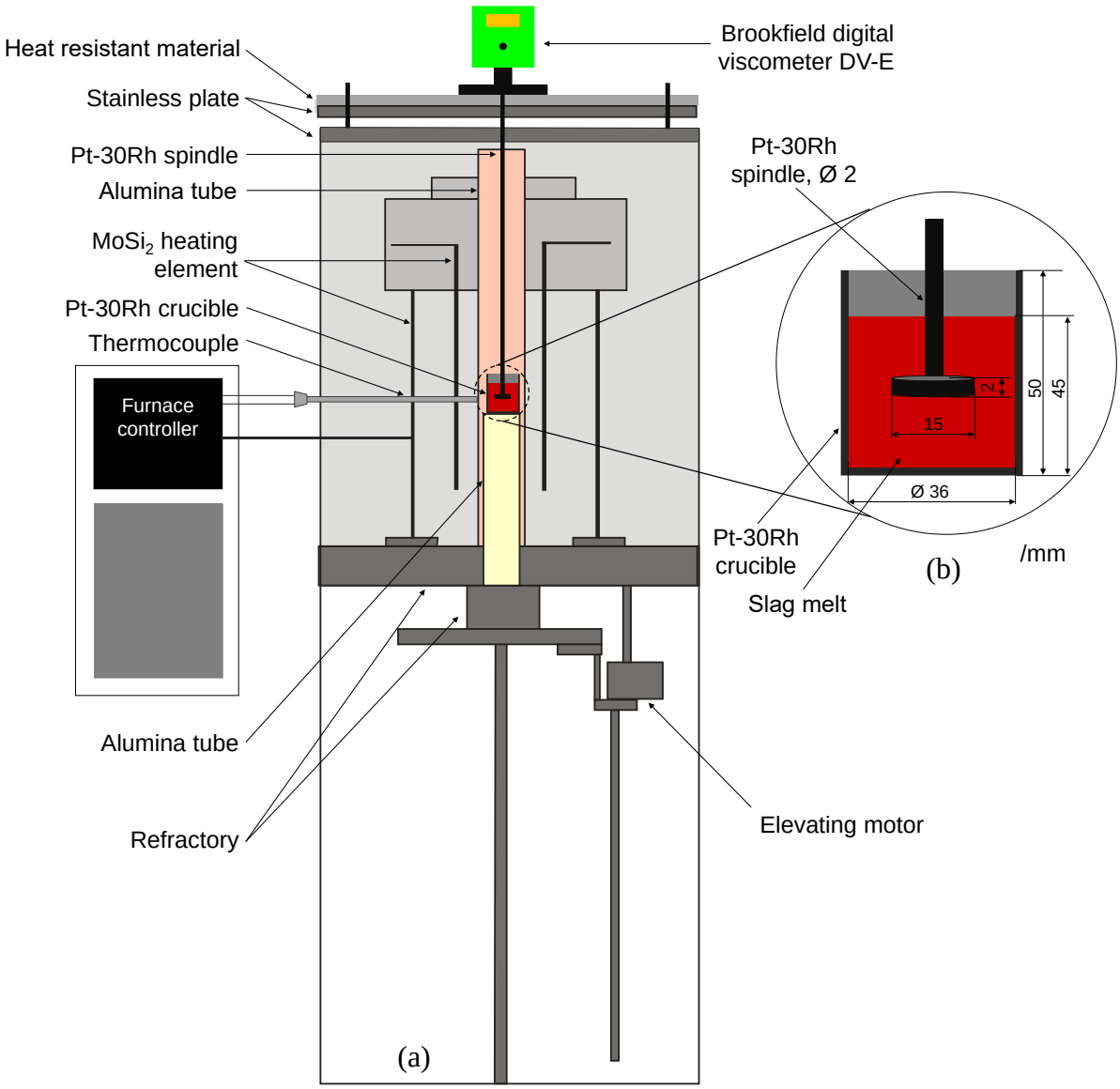

Fig. 2.2. Schematic apparatus for measuring viscosity of slag melts: (a) whole diagram, (b) the Pt–30wt% Rh crucible and Pt–30wt% Rh spindle for rotating cylinder method.

The determination of viscosity by rotating the cylinder at a constant speed can be calculated using the Margules equation of **Eq. (2-1)** [2.43]:

$$\eta = M/4\pi\,\omega h \times [1/r_i^2 - 1/r_0^2] \quad (2\text{-}1)$$

where M is the torque, ω is the cylinder rotation speed, h is the depth of immersion, r_i and r_0 are the radii of inner and outer cylinders. Since the viscosity measurement of slag melts is conducted at high temperatures, it is needed to correct the error term derived from the thermal expansion of the cylinder. The thermal expansion coefficient to calculate the viscosity is considered by the following **Eq. (2-2**):

$$\eta = \eta'/(1 + 3\alpha\Delta T) \quad (2\text{-}2)$$

where η is the viscosity determined, η' is the viscosity measured experimentally by the cylinder at high temperatures, α is the thermal expansion coefficient of cylinder [2.44], and ΔT is the difference between the measuring and room temperatures. In order to confirm the accuracy and the reproducibility of viscosity values for slag melts, the viscometer was calibrated at room temperature (25 °C) using Brookfield standard silicone fluids with four types of known viscosities (0.01, 0.502, 4.850, and 29.44 Pa·s). The viscometer was calibrated two or three times with different speeds of rotation cylinder, and the measured deviation from the mean was within 1.04%. The reproducibility of the measurement at high temperatures was also evaluated for the viscosities of 50CaO–50SiO_2 (mol%) melt as a standard sample.

2.3 Results and Discussion

2.3.1 Error estimation

A previous study [2.45] identified that the error estimation of the rotational viscometer method was taken by the following factors: the thermal expansion of the crucible and the cylinder, the geometric arrangement of the crucible and the cylinder, the error due to temperature measurement, and the composition change of the melt during the measurement. The total error thus was estimated as ~6.7% in the previous study. Another previous study reported that the error of rotational cylinder method was estimated with a uncertainty of ≤ 10% [2.46].

The viscosity of 50CaO–50SiO_2 (mol%) slag melt was measured at 1550–1600 °C. **Fig. 2.3** shows variation of viscosity with temperature for 50CaO−50SiO_2 slag melt (mol%) with the previously reported values of Mizoguchi et al. [2.47] with the same composition and Bockris and Lowe [2.48] with a similar composition of 49.7CaO−50.3SiO_2 (mol%). The comparison of present study and the previous studies shows that our result is in better agreement with the result of Mizoguchi et. al. [2.47] with the deviation of 1.5 % in comparison to that of Bockris and Lowe [2.48] with the deviation of 3.3%.

2.3.2 Viscosity measurements

Table 2.3 summarizes measured results of viscosity in gasified coal and synthesized slag melts.

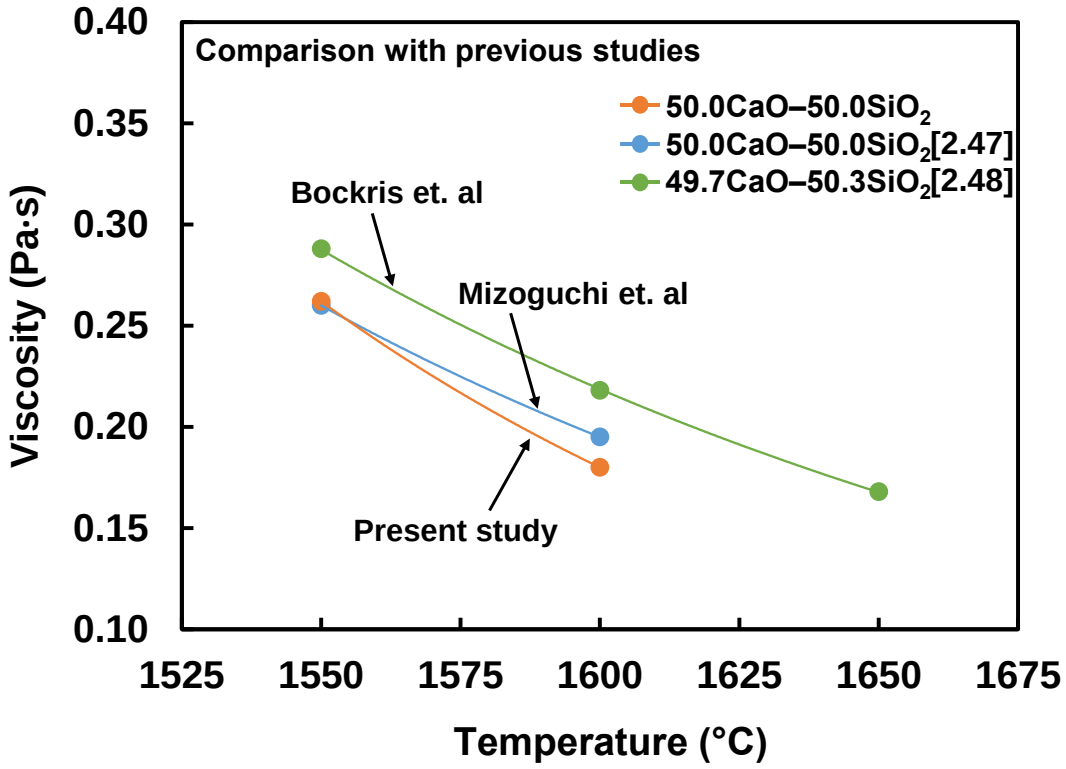

Fig. 2.3. Variation of viscosity with temperature for 50CaO–50SiO_2 slag melt (mol%) with the previously reported values of Mizoguchi *et al.* [2.47] with the same composition and Bockris and Lowe [2.48] with a similar composition of 49.7CaO–50.3SiO_2 (mol%). The solid lines are exponential fits to the data of the slag melts.

Table 2.3 Measured results of viscosity for gasified coal and synthesized slag melts.

Series	Sample	Viscosity (Pa·s) at temperature (°C)							
		1650	1600	1550	1500	1450	1400	1350	1300
(60-x)RO−xA_2O_3−40SiO_2	CA10.40	-	0.4	0.5	0.7	1.0	1.5	-	-
	CA20.40	-	0.7	1.0	1.6	2.6	4.4	-	-
	CA30.40	0.8	1.3	1.9	3.6	-	-	-	-
	CF08.39	-	-	-	-	-	0.2	0.2	0.3
	CAF15.11.39	-	-	0.2	0.2	0.3	0.4	0.6	
(50-x)RO−xA_2O_3−50SiO_2	CA00.50	-	0.2	0.3	-	-	-	-	-
	CA12.50	-	1.5	2.2	3.3	5.2	8.4	-	-
	CF07.49	-	-	-	-	0.2	0.3	0.3	0.5
(40-x)RO−xA_2O_3−60SiO_2	CA00.60	-	0.5	0.6	0.8	-	-	-	-
	CA10.60	2.2	3.2	4.8	7.3	11.6	-	-	-
	MA10.60	0.8	1.1	1.5	2.2	3.5	5.8	-	-
	CF07.58	-	0.3	0.4	0.5	0.6	0.9	1.3	-
	CF14.57	-	0.2	0.2	0.3	0.3	0.5	-	-
Coal slag	CV	6.2	9.7	15.4	-	-	-	-	-
	TH	3.0	4.4	6.8	10.6	-	-	-	-
	MA	2.3	3.3	5.0	8.0	-	-	-	-
	AD	-	0.2	-	0.4	-	0.8	2.3	10.8

2.3.2.1 Gasified coal slag melts

Fig. 2.4 shows the temperature dependences of the viscosity of coal slag melts in the temperature range 1300 to 1650 °C. The viscosities of CV, TH, and MA coal slag melts gradually increase with decreasing temperature as a general trend in slag melts [2.16], while the viscosity of AD slag melt exhibits the rapid increase at 1300 °C. The viscosity of slag melts rapidly increases below the temperature of critical viscosity, T_{cv} [2.49]. T_{cv} is defined as a temperature at which the composition of slag is changed from a one-phase to a two-or-more-phase mixture, and this may correspond to flow changes from Newtonian (above T_{cv}) to non-Newtonian (below T_{cv}) due to crystallization [2.49]. Therefore, the rapid increase in viscosity of AD coal slag melts at 1300 °C is expected due to the presence of the crystal phases.

Table 2.1 shows the main components of the coal slag samples determined by X-Ray fluorescence (XRF) analysis after viscosity measurements. It exhibits the contents of coal slag components in mol% and mass% of SiO_2, Al_2O_3, CaO, MgO, FeO, and Fe_2O_3. **Table 2.3** indicates that the viscosity of gasified coal slag melts varies from 0.2 to 9.7 Pa·s at 1600 °C. The viscosity was found to decrease in the order of CV > TH > MA > AD for coal slag melts. The higher total contents of SiO_2 and Al_2O_3 in coal slag melts give the higher viscosities. In contrast, the viscosity of coal slag melts decreases with increasing contents of CaO, MgO, FeO, and Fe_2O_3.

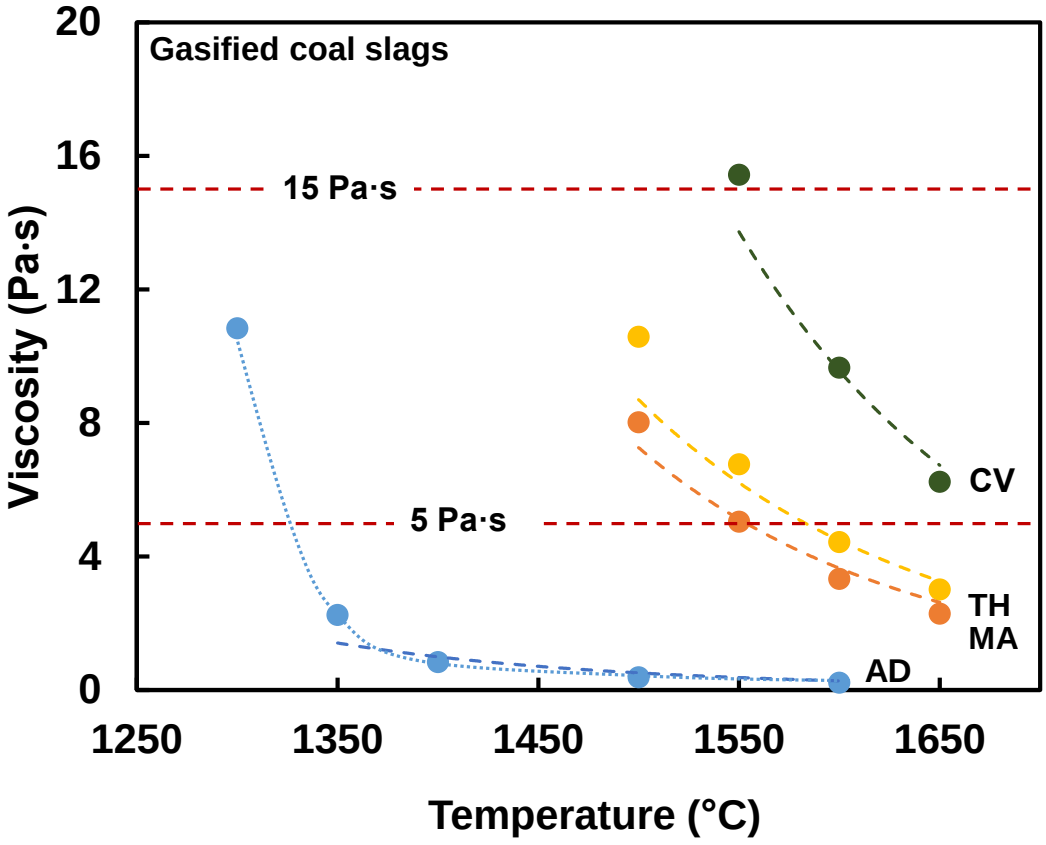

Fig. 2.4. Variations of viscosity with temperature for coal slag melts. The dashed lines are the fitted Arrhenius model according to **Eq. (2-5)** and the dotted line for AD slag melt is a fit of viscosity experimental results. The AD coal slag melt shows a rapid viscosity increase between 1300 and 1350 °C. The red dashed lines are the guides to eyes for moderate viscosities of 5 and 15 Pa·s.

2.3.2.2 Synthesized coal slag melts

Table 2.2 gives the analyzed values of Fe^{3+}/Fe_{tot} in quenched samples. The experiments were conducted two or three times for each sample. The percentage of Fe^{3+} was accounted for 47–56% of gasified coal slags and 69–80% of synthesized slags. A close agreement is found with previous data [2.32] for the similar compositions with the Fe^{3+} percentage of 45–90%.

Table 2.2 also shows calculated and measured values of T_L and T_{hm} for synthesized and coal slag samples, respectively. The calculated result of T_L for 60CaO–40SiO_2 (CA00.40) slag melt is 1769 ℃ and is reduced to 1351 ℃ with adding 10 mol % Al_2O_3 for 40 mol% SiO_2 series. The T_L increases from 1351 ℃ to 1509 ℃ with increasing Al_2O_3 content in the range of 10 and 30 mol% for the same series. The T_L decreases when Al_2O_3 or Fe_2O_3 is added to binary slag melts of 50CaO–50SiO_2 (CA00.50) and 40CaO–60SiO_2 (CA00.60). The T_L values of CAS slags with compositions of 40CaO–10Al_2O_3–50SiO_2 (CA10.50) and 30CaO–10Al_2O_3–60SiO_2 (CA10.60) are higher than those of CFS slags with compositions of 38.8CaO–6.1FeO–6.7Fe_2O_3–48.5SiO_2 (CF07.49) and 29.2CaO–5.6FeO–6.9Fe_2O_3–58.3SiO_2 (CF07.58). The T_L value of CA10.60 (1317 ℃) is lower than that of MA10.60 of (1363 ℃) due to the substitution of CaO for MgO.

Fig. 2.5 shows the temperature dependences of viscosity in a series of (60-x)RO−xA_2O_3−40SiO_2 synthesized slag melts with various Al_2O_3 and/or Fe_2O_3 contents. The viscosities of synthesized slag melt gradually decrease with increasing temperature in a similar manner of coal slag melts (**Fig. 2.4**). The viscosity increases as Al_2O_3 content increases in the range of 10 and 30 mol% (CA10.40<CA20.40<Ca30.40). The viscosity monotonically decreases

when Al_2O_3 in CA10.40 slag melt is replaced by FeO and Fe_2O_3 in CF8.39 (49CaO–4FeO–7.8Fe_2O_3–39.2SiO_2) slag melt. The viscosity decreases monotonically when a part of Al_2O_3 is substituted by Fe_2O_3 for synthesized slag melts with a constant SiO_2 content of 40 mol% for CA30.40 and CAF15.11.39 slag samples. Furthermore, the viscosity of CAF15.11.39 is higher than that of CF8.39 even though FeO and Fe_2O_3 contents in CAF15.11.39 are larger than those in CF8.39. The higher viscosity of CAF15.11.39, compared to that of CF8.39, is related to the effect of Al_2O_3 addition.

Fig. 2.6 shows the temperature dependences of viscosity in a series of (50-x)RO−xA_2O_3−50SiO_2 and (40-x)RO−xA_2O_3−60SiO_2 slag melts with various Al_2O_3 and Fe_2O_3 contents. The viscosity increases when Al_2O_3 is added to binary slag melts named CA00.50 and CA00.60 at constant SiO_2 contents of 50 and 60 mol%. On the contrary, it decreases with FeO and Fe_2O_3 additions. In the series of (40-x)RO−xA_2O_3−60SiO_2 slag melts, the viscosity decreases as FeO and Fe_2O_3 contents increase in the range of 0 and 14.1 mol% (**Tables 2.2 and 2.3**). The viscosity of CA10.60 is higher than that of MA10.60 slag melt due to the substitution of CaO for MgO.

In summary, the viscosities of CAS and CFS synthesized slag melts show different trends with respect to increase in contents of Al_2O_3 and Fe_2O_3 as amphoteric oxides. Namely, the viscosity of synthesized slag melts increases monotonically with increasing Al_2O_3 content and decreases with increasing Fe_2O_3 content.

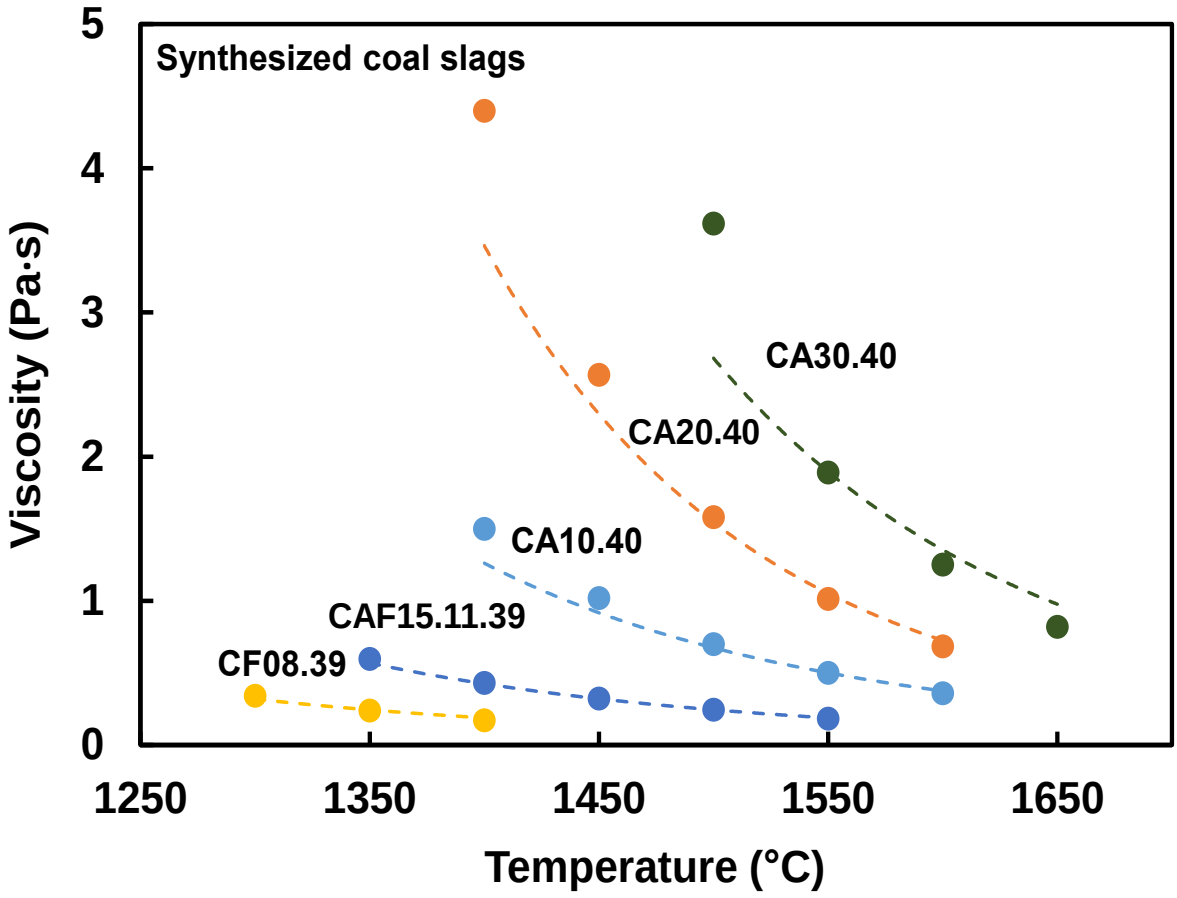

Fig. 2.5. Variations of viscosity with temperature in a series of (60-x)CaO−xA_2O_3−40SiO_2 slag melts with various Al_2O_3 and/or Fe_2O_3 contents, where A = Al and/or Fe. The dashed lines are the same as those of **Fig. 2.4.**

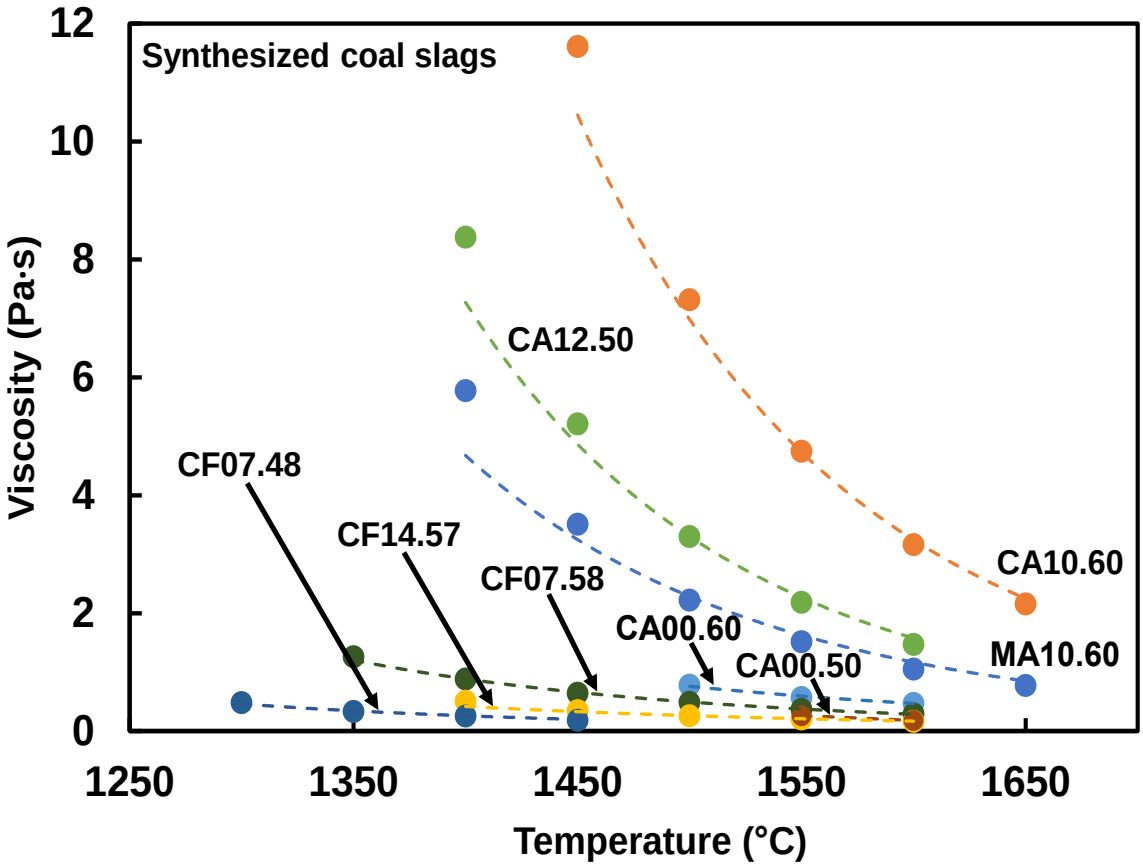

Fig. 2.6. Variations of viscosity with temperature in a series of (50-x)CaO−xA_2O_3−50SiO_2 and (40-x)RO−xA_2O_3−60SiO_2 slag melts with various Al_2O_3 or Fe_2O_3 contents, where R = Ca or Mg and A = Al or Fe. The dashed lines are the same as those of **Fig. 2.4.**

2.3.3 The behavior of slag melt components

The previous studies reported that the definition of acid-based theory is an acid as an oxide ion (O^{2-}) acceptor and a base as an oxide ion donor [2.50] by the scheme of reaction:

$$Acid + O^{2-} = Base \quad (2\text{-}3)$$

According to this definition, the oxides to form acids and bases in slag melts have reactivity reflecting their acidic, basic, and amphoteric characteristics. **Fig. 2.7** shows the simplified drawing of slag melt structure. SiO_2 as an acidic oxide consists of three-dimensional interconnected network of SiO_4 tetrahedra with bridging oxygens and plays a role of network former (NWF) [2.51] in the slag melts. The basic oxides such as CaO and MgO break the silicate network to form non-bridging oxygens as network modifiers (NWM) [2.31, 2.52]. On the other hand, Al_2O_3 and Fe_2O_3 as amphoteric oxides play dual roles as NWF and NWM depending on slag composition [2.32]. NWF contributes to increase the viscosity, on the contrary, NWM affects to decrease the viscosity.

The previous studies [2.10, 2.20] reported that the major chemical composition of coal slag varies within wide ranges as following: SiO_2 as the major component is often encountered in concentration range between 25 and 76 mol%. Al_2O_3 is generally the second-most concentrated species with concentration range between 8 and 26 mol%. Iron oxides are found in concentration range between 0 and 14 mol%. CaO is encountered in concentration range between 0 and 30 mol%, on the other hand, MgO concentration is found as lower than 20 mol%. These composition ranges are in good agreement with the chemical compositions of coal slag components in the present study, as shown in **Tables 2.1 and 2.2**. The effects of the major components on melt viscosity are discussed hereinafter.

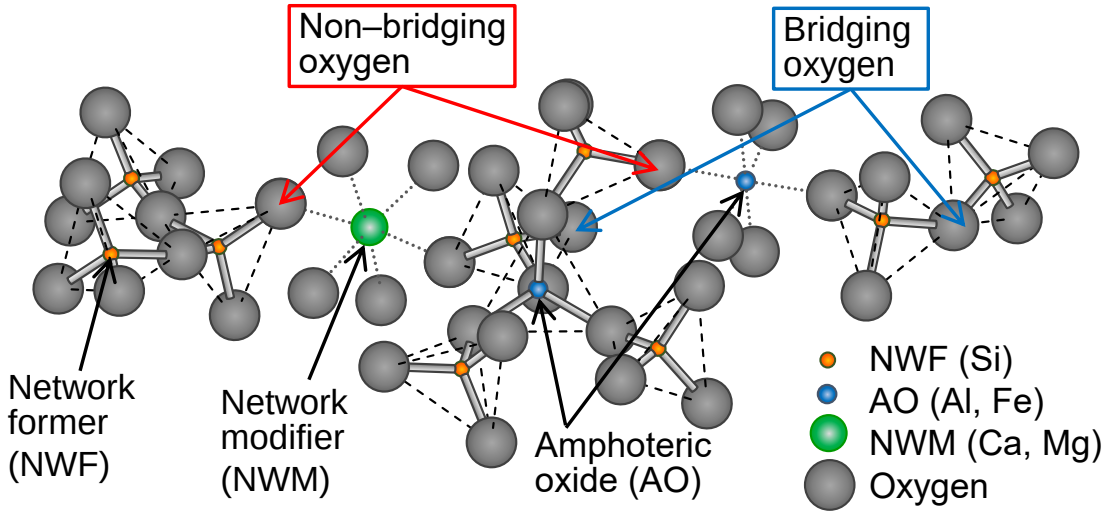

Fig. 2.7. Simplified drawing of slag melt structure. The presence of NWF contributes to increase viscosity, on the contrary, NWM affects to decrease viscosity in the slag melts.

2.3.3.1 Behavior of SiO_2, CaO, and MgO on viscosity

The viscosities of CAS and CFS slag melts were compared to evaluate the effect of SiO_2 addition. **Table 2.3** shows that the viscosity gradually increases with increasing SiO_2 content at a constant Al_2O_3 content of ~10 mol% in CA10.40, CA12.50, and CA10.60 slag melts and at a constant Fe_2O_3 content of ~7 mol% in CF08.39, CF07.49, and CF07.58 ones.

Figs. 2.5 and 2.6 also exhibit that the increase of SiO_2 content increases the viscosity for binary CaO-SiO_2 (CA00.50 and CA00.60 slag melts) and ternary CAS and CFS synthesized slag melts. In the slag melts, the increase of SiO_2 content enhances the degree of polymerization due to the formation of SiO_4 tetrahedral network. SiO_4 in tetrahedral site is connected in three-dimensional polymerized structure with bridging oxygens [2.51]. The viscosity also was found to decrease in the order of CV > TH > MA > AD coal slag melts with increasing SiO_2 content (**Table 2.3**).

The alkaline earth oxides (RO), where R=Ca, Mg, tend to break the Si-O bonds to de-polymerize the SiO_4 network by forming non-bridging oxygens [2.53, 2.54] and contribute to the decrease of viscosity. A previous study reported that among RO oxides, BaO most contributes to the reduce of viscosity, followed by Sr, Ca and Mg oxides [2.43] from the point of cation-oxide ion interaction [2.55]. However, the other researchers have studied that the viscosities of $CaO{-}Al_2O_3{-}SiO_2$ melts are larger than $MgO{-}Al_2O_3{-}SiO_2$ melts at fixed 50, 67, and 75 mol% SiO_2 contents [2.56]. Our result shown in **Fig. 2.6** is in good agreement that the viscosity of CA10.60 is larger than that of MA10.60 at a fixed SiO_2 content of 60 mol%. Further study is needed to understand the effect of CaO and MgO on viscosity and structure of coal slag melts.

2.3.3.2 Behavior of Al_2O_3 on viscosity

The study on SiO_2−Al_2O_3 binary slag melts indicates the structural roles of Al_2O_3 vary from AlO_4 to AlO_6 polyhedra with increasing Al_2O_3 content [2.30]. The Al_2O_3 in silicate melts plays the role of amphoteric oxide and its behavior depends on the addition of R_2O and RO [2.57]. In the case of the molar ratio $[Al_2O_3]/[RO] < 1$, Al_2O_3 mainly behaves NWF as described in previous studies of alumino-slicate melts and glasses [2.31, 2.38]. Several authors reported that viscosity increased with increasing the polymerization degree of network structure by Al_2O_3 addition [2.58, 2.59]. In other words, Al_2O_3 ideally plays the role of NWF for AlO_4 formation in order to link and share the corner between AlO_4 tetrahedra and with SiO_4 tetrahedra when the charge compensating cation such as CaO co-exists enough for Al at $[Al_2O_3]/[CaO] \leq 1$ [2.30, 2.38, 2.52]. The addition of Al_2O_3 to CaO-SiO_2 synthesized slag melts due to the formation of AlO_4 tetrahedra [2.31] corresponds to the increase of viscosity [2.59], as shown in **Fig. 2.5**.

Several slag melts of gasified coals have compositions that the total content of R_2O and RO exceeds Al_2O_3 content on a molar basis ($[Al_2O_3]/[R_2O, RO] \geq 1$) [43,60]. In the present study, the total contents of R_2O and RO oxides are larger than Al_2O_3 in the CV and AD coal slags melts. As shown in **Table 2.3**, the viscosity of coal slag melts increases with increasing total contents of SiO_2 and Al_2O_3 at all temperatures. It is expected that the coal slag melts enriched the SiO_2 and Al_2O_3 contents result in higher viscosity. The Al_2O_3 probably behaves as NWF in the present coal slag melts. The polymerization degree of network structure increases with the formation of both SiO_4 and AlO_4 tetrahedra in the gasified coal slag melts.

2.3.3.3 Behavior of iron oxide on viscosity

The viscosities of CFS slag melts were measured to evaluate the effect of FeO and Fe_2O_3 additions. The viscosity decreases with increasing FeO and Fe_2O_3 contents at a fixed SiO_2 content of ~60 mol% (**Fig. 2.6**). The present study has a good agreement with the previous results that the viscosity decreases with increasing iron oxides in $CaO-FeO-Fe_2O_3-SiO_2$ based slag melts [2.61–2.63]. The viscosity of CFS slag melts was decreased by the addition of iron oxides, indicating that not only RO (CaO and MgO) but also FeO and Fe_2O_3 reduce the polymerization degree of the network. Iron oxide plays roles of both NWM (Fe^{2+}) and amphoteric oxide (Fe^{3+}) and the behavior depends on temperature, composition, pressure, and atmosphere of slag melts [2.37, 2.64, 2.65]. The iron oxides existed in the slag melts are of structural important information due to polymerisation degree of silicate melt depending on the Fe^{3+}/Fe_{tot} [2.66]. This ratio was not evaluated during viscosity measurements at high temperatures. Therefore, several studies have been measured by Mössbauer spectroscopies and chelate titration method for quenched samples with a postulation of structural similarity in between melt and glass solid states. There is a general tendency of the Fe^{3+}/Fe_{tot} to increase with R_2O and RO contents [2.40, 2.43, 2.67]. This tendency is in close agreement in CFS slag system, as shown in **Table 2.2.** The Fe^{3+}/Fe_{tot} of CV coal slag is higher than those of TH and MA at a similar SiO_2 content of ~60 mol%. The Fe^{3+}/Fe_{tot} of the coal slag melts was found to decrease in the order of CV > MA > TH with increasing total contents of R_2O and RO (CaO, MgO, K_2O, SrO, BaO and Na_2O) in the order of 20 > 17.9 > 16.6 mol%, as shown in **Table 2.1**.

One of previous studies reported that the oxygen coordination number of Fe^{3+} ions can be determined by the ratio $[RO]/[Fe_2O_3]$ [2.31, 2.62]. In the similar compositions of the CFS

quenched slag samples, Fe^{3+} as NWF and NWM are favored at ≤ 10 mol% and at 10–20 mol% Fe_2O_3, respectively [2.32, 2.68]. In this study, the valence states of Fe^{3+}/Fe_{tot} of quenched sample has been investigated, as shown in **Table 2.2.** The increase of Fe_2O_3 content decreases the viscosity of gasified and synthesized coal slag melts, as shown in **Figs. 2.4, 2.5, and 2.6**. A previous study [2.32] also suggested that in relatively-acidic silicate melts of CaO–FeO– Fe_2O_3–SiO_2 with a CaO/SiO_2 molar ratio of 0.5, Fe^{3+} ions have mainly octahedral oxide coordination. In the acidic silicate melts, Fe_2O_3 acts as a basic oxide with partial dissociation [2.32] by the following **Eq. (2-4)**:

$$Fe_2O_3 \rightarrow 2FeO^{+} + O^{2-} \quad (2\text{-}4)$$

Therefore, it is estimated that Fe_2O_3 would behave as a NWM in the acidic synthesized and gasified coal slag melts mainly with $(CaO + MgO + FeO)/(Al_2O_3 + SiO_2)$ molar ratios of ≤ 1 as a basicity composition parameter (base/acid ratio) (**Table 2.2**). The Fe_2O_3 contribution results that the viscosity decreases with increasing Fe_2O_3 content in the gasified coal and synthesized slag melts.

The effect of Fe_2O_3 on coal slag melts would be more significant in the larger Fe_2O_3 content due to decreases of melting temperatures and of viscosity for slag melts [60]. The viscosity was found to decrease in the order of CV > TH > MA > AD coal slag melts with Fe_2O_3 contents of 1.4 < 2.6 < 3.9 < 8 mol%, as shown in **Fig 2.4** and **Tables 2.1 and 2.2**.

2.3.4 The temperature dependence of viscosity

Large numbers of researches concerning the temperature dependence of viscosity were described for synthesized and gasified coal slag melts. The viscosity data has been fitted

based on two models for Newtonian and non-Newtonian fluids [2.12]. The Arrhenius model can be obtained an expression between viscosity and temperature for silicate melts using only two parameters [2.43]:

$$Log\ \eta = \log a + \ b/T \tag{2-5}$$

where *a* and *b* are the fitting parameters as shown in **Table 2.4**, and *T* is the temperature. The viscosity data shown in **Figs. 2.4, 2.5, and 2.6** has been fitted with dashed line using the approximation of Arrhenius viscosity–temperature relationship by **Eq. (2-5)**.

Several models have been developed to explain or fit the temperature dependence of viscosity considering simplified melt composition of slag melts [43]. All the viscosity models are the result of an empirical fitting based on roles of constituents in slag melts. The empirical fitting of Urbain model is one of the viscosity predictions used widely for coal gasification slag melts [2.8, 2.26, 2.27]. The Urbain's model based on the role of the slag melts are grouped components of oxygen content as glass formers, glass modifiers or as amphoteric oxides by **Eq. (2-6)** through **Eq. (2-10)** [2.43, 2.66]:

$$x_g = SiO_2 + P_2O_5$$

$$x_m = FeO + CaO + MgO + Na_2O + K_2O + MnO + NiO + 2(TiO_2 + ZrO_2) + 3CaF_2$$

$$x_a = Al_2O_3 + Fe_2O_3 + B_2O_3. \tag{2-6}$$

Then α is calculated,

$$\alpha = x_m/x_m + x_a \tag{2-7}$$

and the parameter *b* (K) is calculated by combination of four parabolic equations in a with the molar ratio of silica, SiO_2,

$$b_0 = 13.8 + \ 39.9355 * \alpha + \ 244.049 * \alpha^2$$

$$b_1 = 30.481 - 117.1505 * \alpha + 129.9978 * \alpha^2$$

$$b_2 = -240.9429 + 234.0486 * \alpha - 300.04 * \alpha^2$$

$$b_3 = 60.7619 - 153.9276 * \alpha + 211.1616 * \alpha^2$$

$$b = b_0 + b_1 * SiO_2 + b_2 * SiO_2^2 + b_3 * SiO_2^3 \quad (2\text{-}8)$$

and parameter α (Pa·s/K) is given from b as,

$$-\ln a = 0.2693 * b + 13.9751 \quad (2\text{-}9)$$

The viscosity (Pa·s) is computed as a function of temperature (K) according to the Weyman equation:

$$\eta = a * T * e^{(b*10^3)/T} \quad (2\text{-}10)$$

The viscosity data of gasified coal slags have been fitted using **Eqs. 2-5 and 2-10**, as shown in **Fig. 2.8**. It shows that the two models are able to predict viscosities and capable of describing trends of temperature and composition dependences. It is demonstrated in close agreement between viscosity measurements and predictions of the Arrhenius and Urbain models for the coal slag melts. However, the prediction of viscosity data by **Eq. (2-10)** of Urbain's model is not accurate for AD slag melt containing relatively-high Fe_2O_3. The prediction is found to deviate from the experimental results of coal slag melts. The large deviation was found to decrease in the order of CV < TH < MA < AD (Dot lines in **Fig 2.8**). The deviation increases with increasing Fe_2O_3 content in the range from 1.4 to 8 mol%. Mills [2.28] also pointed out the large deviation of the Urbain model for $CaO–Fe_2O_3–SiO_2$ slag melts with high Fe_2O_3 concentrations. Thus the other composition parameter to predict melt viscosity is needed for gasified coal slags with high Fe_2O_3 concentrations.

Table 2.4 The fitting parameters of *a* and *b* of the Arrhenius model.

Series	Sample	*a*	*b*	R^2
$(60-x)RO{-}xA_2O_3{-}40SiO_2$	CA10.40	7.8E-05	5.9E+03	0.989
	CA20.40	1.3E-05	7.6E+03	0.988
	CA30.40	4.0E-05	7.2E+03	0.959
	CF08.39	2.0E-04	4.2E+03	0.981
	CAF15.11.39	1.1E-04	5.0E+03	0.998
$(50-x)RO{-}xA_2O_3{-}50SiO_2$	CA12.50	3.6E-05	7.4E+03	0.994
	CF07.49	1.4E-04	4.6E+03	0.994
$(40-x)RO{-}xA_2O_3{-}60SiO_2$	CA00.60	3.5E-04	5.0E+03	0.989
	CA10.60	3.3E-05	8.0E+03	0.996
	MA10.60	6.2E-05	6.8E+03	0.988
	CF07.58	1.3E-04	5.4E+03	0.977
	CF14.57	3.0E-04	4.4E+03	0.994
Coal Slag	CV	1.1E-04	7.9E+03	0.985
	TH	1.8E-04	7.0E+03	0.981
	MA	1.0E-04	7.3E+03	0.986
	AD	4.4E-05	6.1E+03	0.931

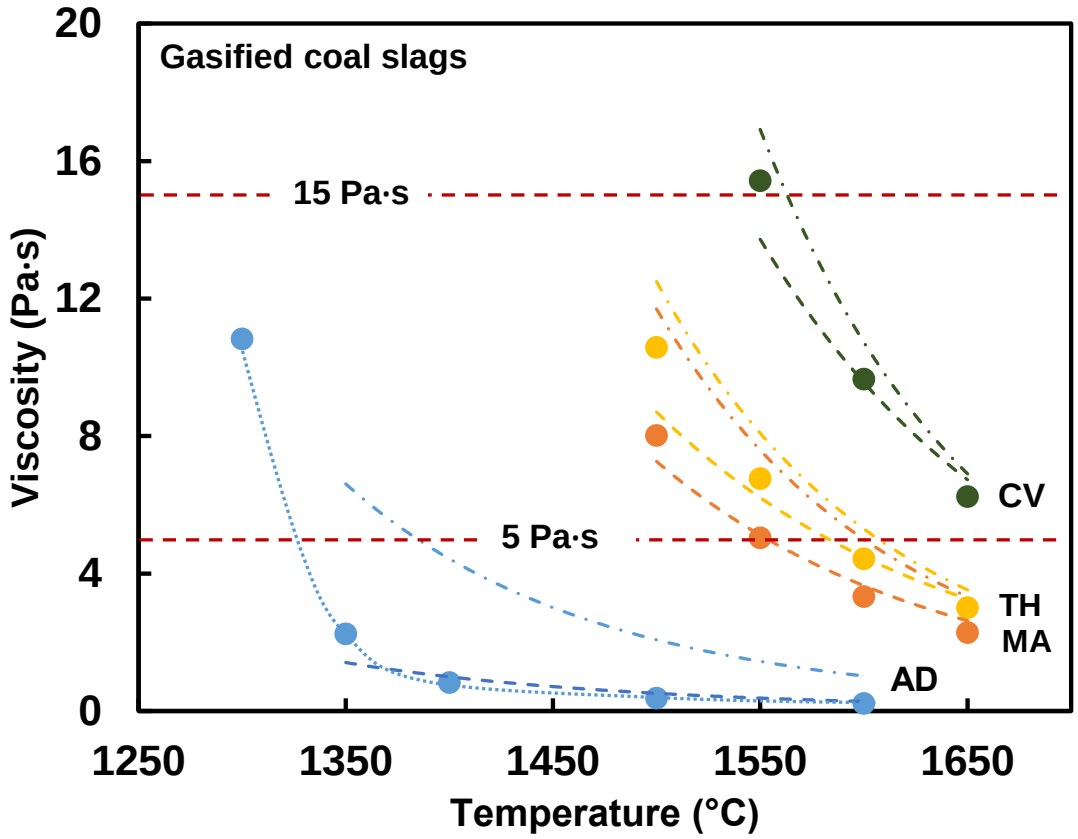

Fig. 2.8. Variations of viscosity with temperature for coal slag melts. The dashed and dot lines are the same as those of **Fig. 2.4.** The dash-dot lines are the fitted Urbain model according to **Eq. (2-10)**.

2.3.5 Composition parameter

An empirical composition parameter is here proposed for viscosity based on the studied compositions and the roles of their components. The major components in the coal slags are confirmed as SiO_2, Al_2O_3, CaO, MgO, FeO, and Fe_2O_3 in this study. It was found experimentally that the roles of these components on melt viscosity are classified into two types of network former (NWF) for SiO_2 and Al_2O_3 and network modifier (NWM) for CaO, MgO, FeO, and Fe_2O_3.

2.3.5.1 Based on measured data

Based on measured viscosity data of slag melts, a composition parameter is proposed to predict densities from the corresponding components determined by **Eq**. **(2-11)**:

$$P_\eta = 16.20 \cdot f_{SiO_2} + 10.05 \cdot f_{Al_2O_3} - 16.37 \cdot f_{CaO} - 24.99 \cdot f_{MgO} - 33.15 \cdot f_{FeO} - 2.09 \cdot f_{Fe_2O_3} \quad (2\text{-}11)$$

where P_η is composition parameter of viscosity, and f is the fraction of each component expressed by mol%.

Fig. 2.9 shows the relationship between viscosity and the composition parameter for the viscosity values measured at 1550°C. It can be seen that there are good correlation between P_η and the densities of each system. The calculated value of the correlation coefficient R^2 is 98%, which indicates a positive correlation between measured viscosity and composition parameter for gasified and synthesized slag melts. This new model has the capability to predict the viscosity of slag melts based on mole percentage by the analysis of their chemical compositions without viscosity measurements.

2.3.5.2 Based on the role of components

The composition parameter is approached using the influence the major components of coal slags on measured viscosity data. **Table 2.5** shows composition parameter P_η calculated from the sum of molar or mass for NWF (SiO_2 and Al_2O_3) and for NWM (CaO, MgO, FeO, and Fe_2O_3). Fe valence state was not taken into account in the latter mass-based parameter. The mass-based parameter without considering Fe valency state may be much convenient for engineering applications. Based on measured viscosity data, a factor 2 for MgO, FeO, and Fe_2O_3 is proposed to account for the sum of molar or mass ratios for NWM.

$$P_\eta = \Sigma NWM/\Sigma NWF \quad (2\text{-}12)$$

Figs. 2.10 and 2.11 show correlation between viscosity and the composition parameter P_η proposed for synthesized and gasified coal slag melts. Solid lines represent the relationships between η and P_η at 1500–1650 °C. The empirical composition parameter (**Table 2.6**) can be approximately used to predict viscosity of gasified coal slag melts. The composition parameter P_η also gives a prediction that the moderate flow of slag melts with ≤15 Pa·s at ≥1500 °C achieves by the composition design of slag melts with a P_η value of >0.43 for molar basis (**Fig. 2.10**) and a P_η value of >0.36 for mass basis without considering Fe valency state (**Fig. 2.11**). Moreover, slag melts with low viscosities of < 1 Pa·s and with higher P_η values of >1.1, including relatively-high FeO and Fe_2O_3 contents > 8 mol%, may have a possibility existing the critical temperature of T_{cv} with rapid viscosity increase in a similar manner of AD slag melts. The result is in good agreement with our previous study of melt density [2.29] that the larger Fe_2O_3 content of ≥ 7.5 mol% may form inhomogeneous melt structure including small crystals in melt state.

Table 2.5 Composition parameter P_η of gasified coal and synthesized slags based on the total contents of NWF and NWM.

Series	Sample	Molar ratio (mass ratio) or mol% (mass%)				NWF[a]		Molar ratio (mass ratio) or mol% (mass%)								NWM[b]		P_η = NWM/ ΣNWF	
		SiO_2		Al_2O_3				CaO		MgO		FeO		Fe_2O_3					
Coal slag	CV	61.5	(54.8)	13.9	(21.1)	75.4	(75.9)	14.2	(11.9)	3.6	(2.1)	2.2	(2.3)	1.4	(3.3)	28.6	(27.3)	0.38	(0.36)
	TH	57.8	(49.8)	16.0	(23.4)	73.8	(73.2)	9.2	(7.4)	4.8	(2.8)	5.8	(6.0)	2.6	(6.0)	35.6	(37.0)	0.48	(0.51)
	MA	54.6	(46.2)	15.0	(21.6)	69.6	(67.8)	8.0	(6.3)	6.3	(3.6)	7.1	(7.2)	3.9	(8.7)	42.6	(45.3)	0.61	(0.67)
	AD	39.0	(34.3)	10.0	(14.9)	49.0	(49.2)	24.5	(20.1)	16.4	(9.7)	0.0	(0.0)	8.0	(18.7)	73.3	(76.9)	1.50	(1.56)
(60-x)RO−xA_2O_3−40SiO_2	CA10.40	40.0	(38.6)	10.0	(16.4)	50.0	(55.0)	50.0	(45.0)	0.0	(0.0)	0.0	(0.0)	0.0	(0.0)	50.0	(45.0)	1.00	(0.82)
(A=Al and/or Fe)	CA20.40	40.0	(35.9)	20.0	(30.5)	60.0	(66.4)	40.0	(33.6)	0.0	(0.0)	0.0	(0.0)	0.0	(0.0)	40.0	(33.6)	0.67	(0.51)
(R=Ca or Mg)	CA30.40	40.0	(33.6)	30.0	(42.8)	70.0	(76.4)	30.0	(23.5)	0.0	(0.0)	0.0	(0.0)	0.0	(0.0)	30.0	(23.5)	0.43	(0.31)
	CF08.39	39.2	(35.5)	0.0	(0.0)	39.2	(35.5)	49.0	(41.4)	0.0	(0.0)	4.0	(4.3)	7.8	(18.8)	72.6	(87.6)	1.85	(2.47)
	CAF15.11.39	38.6	(30.2)	14.5	(19.3)	53.1	(49.5)	29.0	(21.2)	0.0	(0.0)	6.9	(6.5)	11.0	(22.9)	64.8	(80.0)	1.22	(1.62)
(50-x)RO−xA_2O_3−50SiO_2	CA00.50	50.0	(51.7)	0.0	(0.0)	50.0	(51.7)	50.0	(48.3)	0.0	(0.0)	0.0	(0.0)	0.0	(0.0)	50.0	(48.3)	1.00	(0.93)
(A=Al or Fe)	CA12.50	50.0	(47.1)	12.5	(20.0)	62.5	(67.1)	37.5	(33.0)	0.0	(0.0)	0.0	(0.0)	0.0	(0.0)	37.5	(33.0)	0.60	(0.49)
(R=Ca or Mg)	CF07.49	48.5	(44.2)	0.0	(0.0)	48.5	(44.2)	38.8	(33.0)	0.0	(0.0)	6.1	(6.6)	6.7	(16.2)	64.4	(78.6)	1.33	(1.78)
(40-x)RO−xA_2O_3−60SiO_2	CA00.60	60.0	(61.6)	0.0	(0.0)	60.0	(61.6)	40.0	(38.4)	0.0	(0.0)	0.0	(0.0)	0.0	(0.0)	40.0	(38.4)	0.67	(0.62)
(A=Al or Fe)	CA10.60	60.0	(57.2)	10.0	(16.2)	70.0	(73.4)	30.0	(26.7)	0.0	(0.0)	0.0	(0.0)	0.0	(0.0)	30.0	(26.7)	0.43	(0.36)
(R=Ca or Mg)	MA10.60	60.0	(61.8)	10.0	(17.5)	70.0	(79.3)	0.0	(0.0)	30.0	(20.7)	0.0	(0.0)	0.0	(0.0)	60.0	(41.4)	0.86	(0.52)
	CF07.58	58.3	(52.7)	0.0	(0.0)	58.3	(52.7)	29.2	(24.6)	0.0	(0.0)	5.6	(6.1)	6.9	(16.6)	54.2	(70.0)	0.93	(1.33)
	CF14.57	57.1	(46.0)	0.0	(0.0)	57.1	(46.0)	19.0	(14.3)	0.0	(0.0)	9.8	(9.4)	14.1	(30.2)	66.8	(93.5)	1.17	(2.03)

[a] Summation of molar ratio (mass ratio) or mol% (mass%) for SiO_2 and Al_2O_3.
[b] Summation of molar ratio (mass ratio) or mol% (mass%) for CaO + 2 × (MgO + FeO + Fe_2O_3).

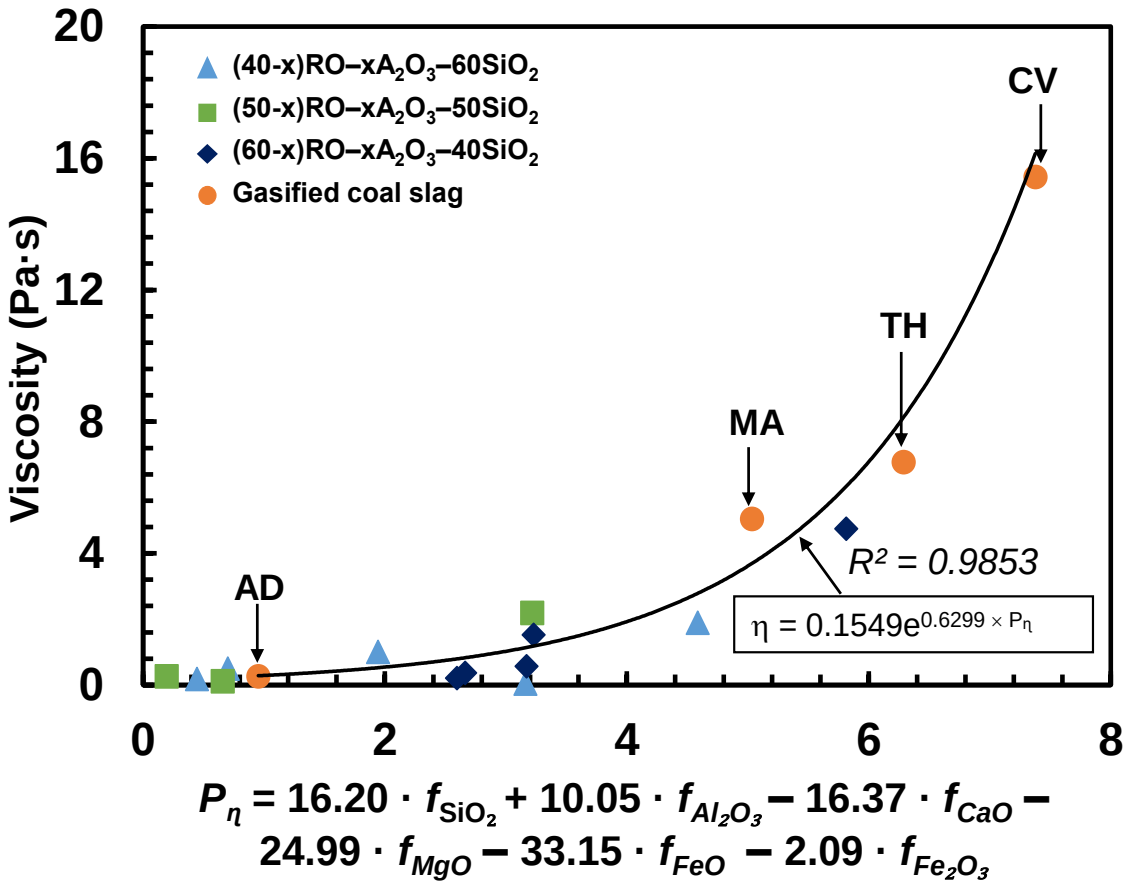

Fig. 2.9. Variations of viscosity with the parameter P_η of molar basis of gasified coal and synthesized slag melts at 1550 °C. The solid line is exponential fit to the data.

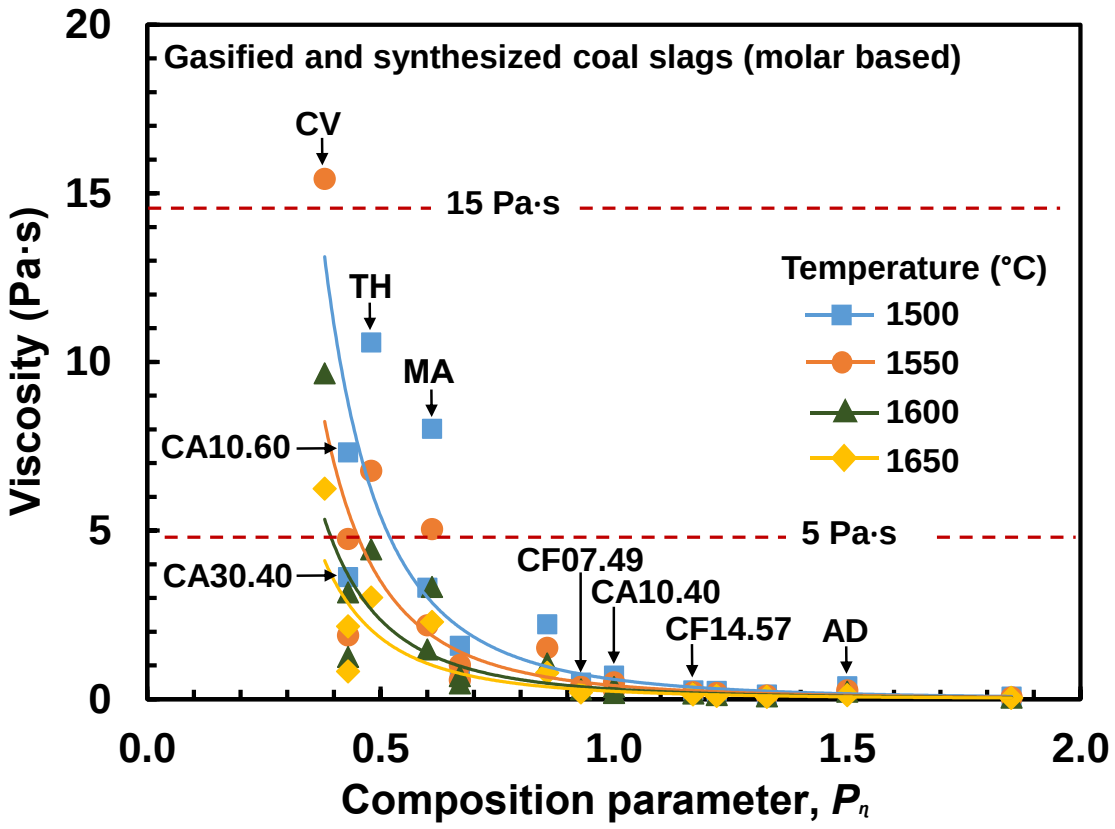

Fig. 2.10. Variations of viscosity with the parameter P_η of the molar basis for synthesized and gasified coal slag melts series at 1500, 1550, 1600 and 1650 °C. Solid lines represent the fitting (**Table 2.6**) by the empirical composition parameter for the viscosity data. The red dashed lines are the guides to eyes for moderate viscosities of 5 and 15 Pa·s.

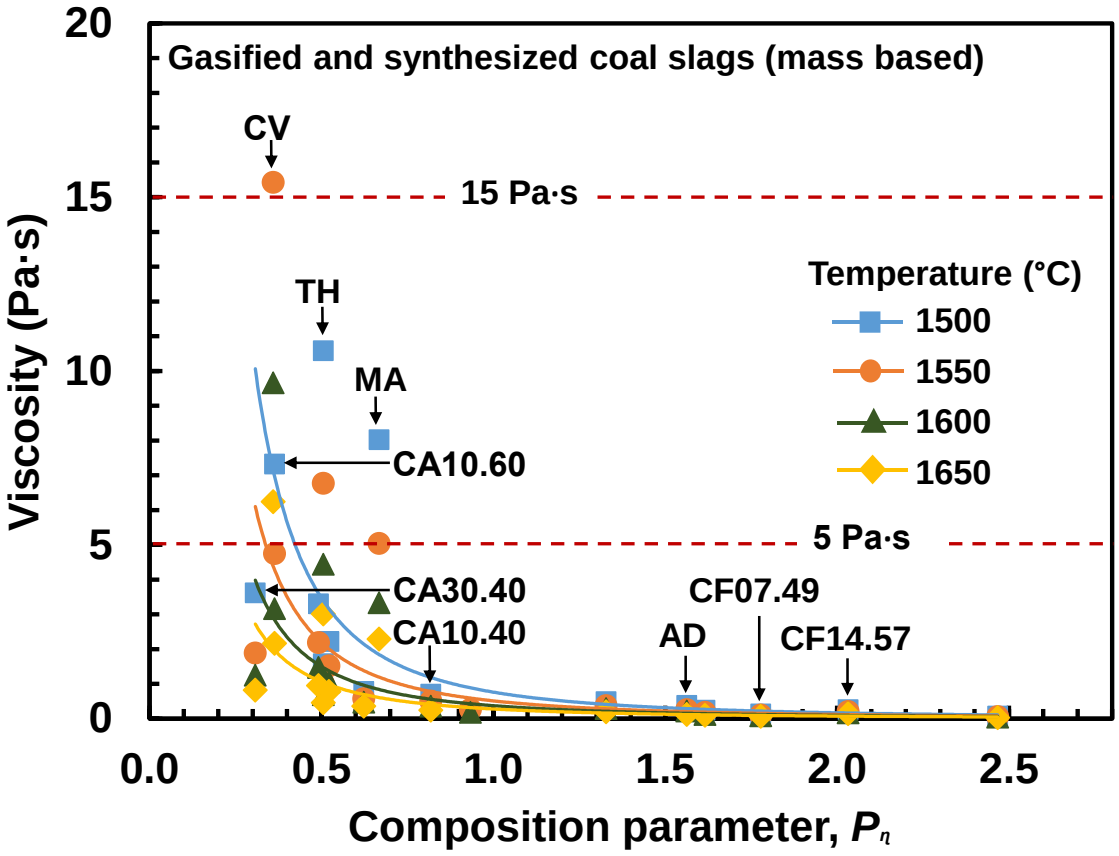

Fig. 2.11. Variations of viscosity with the parameter P_η of the mass basis for synthesized and gasified coal slag melts series at 1500, 1550, 1600 and 1650 °C. It is postulated all iron oxide exists as Fe_2O_3. The solid and dashed lines are the same as those of **Fig. 2.9.**

Table 2.6 The equations for the fitting of the data of molar and mass basis at each temperature.

Temperature (°C)	molar basis		mass basis	
	Equation	R^2	Equation	R^2
1500	$\eta = 0.5873 \cdot P_{\eta}^{-3.210}$	0.868	$\eta = 0.7618 \cdot P_{\eta}^{-2.189}$	0.803
1550	$\eta = 0.4039 \cdot P_{\eta}^{-3.116}$	0.859	$\eta = 0.5102 \cdot P_{\eta}^{-2.104}$	0.771
1600	$\eta = 0.2968 \cdot P_{\eta}^{-2.986}$	0.854	$\eta = 0.3718 \cdot P_{\eta}^{-2.011}$	0.763
1650	$\eta = 0.2322 \cdot P_{\eta}^{-2.970}$	0.883	$\eta = 0.2769 \cdot P_{\eta}^{-1.938}$	0.770

2.4 Conclusions

The viscosity of gasified and synthesized coal slag melts with homogeneous melting state gradually increases with decreasing temperature. The viscosity of AD slag melt rapidly increases at ≤1300 °C supposedly due to crystallization.

The viscosity of gasified coal slag melts was found to decrease in the order of CV > TH > MA > AD. The viscosity increases with increasing total contents of SiO_2 and Al_2O_3 and decreases with increasing total contents of CaO, MgO, FeO, and Fe_2O_3.

The viscosity of CAS and CFS synthesized slag melts shows different trends with respect to increase in Al_2O_3 and Fe_2O_3 contents. The viscosity of slag melts increases monotonically with increasing Al_2O_3 content and decreases with increasing Fe_2O_3 content.

An empirical composition parameter P_η was calculated from the ratio of ΣNWM (SiO_2 and Al_2O_3) and ΣNWF (CaO, MgO, FeO, and Fe_2O_3) based on the chemical composition of the main components. The viscosity of various coal slag melts has a good correlation with P_η. The design of slag composition due to blending of various coals for good flow at tapping temperature can be estimated from the composition parameter of melt viscosity.

References

[2.1] Oki Y, Hara S, Umemoto S, Kidoguchi K, Hamada H, Kobayashi M, Nakano Y. Development of high-efficiency oxy-fuel IGCC system. Energy Procedia 2014;63:471–5. doi:10.1016/j.egypro.2014.11.050.

[2.2] Kobayashi M, Nakao Y. Inhibition and elimination of carbon deposition in dry gas desulfurization process under oxy-fuel IGCC derived coal gas environment. Fuel 2015;152:19–28. doi:10.1016/j.fuel.2015.02.092.

[2.3] Minchener AJ. Coal gasification for advanced power generation. Fuel 2005;84:2222–35. doi:10.1016/j.fuel.2005.08.035.

[2.4] Aineto M, Acosta A, Rincon J, Romero M. Thermal expansion of slag and fly ash from coal gasification in IGCC power plant. Fuel 2006;85:2352–8. doi:10.1016/j.fuel.2006.05.015.

[2.5] Song W, Tang L, Zhu X, Wu Y, Zhu Z, Koyama S. Flow properties and rheology of slag from coal gasification. Fuel 2010;89:1709–15. doi:10.1016/j.fuel.2009.07.013.

[2.6] Wang P, Massoudi M. Slag behavior in gasifiers part I: Influence of coal properties and gasification conditions. Energies 2013;6:784–806. doi:10.3390/en6020784.

[2.7] Kong L, Bai J, Li W, Wen X, Li X, Bai Z, Guo Z, Li H. The internal and external factor on coal ash slag viscosity at high temperatures, Part 1: Effect of cooling rate on slag viscosity, measured continuously. Fuel 2015;158:968–75. doi:10.1016/j.fuel.2015.02.055.

[2.8] Hurst HJ, Novak F, Patterson JH. Viscosity measurements and empirical predictions for fluxed Australian bitumnous coal ashes. Fuel 1999;78:1831–40. doi:10.1016/S0016-2361(99)00094-0.

[2.9] Patterson JH, Hurst HJ. Ash and slag qualities of Australian bituminous coals for use in slagging gasifiers. Fuel 2000;79:1671–8. doi:10.1016/S0016-2361(00)00032-6.

[2.10] Ilyushechkin AY, Hla SS. Viscosity of high-iron slags from Australian coals. Energy and Fuels 2013;27:3736–42. doi:10.1021/ef400593k.

[2.11] Hsieh PY, Kwong KS, Bennett J. Correlation between the critical viscosity and ash fusion temperatures of coal gasifier ashes. Fuel Process Technol 2016;142:13–26. doi:10.1016/j.fuproc.2015.09.019.

[2.12] Massoudi M, Wang P. Slag behavior in gasifiers. Part II: Constitutive modeling of slag. vol. 6. 2013. doi:10.3390/en6020807.

[2.13] Wu G, Yazhenskikh E, Hack K, Wosch E, Muller M. Viscosity model for oxide melts relevant to fuel slags. Part 1: Pure oxides and binary system in the SiO_2–Al_2O_3–CaO–MgO–Na_2O–K_2O. Fuel Process Technol 2015;137:93–103. doi:10.1016/j.fuproc.2015.03.025.

[2.14] Wu G, Yazhenskikh E, Hack K, Wosch E, Muller M. Viscosity model for oxide melts relevant to fuel slags. Part 2: The system SiO_2–Al_2O_3–CaO–MgO–Na_2O–K_2O. Fuel Process Technol 2015;137:93–103. doi:10.1016/j.fuproc.2015.03.025.

[2.15] Hurst HJ, Novak F, Patterson JH. Viscosity measurements and empirical predictions for some model gasifier slags - II. Fuel 2000;79:1797–9. doi:10.1016/S0016-2361(00)00043-0.

[2.16] Yun Y, Yoo YD, Chung SW. Selection of IGCC candidate coals by pilot-scale gasifier operation. Fuel Process Technol 2007;88:107–16. doi:10.1016/j.fuproc.2004.08.009.

[2.17] Song W, Sun Y, Wu Y, Zhu Z, Koyama S. Measurement and simulation of flow

properties of coal asg slag in coal gasification. Am Inst Chem Eng 2011;57:801–18. doi:10.1002/aic.

[2.18] Lin X, Ideta K, Miyawaki J, Takebe H, Yoon SH, Mochida I. Correlation between fluidity properties and local structures of three typical Asian coal ashes. Energy and Fuels 2012;26:2136–44. doi:10.1021/ef201771f.

[2.19] Jiang Y, Lin X, Ideta K, Takebe H, Miyawaki J, Yoon SH, Mochida I. Microstructural transformations of two representative slags at high temperatures and effects on the viscosity. J Ind Eng Chem 2014;20:1338–45. doi:10.1016/j.jiec.2013.07.015.

[2.20] Ilyushechkin AY, Roberts D. Slagging behaviour of Australian brown coals and implications for their use in gasification technologies. Fuel Process Technol 2015:1–10. doi:10.1016/j.fuproc.2015.10.028.

[2.21] Jak E, Degterov S, Hayes PC, Pelton AD. Thermodynamic modelling of the system Al_2O_3–SiO_2–CaO–FeO–Fe_2O_3 to predict the flux requirements for coal ash slags. Fuel 1998;77:77–84. doi:10.1016/S0016-2361(97)00137-3.

[2.22] Li H, Yoshihiko N, Dong Z, Zhang M. Application of the FactSage to predict the ash melting behavior in reducing conditions. Chinese J Chem Eng 2006;14:784–9. doi:10.1016/S1004-9541(07)60012-3.

[2.23] Song W, Dong Y, Wu Y, Zhu Z. Prediction of temperature of critical viscosity for coal ash slag. Am Inst Chem Eng 2011;57:2921–5. doi:10.1002/aic.12500.

[2.24] Duchesne MA, Bronsch AM, Hughes RW, Masset PJ. Slag viscosity modeling toolbox. Fuel 2013;114:38–43. doi:10.1016/j.fuel.2012.03.010.

[2.25] Ye I, Ryu C. Numerical modeling of slag flow and heat transfer on the wall of a coal gasifier. Fuel 2015;150:64–74. doi:10.1016/j.fuel.2015.01.111.

[2.26] Kondratiev A, Jak E. Predicting coal ash slag flow characteristics (viscosity model for the Al_2O_3–CaO–"FeO"–SiO_2 system). Fuel 2001;80:1989–2000. doi:10.1016/S0016-2361(01)00083-7.

[2.27] Van Dyk JC, Waanders FB, Benson SA, Laumb ML, Hack K. Viscosity predictions of the slag composition of gasified coal, utilizing FactSage equilibrium modelling. Fuel 2009;88:67–74. doi:10.1016/j.fuel.2008.07.034.

[2.28] Mills KC. Estimation of physicochemical properties of coal slag and ashes. Miner Mater Ash Coal, Am Chem Soc Washinton, DC 1986;301:195–214. doi:10.1021/bk-1986-0301.ch015.

[2.29] Arman, Okada A, Takebe H. Density measurements of gasified coal and synthesized slag melts for next-generation IGCC. Fuel 2016;182:304–13. doi:10.1016/j.fuel.2016.05.117.

[2.30] Aksay I, Pask J, Davis R. Densities of SiO_2–Al_2O_3 Melts. J Am Ceram Soc 1973;62 (7-8):332–6. doi:10.1111/j.1151-2916.1979.tb19071.x.

[2.31] Morinaga K, Suginohara Y, Yanagase T. Density of CaO–SiO_2–Fe_2O_3, –Al_2O_3 melts. Tech Rep Kyushu Univ 1975;48 (6):859–65.

[2.32] Morinaga K, Suginohara Y, Yanagase T. Oxygen coordination number of Fe ions in CaO–SiO_2 and Na_2O–SiO_2 systems. J Japan Ints Met 1976;40 (05):480–6.

[2.33] Dingwell DB, Brearley M. Melt densities in the CaO–FeO–Fe_2O_3–SiO_2 system and the compositional dependence of the partial molar volume of ferric iron in silicate melts. Geochim Cosmochim Acta 1988;52:2815–25. doi:10.1016/0016-7037(88)90149-4.

[2.34] Mills KC, Jeffrey M. Rhine. The measurement and estimation of the physical properties of slags formed during coal gasification: 1. Properties relevant to fluid

flow. Fuel 1989;68:193–200. doi:10.1017/CBO9781107415324.004.

[2.35] Nowok JW, Bieber JA, Benson SA, Jones ML. Physicochemical effects influencing the measurements of interfacial surface tension of coal ashes. Fuel 1991;70:951–6. doi:10.1016/0016-2361(91)90050-K.

[2.36] Neuville DR, Cormier L, Massiot D. Al coordination and speciation in calcium aluminosilicate glasses: Effects of composition determined by ^{27}Al MQ-MAS NMR and Raman spectroscopy. Chem Geol 2006;229:173–85. doi:10.1016/j.chemgeo.2006.01.019.

[2.37] Chevrel MO, Giordano D, Potuzak M, Courtial P, Dingwell DB. Physical properties of $CaAl_2Si_2O_8$–$CaMgSi_2O_6$–FeO–Fe_2O_3 melts: analogues for extra-terrestrial basalt. Chem Geol 2013;346:93–105. doi:10.1016/j.chemgeo.2012.09.004.

[2.38] Takahashi S, Neuville DR, Takebe H. Thermal properties, density and structure of percalcic and peraluminus CaO–Al_2O_3–SiO_2 glasses. J Non Cryst Solids 2015;411:5–12. doi:10.1016/j.jnoncrysol.2014.12.019.

[2.39] Takeshita R, Yoshida I, Ueno K. Adsorption behaviour of phosphate ion on the iron (III) compleks of a chelating Resin. Bul Chem Soc Japan 1979;52 (9):2577–80.

[2.40] Nowok JW, Hurley JP, Stanley DC. Local structure of a lignitic coal ash slag and its effect on viscosity. Energy and Fuels 1993;7:1135–40. doi:10.1021/ef00042a063.

[2.41] www.factsage.com.

[2.42] Ohta Y, Morinaga K, Yanagase T. Aplication of hot-thermocouple to high temperature chemistry. Bull Japan Inst Met 1980;19 (4):239–45.

doi:10.11311/jscta1974.13.90.

[2.43] Vargas S, Frandsen FJ, Dam-Johansen K. Rheological properties of high-temperature melts of coal ashes and other silicates. Prog Energy Combust Sci 2001;27:237–429. doi:10.1016/S0360-1285(00)00023-X.

[2.44] Barter BB, Darling AS. Thermal expansion of rhodium-platinum alloys. Platin Met Rev 1960;4:138–40.

[2.45] Shiraishi Y, Ikeda K, Tamura A, Saito T. On the viscosity and density of the molten $FeO–SiO_2$ system. Mater Trans JIM 1978;19 (5):264–74. doi:10.2320/matertrans1960.19.264.

[2.46] Quested PN, Monaghan BJ. The measurement of thermophysical properties of molten slags and fluxes. High Temp Mater Process 2001;20:219–33. doi:10.1515/HTMP.2001.20.3-4.219.

[2.47] Mizoguchi K, Yamane M, Suginohara Y. Viscosity measurements of the molten MeO (Me=Ca, Mg, Na)–SiO_2–Ga_2O_3 silicate system. J Japan Ins Met 1986;50:76–82.

[2.48] Bockris JO, Lowe DC. Viscosity and the structure of molten silicates. Proc R Soc 1954;226:423–35. doi:10.1098/rspa.1954.0266.

[2.49] Oh MS, Brooker DD, de Paz EF, Brady JJ, Decker TR. Effect of crystalline phase formation on coal slag viscosity. Fuel Process Technol 1995;44:191–9. doi:10.1016/0378-3820(95)00012-V.

[2.50] Flood H, Förland T. The acidic and basic properties of oxides. Acta Chem Scand 1947:592–604.

[2.51] Mysen BO, Virgo D, Seifert FA. The structure of silicate melts: Implications for chemical and physical properties of natural magma. Rev Geophys Sp Phys

1982;20:353–83. doi:10.1029/RG020i003p00353.

[2.52] Mills KC, Yuan L, Jones RT. Estimating the physical properties of slags. J South African Inst Min Metall 2011;111:649–58.

[2.53] Mills KC. The influence of structure on the physico-chemical properties of slags. ISIJ Int 1993;33:148–55. doi:10.2355/isijinternational.33.148.

[2.54] Xu J, Zhang J, Jie C, Tang L, Chou K. Measuring and modeling of density for selected CaO–MgO–Al_2O_3–SiO_2 slag with low silica. J Iron Steel Res Int 2012;19:26–32. doi:10.1016/S1006-706X(12)60109-5.

[2.55] Moringa K, Yoshida H, Takebe H. Compositional dependence of absorption spectra of Ti^{3+} in silicate, borate, and phosphate glasses. J Am Ceram Soc 1994;77:3113–8. doi:10.1111/j.1151-2916.1994.tb04557.x.

[2.56] Toplis MJ, Dingwell DB. Shear viscosities of CaO–Al_2O_3–SiO_2 and MgO–Al_2O_3–SiO_2 liquids: Implications for the structural role of aluminium and the degree of polymerisation of synthetic and natural aluminosilicate melts. Geochim Cosmochim Acta 2004;68:5169–88. doi:10.1016/j.gca.2004.05.041.

[2.57] Nakashima K, Saito N, Sukenaga S. Viscosity of iron oxide containing slag. J MMIJ 2011;127:111–6. doi:10.2473/journalofmmij.127.111.

[2.58] Riebling EF. Structural similarities between a glass and its melt. J Am Ceram Soc 1968;51:143–9. doi:10.1111/j.1151-2916.1968.tb11857.x.

[2.59] Kou T, Mizoguchi K, Suginohara Y. The effect of Al_2O_3 on viscosity silicate melts. J Japan Ins Met 1978;41:775–81.

[2.60] Nowok JW. Viscosity and phase transformation in coal ash slags near and below the temperature of critical viscosity. Energy and Fuels 1994;8:1324–36. doi:10.1021/ef00048a022.

[2.61] Lee YS, Min DJ, Jung SM, Yi SH. Influence of basicity and FeO content on viscosity of blast furnace type slags containing FeO. ISIJ Int 2004;44:1283–90. doi:10.2355/isijinternational.44.1291.

[2.62] Saito N, Hori N, Nakashima K, Mori K. Viscosity of blast furnace type slags. Metall Mater Trans B 2003;34:509–16.

[2.63] Sumita S, Mimori T, Morinaga K, Yanagase T. Viscosity of slag melts containing Fe_2O_3. J Japan Inst Met Mater 1980;44:94–9.

[2.64] Partzsch GM, Lattard D, McCammon C. Mössbauer spectroscopic determination of Fe^{3+}/Fe^{2+} in synthetic basaltic glass: a test of empirical fO_2 equations under superliquidus and subliquidus conditions. Contrib to Mineral Petrol 2004;147:565–80. doi:10.1007/s00410-004-0571-5.

[2.65] Guo X, Lange R, Ai Y. The density and compressibility of CaO–FeO–SiO_2 liquids at one bar: Evidence for four-coordinated Fe^{2+} in the $CaFeO_2$ component. Geochim Cosmochim Acta 2013;120:206–19. doi:10.1016/j.gca.2013.06.007.

[2.66] Urbain G, Bottinga Y, Richet P. Viscosity of liquid silica, silicates and alumino-silicates. Geochim Cosmochim Acta 1982;46:1061–72. doi:10.1016/0016-7037(82)90059-X.

[2.67] Nowok JW. Viscosity and structural state of Iron in coal ash slags under gasification conditions. Energy and Fuels 1995;9:534–9. doi:10.1021/ef00051a019.

[2.68] Sumita S, Morinaga K, Yanagase T. Physical properties and structure of binary ferrite melts. Trans Japan Inst Met 1983;24 (1):35–41. doi:10.2320/matertrans1960.24.35.

Chapter 3

Density Measurements of Gasified Coal and Synthesized Slag Melts

3.1. Introduction

Physical property data e.g., viscosity, density, surface tension for coal slags are required in the design, operation, and the development of gasifier in the Integrated Gasification Combined Cycle (IGCC) [3.1–3.4]. The density of slag melts is one of fundamental and important properties for IGCC process [3.5, 3.6]. However, limited studies on reliable data of density have been reported for coal slag melts [3.7]. Furthermore, the chemical compositions of coal slag melts from different origin countries can vary significantly [3.8] and consequently the density of these coal slags can show appreciable variability.

Density of melts is necessary for the calculation of other properties, such as molar volume and coefficient of volume expansion in order to discuss the molecular structure of slag melts [3.9–3.11]. The coefficient of volume expansion also is one of important physical properties to control the melting process of slag melts [3.12, 3.13].

The density measurements at high temperatures have been mainly carried out using maximum bubble pressure, pycnometer and Archimedean single- or double-bob methods

[3.14–3.18]. The Archimedean methods give reproducible data sets with better precision [3.19]. Therefore, the Archimedean double-bob method is selected in this work.

The slags formed during the coal gasification process mainly contain SiO_2, Al_2O_3, CaO, MgO, FeO, and Fe_2O_3 with small amounts of Na_2O, K_2O, TiO_2, P_2O_5, SrO, MnO, and other compounds [3.10]. Synthesized coal slags with simplified silicate systems have been prepared to understand the role of components on melt properties [3.20–3.22]. The synthesized coal slags were used to discuss degree of polymerization and crystallization behavior of the melts [3.9].

The effects of Al_2O_3 and Fe_2O_3 on the density of CaO–Al_2O_3–SiO_2 (CAS) and CaO–Fe_2O_3–SiO_2 (CFS) slags are evaluated here as a start to study the structures of gasified coal slag melts. The behavior of Al_2O_3 and Fe_2O_3 in silicate glasses, crystals and slag melts has been widely studied by various techniques such as Raman and Mössbaeur spectroscopies and melt properties of density at high temperatures [3.23–3.30].

The previous studies have reported that Al^{3+} generally was NWF in silicate glasses, whereas compositional dependences of properties were qualitatively related to the glass structure examined by IR spectroscopy [3.30]. The proportions of AlO_x (x= 4, 5, 6) species were evaluated by using ^{27}Al MQ NMR spectroscopy [3.28]. In the CAS slag melts, behavior of adding Al_2O_3 shows the monotonic increase of molar volume as NWF in the composition region of $[Al_2O_3]/[CaO] < 1.00$ [3.24].

In silicate glasses and slag melts containing iron oxide, the structural role of iron oxide is still not well understood [3.29, 3.31]. A previous study reported that the behavior of iron oxide species in CFS melts differs significantly from that in Na_2O–FeO–Fe_2O_3–SiO_2 (NFS) melts due to the behavior of Fe^{3+} ions [3.15]. Fe_2O_3 in NFS melts has the tetrahedral site, on the contrary, in CFS melts, it has octahedral one from the result of ^{57}Fe Mössbauer

spectra [3.26]. Another study [3.24] reported that the roles of Fe^{3+} varied with tetrahedral and octahedral sites in the CFS slag melts. The Mössbauer spectra of quenched samples indicated that the site of Fe^{3+} ions varied from tetrahedral to octahedral coordination with increasing Fe_2O_3 content [3.25].

According to these scientific and engineering backgrounds, the objectives of this research are (i) to establish an Archimedean double-bob method to measure density of gasified coal and synthesized slag melts in silicate systems containing CaO or MgO and Al_2O_3 and/or FeO/Fe_2O_3, (ii) to study the composition and temperature dependences of density, molar volume, and the coefficient of volume expansion, (iii) to discuss the effect of Al_2O_3 and Fe_2O_3 on these properties, and (iv) to propose a composition parameter to predict the density of coal slag melts based on chemical composition.

3.2. Materials and Methods

3.2.1. Sample preparation

3.2.1.1 Coal slag samples

The samples provided by the CRIEPI, Japan are coal slags collected after rapid quenching with water of molten slag flowing from the gasifier. The samples are denoted as CV (Coal Valley), TH (Tanito Harum) and MA (Malinau). The samples were melted in a Pt crucible at 1600 ^oC for about 2 hours. The density measurements were conducted in the range 1500–1600 ^oC for homogenous melt state. Then the samples were rapidly cooled at room temperature to evaluate their chemical compositions. **Table 3.1** shows the chemical compositions of the coal slag samples determined by X-Ray fluorescence (XRF) analysis. The valence state of iron oxide was evaluated using chelate titration method in the quenched samples [3.32].

Table 3.1 Chemical composition of gasified coal slags.

Element	mol% (mass %)					
	Coal Valley (CV)		Tanito Harum (TH)		Malinau (MA)	
Major component						
SiO_2	61.5	(54.8)	57.8	(49.8)	54.6	(46.2)
Al_2O_3	13.9	(21.1)	16.0	(23.4)	15.0	(21.6)
CaO	14.2	(11.9)	9.2	(7.4)	8.0	(6.3)
MgO	3.6	(2.1)	4.8	(2.8)	6.3	(3.6)
FeO	2.2	(2.3)	5.8	(6.0)	7.1	(7.2)
Fe_2O_3	1.4	(3.3)	2.6	(6.0)	3.9	(8.7)
Minor component						
K_2O	1.1	(1.5)	1.4	(1.9)	1.3	(1.8)
TiO_2	0.6	(0.7)	1.0	(1.1)	1.0	(1.1)
P_2O_5	0.1	(0.4)	0.1	(0.4)	0.2	(0.8)
SrO	0.1	(0.2)	0.1	(0.2)	0.1	(0.1)
ZrO_2	0.1	(0.2)	ND [a]	(ND)	0.1	(0.2)
MnO	0.1	(0.1)	0.1	(0.1)	0.1	(0.1)
Cr_2O_3	0.1	(0.2)	ND	(ND)	0.1	(0.2)
BaO	0.2	(0.5)	ND	(ND)	0.1	(0.2)
Na_2O	0.8	(0.7)	1.1	(0.9)	2.1	(1.9)
Total	100.0	(100.0)	100.0	(100.0)	100.0	(100.0)
$\sum[A_2O_3]^b / \sum[RO]^c$	0.76		0.93		0.88	
$[Al_2O_3] / \sum[RO]$	0.69		0.80		0.70	
$[Fe_2O_3] / \sum[RO]$	0.07		0.13		0.18	

[a] Not detected.
[b] A_2O_3: Amphoteric oxide (Al_2O_3, Fe_2O_3).
[c] RO: Bivalent metal oxide (Fe, Ca, Mg, Sr).
$\sum[A_2O_3] / \sum[RO]$: molar ratio of total contents of amphoteric and bivalent metal oxides.

3.2.1.2 Synthesized slag samples

Table 3.2 shows that the batches of synthesized slag samples were divided into three series of (60-x)RO–xA_2O_3–40SiO_2, (50-x)RO–xA_2O_3–50SiO_2, and (40-x)RO–xA_2O_3–60SiO_2 in molar ratio, where R is the alkaline earth metal: Ca and Mg; A is Al and Fe without considering the valence state of iron oxide. There are compositions containing 40, 50 and 60% SiO_2 (nominal concentration) with various contents of CaO, MgO, Al_2O_3 and Fe_2O_3. The composition series of synthesized slags were systematically varied by considering those of gasified coal slags **(Table 3.1)**.

The samples were prepared from a mixture of SiO_2, Al_2O_3, $CaCO_3$, MgO, and Fe_2O_3 powders with 99.99 % purity as raw materials. Mixed powders were melted in a Pt crucible between 1350 and 1600 ^oC for about 2 hours depending on their homogenous melting temperatures. The synthesized slag melt was poured onto iron mold for cooling.

The cooled sample was crushed, then re-melted at the highest measuring temperature and the sample was kept for 2 hours before density measurements. The nominal contents used in this study are also shown in **Table 3.2.** The sample compositions are labeled by the type and molar fraction of components except for SiO_2, where C, A, and F mean respective oxides: CaO, Al_2O_3, and Fe_2O_3 and x and y are their molar fractions, as shown in **Table 3.2**. The valence state of iron was also determined experimentally in quenched samples after density measurements using chelate titration method. The experimental results of Fe^{3+}/Fe_{tot} are presented in **Table 3.3.** The FeO and Fe_2O_3 mol% are calculated from Fe^{3+}/Fe_{tot} for determining sample composition. The FeO and Fe_2O_3 contents (mol%) in quenched samples are used to discuss their effects on melt density in the section of results and discussion.

Table 3.2 Chemical composition of synthesized coal slag samples.

Series	Samples	mol% (mass %)												Molar ratio		
		SiO_2		Al_2O_3		CaO		MgO		FeO[a]		Fe_2O_3[a]		$\sum[A_2O_3]/\sum[RO]$[b]	$[Al_2O_3]/\sum[RO]$[c]	$[Fe_2O_3]/\sum[RO]$[d]
(60-x)RO−xA_2O_3−40SiO_2	CA10.40	40.0	(38.6)	10.0	(16.4)	50.0	(45.0)	0.0	(0.0)	0.0	(0.0)	0.0	(0.0)	0.00	0.20	0.00
	CA20.40	40.0	(35.9)	20.0	(30.5)	40.0	(33.6)	0.0	(0.0)	0.0	(0.0)	0.0	(0.0)	0.00	0.50	0.00
	CA30.40	40.0	(33.6)	30.0	(42.8)	30.0	(23.5)	0.0	(0.0)	0.0	(0.0)	0.0	(0.0)	0.00	1.00	0.00
	CF08.39	39.2	(35.5)	0.0	(0.0)	49.0	(41.4)	0.0	(0.0)	4.0	(4.3)	7.8	(18.8)	0.15	0.00	0.16
	CAF15.11.39	38.6	(30.2)	14.5	(19.3)	29.0	(21.2)	0.0	(0.0)	6.9	(6.5)	11.0	(22.9)	0.71	0.50	0.38
(50-x)RO−xA_2O_3−50SiO_2	CA12.50	50.0	(47.1)	12.5	(20.0)	37.5	(33.0)	0.0	(0.0)	0.0	(0.0)	0.0	(0.0)	0.00	0.33	0.00
	CF07.48	48.5	(44.2)	0.0	(0.0)	38.8	(33.0)	0.0	(0.0)	6.1	(6.6)	6.7	(16.2)	0.00	0.00	0.17
(40-x)RO−xA_2O_3−60SiO_2	CA00.60	60.0	(61.6)	0.0	(0.0)	40.0	(38.4)	0.0	(0.0)	0.0	(0.0)	0.0	(0.0)	0.00	0.00	0.00
	CA10.60	60.0	(57.2)	10.0	(16.2)	30.0	(26.7)	0.0	(0.0)	0.0	(0.0)	0.0	(0.0)	0.00	0.33	0.00
	MA10.60	60.0	(61.8)	10.0	(17.5)	0.0	(0.0)	30.0	(20.7)	0.0	(0.0)	0.0	(0.0)	0.00	0.33	0.00
	CF02.60	59.5	(59.1)	0.0	(0.0)	37.2	(34.5)	0.0	(0.0)	1.6	(1.9)	1.7	(4.5)	0.04	0.00	0.05
	CF04.59	59.2	(56.9)	0.0	(0.0)	34.5	(30.9)	0.0	(0.0)	2.8	(3.2)	3.5	(8.9)	0.09	0.00	0.10
	CF06.59	58.9	(54.6)	0.0	(0.0)	31.9	(27.6)	0.0	(0.0)	3.8	(4.2)	5.5	(13.6)	0.15	0.00	0.17
	CF07.58	58.3	(52.7)	0.0	(0.0)	29.2	(24.6)	0.0	(0.0)	5.6	(6.1)	6.9	(16.6)	0.20	0.00	0.24
	CF11.58	57.6	(49.1)	0.0	(0.0)	24.0	(19.1)	0.0	(0.0)	7.8	(8.0)	10.5	(23.8)	0.33	0.00	0.44
	CF14.57	57.1	(46.0)	0.0	(0.0)	19.0	(14.3)	0.0	(0.0)	9.8	(9.4)	14.1	(30.2)	0.49	0.00	0.74

[a] The FeO and Fe_2O_3 were determined experimentally using chelate titration method in the quenched samples.
[b] $\sum[A_2O_3]$ / $\sum$[RO]: molar ratio of total contents of amphoteric and bivalent metal oxides.
[c] $[Al_2O_3]$ / $\sum$[RO]: molar ratio of Al_2O_3 and total content of bivalent metal oxides.
[d] $[Fe_2O_3]$ / $\sum$[RO]: molar ratio of Fe_2O_3 and total content of bivalent metal oxides.

Table 3.3 Properties related density of gasified coal and synthesized slag melts.

Samples	Fe^{3+}/Fe_{tot}[a]	Density[b], at temperature (°C)												Molar volume[b]						β[b]
		1350		1400		1450		1500		1550		1600		1350	1400	1450	1500	1550	1600	
CA10.40	-	2.696	(0.002)[c]	2.676	(0.003)	2.675	(0.002)	2.657	(0.003)	2.637	(0.005)	-		23.1	23.3	23.3	23.4	23.6	-	11.2
CA20.40	-	-		2.665	(0.003)	2.639	(0.002)	2.625	(0.003)	2.603	(0.003)	-		-	25.1	25.3	25.5	25.7	-	15.7
CA30.40	-	-		-		-		2.597	(0.005)	2.571	(0.004)	-		-	-	-	27.5	27.8	-	20.4
CF08.39	0.80	2.972	(0.005)	2.964	(0.002)	2.943	(0.002)	2.929	(0.005)	2.918	(0.006)	-		22.3	22.4	22.5	22.7	22.7	-	9.3
CAF15.11.39	0.76	-		3.012	(0.001)	2.998	(0.001)	2.992	(0.002)	2.967	(0.002)	-		-	20.6	20.7	20.7	20.9	-	10.0
CA12.50	-	2.607	(0.006)	2.594	(0.005)	2.563	(0.006)	2.546	(0.007)	2.535	(0.004)	-		24.5	24.6	24.9	25.1	25.2	-	14.2
CF07.48	0.69	2.953	(0.002)	2.931	(0.001)	2.913	(0.001)	2.902	(0.001)	2.879	(0.001)	-		22.3	22.5	22.6	22.7	22.9	-	12.9
CA00.60	-	-		-		2.540	(0.003)	2.525	(0.003)	2.508	(0.002)	-		-	-	23.0	23.2	23.3	-	13.5
CA10.60	-	2.54	(0.02)	2.515	(0.007)	2.495	(0.005)	2.491	(0.003)	2.479	(0.004)	-		24.9	25.1	25.3	25.3	25.5	-	11.4
MA10.60	-	-		-		2.48	(0.05)	2.47	(0.01)	2.453	(0.005)	-		-	-	23.5	23.6	23.8	-	10.6
CF02.60	0.68	-		-		2.589	(0.001)	2.577	(0.001)	2.564	(0.002)	-		-	-	23.4	23.5	23.6	-	9.7
CF04.59	0.72	-		2.677	(0.001)	2.667	(0.002)	2.656	(0.001)	2.644	(0.001)	-		-	23.4	23.4	23.6	23.7	-	8.3
CF06.59	0.75	2.751	(0.002)	2.743	(0.001)	2.731	(0.002)	2.718	(0.001)	2.709	(0.001)	-		23.5	23.6	23.7	23.8	23.9	-	8.2
CF07.58	0.71	2.835	(0.001)	2.826	(0.002)	2.805	(0.001)	2.799	(0.001)	2.793	(0.002)	-		23.5	23.5	23.7	23.7	23.8	-	7.4
CF11.58	0.73	2.930	(0.002)	2.924	(0.001)	2.908	(0.001)	2.893	(0.001)	2.885	(0.002)	-		24.1	24.1	24.2	24.4	24.4	-	7.8
CF14.57	0.74	-		-		3.032	(0.003)	3.019	(0.003)	3.002	(0.004)	-		-	-	24.6	24.7	24.8	-	10.1
CV	0.56	-		-		-		-	-	2.53	(0.01)	2.513	(0.007)	-	-	-	-	26.7	26.8	12.2
TH	0.47	-		-		-		2.566	(0.003)	2.548	(0.003)	2.535	(0.002)	-	-	-	27.2	27.4	27.5	10.4
MA	0.52	-		-		-		2.570	(0.003)	2.559	(0.002)	2.541	(0.001)	-	-	-	27.6	27.7	27.9	14.1

[a] The fraction of Fe^{3+}/Fe_{tot} was analyzed two or three times for quenched samples.

[b] The units of density, molar volume, and coefficient of volume expansion (β) are g/cm^3, cm^3/mol and $10^{-5}/°K$, respectively.

[c] The number in brackets represent individual error's estimation for each temperature and composition.

3.2.2. Density measurements of slag melts

The apparatus used for the Archimedean double-bob method is similar to one that used in the previous studies [3.15, 3.33, 3.34], as illustrated in **Fig. 3.1**. The principle of this method is to measure the buoyancies of two Pt-bobs with different sizes by using an electrical balance (Sartorius ED124S). A computer interface (Sartorius YCC01-USBM2) was added to monitor and record the buoyancy directly. The measuring temperature was selected for homogeneous melting state. The temperature for homogeneous melting was confirmed by hot thermocouple method [3.35] and FactSage data bank [3.36].

The cooled sample was crushed and then re-melted at the highest measuring temperature and was kept for 2 hours before density measurements. After the temperature holding, the Pt-bob was suspended by a Pt–Rh 13 wt% wire with 0.25 mm diameter from the bottom of the electrical balance and then Pt-bob was lowered. When the tip of the bob touched the surface of slag melts, the digital balance displayed a change in weight. From the change, it was confirmed that the bob actually had touched the surface of slag melts. Then the bob was lowered further until the bob reached a depth of 20 mm below the surface of the slag melts.

The buoyancies of the large and small bobs were continuously measured for 30 minutes without removing the bobs from the slag melt in all temperature measurements. The average value of buoyancy was used for density determination. The density of slag melts, ρ, was calculated using the following **Eq. (3-1)**:

$$\rho = (W_1 - W_2)/(V_1 - V_2) \quad (3\text{-}1)$$

where W_1 and W_2 are the buoyancies, and V_1 and V_2 are the submerged volumes of the large and small bobs, respectively. The thermal expansions of the large and small bobs were corrected by **Eq**. **(3-2)** with the data of the thermal expansion of platinum [3.37]:

$$V_1 - V_2 = (1 + 3\alpha\Delta T) \cdot (V_1' - V_2') \quad (3\text{-}2)$$

where α is the thermal expansion coefficient of Pt, ΔT is the difference between measuring and room temperatures, and V_1' and V_2' are the volumes of the large and small bobs at room temperature, respectively. The reproducibility of the measurement was evaluated for the densities of silicone fluids and a slag melt of $40Na_2O–60SiO_2$ (mol%) as standard samples.

The density is strongly dependent on the molar weight and the molar volume. The latter is more sensitive to change in structure than density [3.11]. The molar volume (MV) V_m is calculated using the following **Eq**. **(3-3)**:

$$V_m = \sum(x_i \cdot M_i)/\rho \quad (3\text{-}3)$$

where x_i is the molar fraction, and M_i is the molar weight of a component i.

The coefficient of volume expansion (CVE), β, is calculated from the density change corresponding to the temperature measurements by the following **Eq**. **(3-4)**:

$$\beta = (\rho_1 - \rho_2)/\rho_2 \cdot 1/(T_2 - T_1) \quad (3\text{-}4)$$

where T_1 is the lowest temperature corresponding to ρ_1 and T_2 is the highest one corresponding to ρ_2.

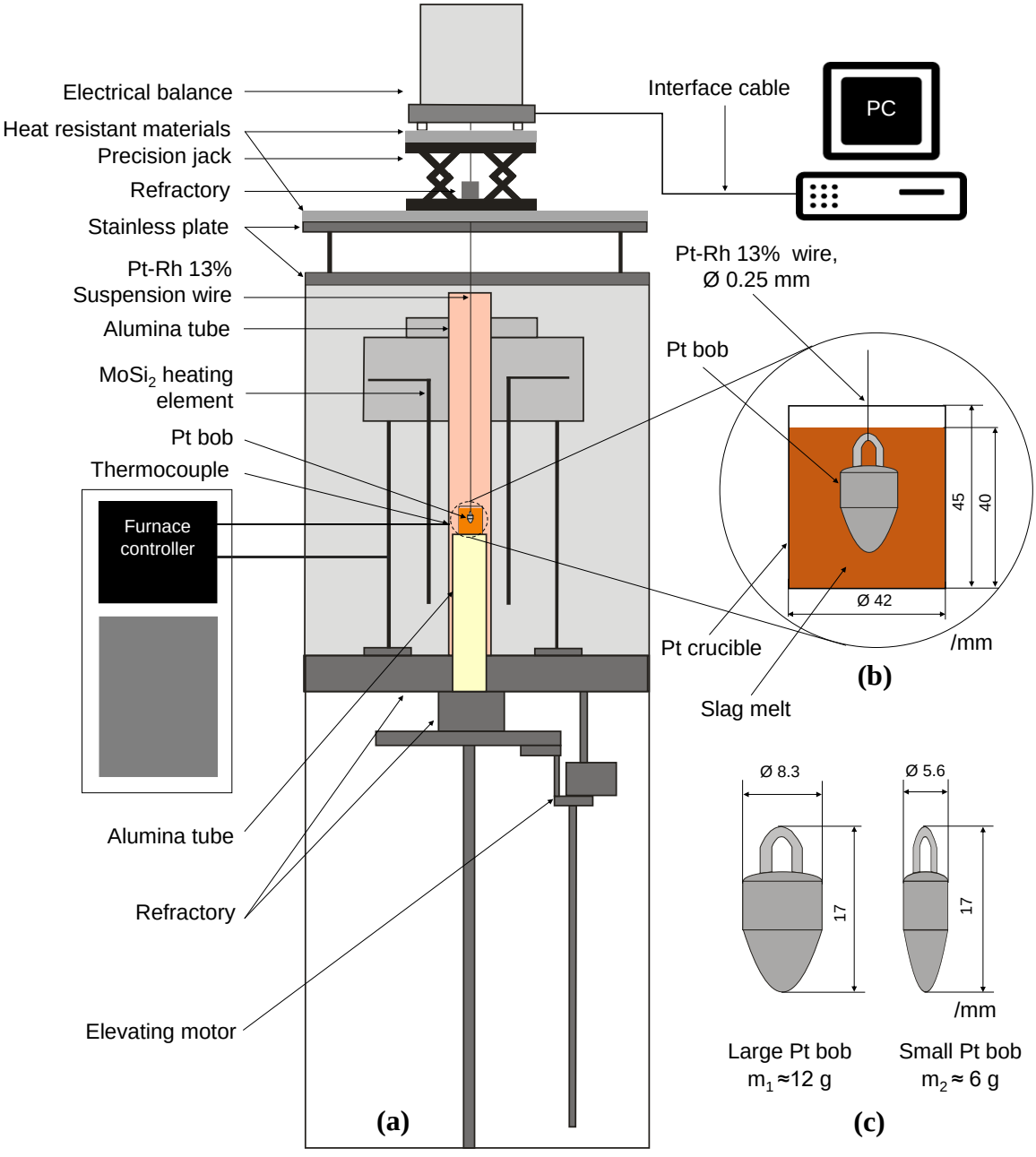

Fig. 3.1. Schematic apparatus for density measurements of slag melts: **(a)** whole diagram, **(b)** sample, and **(c)** large and small bobs.

3.3. Results and Discussion

3.3.1. Error estimation

The error estimation of the above method was taken as the deviations in the determination of buoyancy, temperature, and electrical balance reading [3.38]. The individual errors are summarised in **Table 3.3** for each measuring condition. The errors caused by viscosity and inhomogeneity of the sample in density measurements do not exceed $\pm 1.5 \times 10^{-2}$ g/cm^3 for CA, $\pm 6 \times 10^{-3}$ g/cm^3 for CF, $\pm 2 \times 10^{-3}$ g/cm^3 for CAF, and $\pm 5.2 \times 10^{-2}$ g/cm^3 for MA synthesized slags, $\pm 1.2 \times 10^{-2}$ g/cm^3 for gasified coal slags. The error range was depended on composition in slag melts. The average value of error was 0.37% for all measured densities.

The accuracy of density measurements was determined in the following ways. Firstly, the densities of silicone fluids with the viscosities 0.01, 0.999, 4.850, and 29.44 Pa·s were measured at 25 °C. The densities of silicone fluids were tested to be 0.941, 0.972, 0.973, and 0.974 g/cm^3, respectively. The measured densities have good agreement with the data of silicone fluid standards [39] with a precision of 0.16%. Secondly, the density of $40Na_2O$–$60SiO_2$ (mol%) melt was measured at 1350–1500 °C. The density results of $40Na_2O$–$60SiO_2$ melts are shown in **Fig. 3.2**. The results show that the mean difference between the first and second measurements is within 0.61 % of the density values. The reproducibility of this work is within the error estimation of density measurements. Furthermore, the density values are good agreement with previously reported values [3.33] within a deviation of 0.10%. The accuracy and reproducibility of density for silicone fluids and the $40Na_2O$–$60SiO_2$ (mol%) melt support the reasonable results of density measurements in this work.

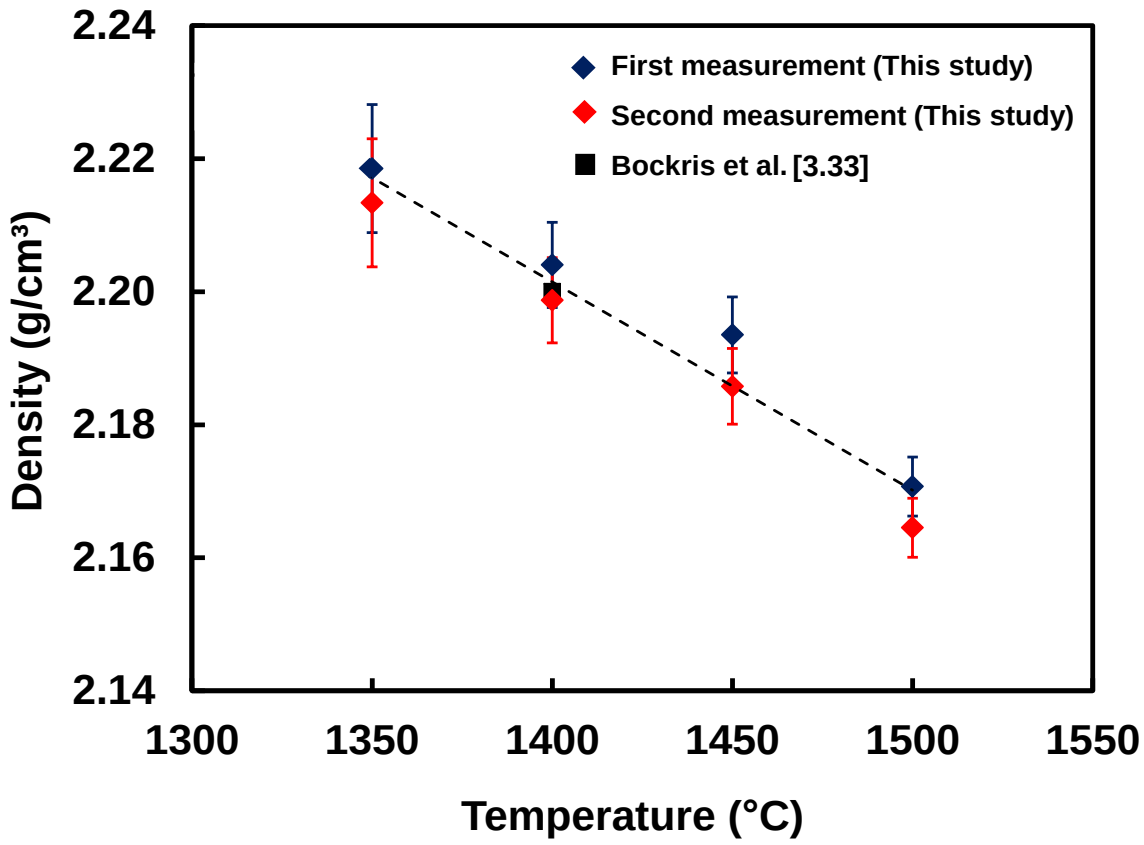

Fig. 3.2. Variation of density with temperature for $40Na_2O{-}60SiO_2$ slag melt (mol%) with the previously reported value Bockris et.al [3.33]. The dashed line represents the average linear fit of densities measured in this study.

3.3.2. Density measurements

Table 3.3 summarizes the results of density, MV and CVE for gasified coal and synthesized slag melts. **Table 3.3** also gives the analyzed values of Fe^{3+}/Fe_{tot} in quenched samples. The experiments were conducted two or three times for each sample. The experimental results showed that the percentage of Fe^{3+} was accounted for 47–56% and 68–80% for gasified and synthesized quenched samples, respectively. A close agreement is found by data of previous study with the similar compositions with the Fe^{3+} percentage of 45–90% [3.25].

Fig. 3.3 shows the temperature dependences of density for coal slag melts. There are linear relationships between density and temperature for all coal slag melts between 1500 and 1600 °C. The densities of the coal slag melts decrease linearly with increasing temperature. The density varied from 2.513 to 2.570 g/cm^3. The density was found to increase in the order of CV < TH < MA with increasing Fe_2O_3 and FeO contents, as shown in **Table 3.1**. In addition, the density decreases with increasing Al_2O_3 and SiO_2 contents.

Figs. 3.4 and 3.5 show the temperature dependences of density for synthesized slag melts with various Al_2O_3 and Fe_2O_3 contents. The density decreases linearly with increasing temperature as a general trend in slag melts [3.11]. The slag melt containing the largest Fe_2O_3 concentration of 14 mol%, named as CF14.57, has larger density values, compared to all the other samples at 1350–1550 °C. The density monotonically decreases when Fe_2O_3 is replaced by Al_2O_3 for synthesized slag melts with constant SiO_2 contents (40, 50, and 60 mol%), as shown in **Table 3.3 and Figs. 3.4 and 3.5**. The density is also found to decrease as Al_2O_3 content increases in the range of 10 and 30 mol%. The density of $30CaO–10Al_2O_3–60SiO_2$

(CA10.60) slag melt is slightly bigger than that of $30MgO–10Al_2O_3–60SiO_2$ (MA10.60) sample due to the substitution of CaO for MgO.

Densities of gasified and synthesized coal slag melts are shown in **Figs. 3.3, 3.4, and 3.5** and are summarized in **Table 3.3**. The densities of CAS and CFS slag melts show different trends with respect to increase in Al_2O_3 and Fe_2O_3 contents. The density of slag melts decreases almost monotonically with increasing Al_2O_3 content and increases with increasing Fe_2O_3 content.

Fig. 3.6 shows the relationship between density and A_2O_3 content (A=Al or Fe) for slag melts of CAS with 40 mol% SiO_2 and CFS with 60 mol% SiO_2. The densities shown in **Fig. 3.6** are the measured values at 1550 °C. A comparison between our results and reported values in the CAS slag melts shows slight deviation [3.24] and has a good agreement in the CFS slag melts [3.26].

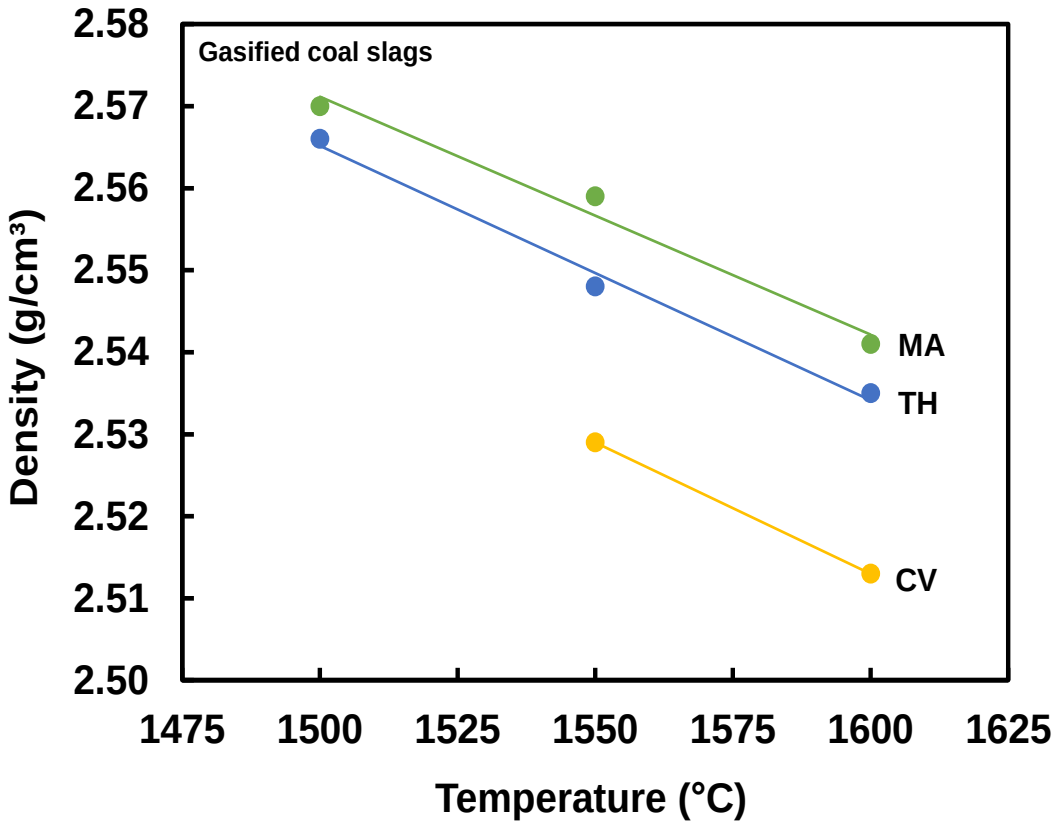

Fig. 3.3. Variations of density with temperature for coal slag melts. The straight lines are least square fit to the data of the coal slag melts at measuring temperatures.

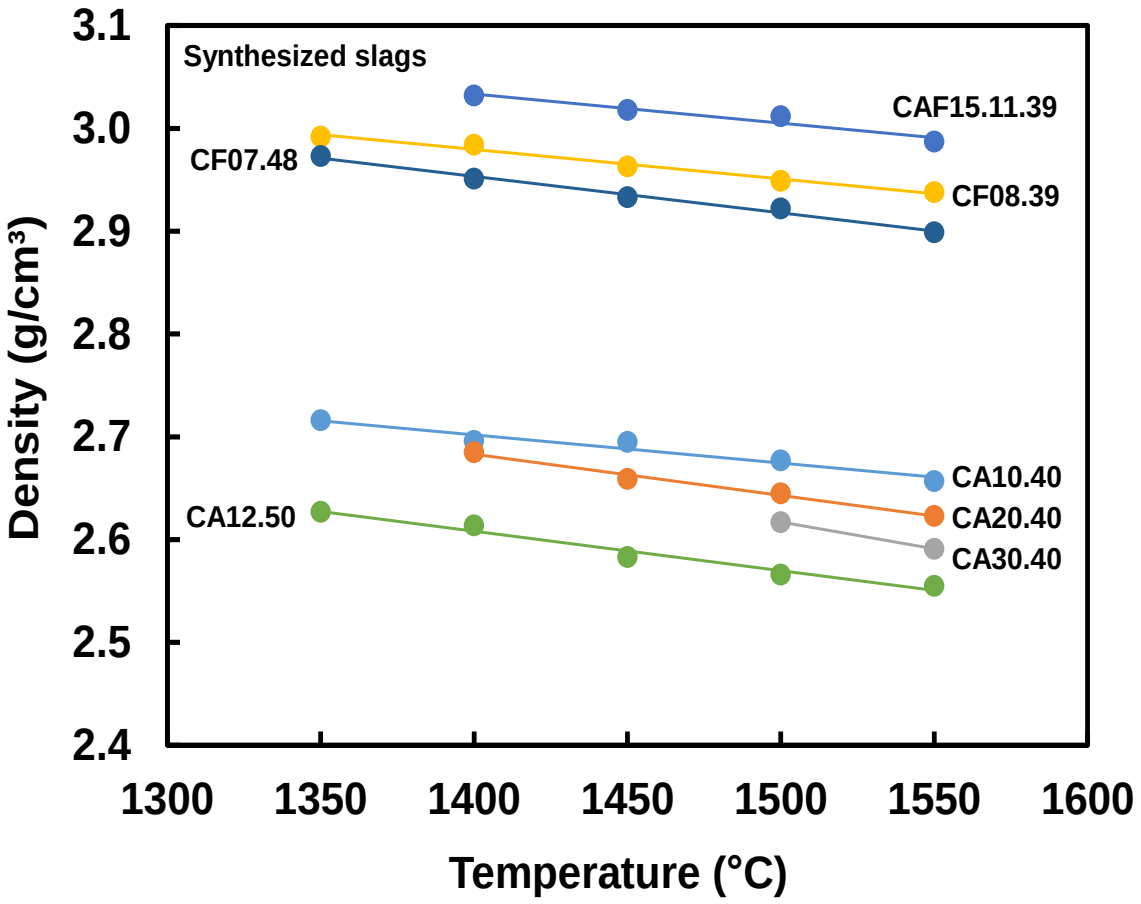

Fig. 3.4. Variations of density with temperature in a series of (60-x)RO−xA_2O_3−40SiO_2 and (50-x) RO−xA_2O_3−50SiO_2 slag melts (**Table 3.2**) with various Al_2O_3 and Fe_2O_3 contents. The straight lines are least square fit to the data of the synthesized slag melts at measuring temperatures.

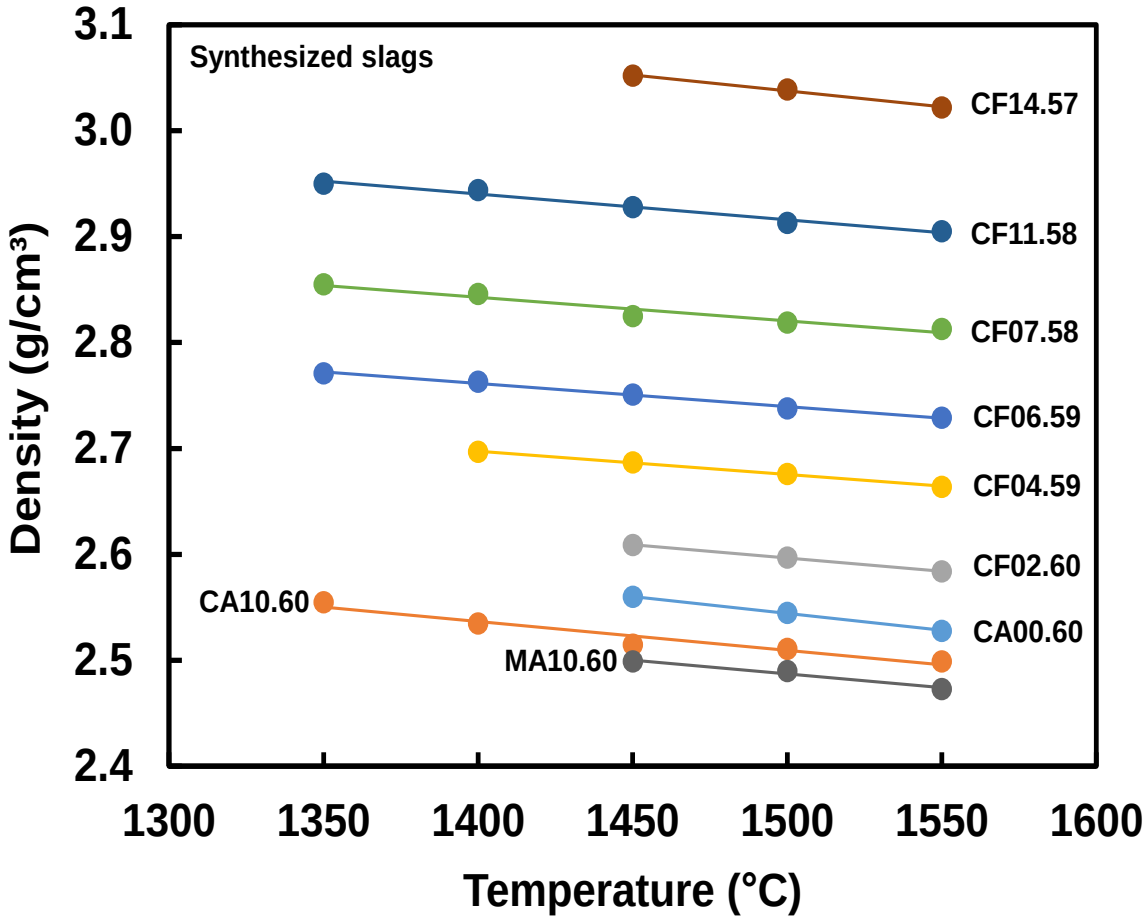

Fig. 3.5. Variations of density with temperature in a series of (40-x)RO−xAl_2O_3−60SiO_2 slag melts (**Table 3.2**) with various Al_2O_3 and Fe_2O_3 contents. The lines are the same as those in **Fig. 3.4**.

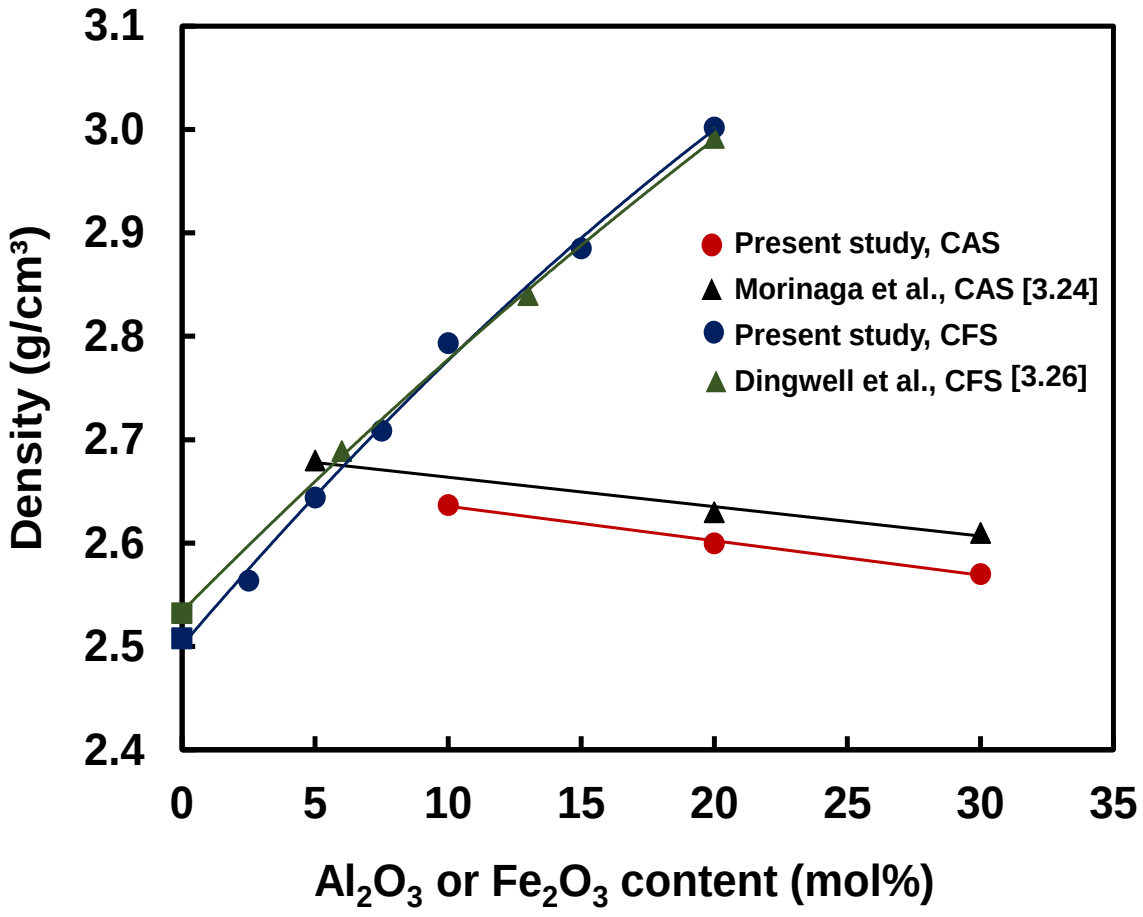

Fig. 3.6. Variation of density with Al_2O_3 or Fe_2O_3 content in a series of $(60-x)CaO-xAl_2O_3-40SiO_2$ (CAS) and $(40-x)CaO-xFe_2O_3-60SiO_2$ (CFS) slag melts (**Table 3.2**) at 1550 °C, respectively. Solid circles (red and blue) are the results of present studies. Solid triangles (black and green) are reported values by Morinaga et al. [3.24] and Dingwell et al. [3.26]. Solid squares (blue and green) are binary slag melts of $40CaO-60SiO_2$. The solid lines of CAS and CFS are least square and polynomial fits to the data, respectively.

3.3.3. Molar volume

The molar volumes of synthesized slag melts with various Al_2O_3 and Fe_2O_3 contents are shown in **Figs. 3.7 and 8**. **Fig. 3.7** shows the relationship between molar volume (MV) and Al_2O_3 content in a series of CAS slag melts with 40 mol% SiO_2. MVs of the slag melts at 1400–1550 °C increase monotonically with increasing Al_2O_3 content. MVs of CAS slag melts are in the range of 23.6–27.8 cm^3/mol **(Table 3.3)**. A good agreement of MV is found with data of CAS slag melts with similar compositions [3.24]. MV increases with increasing Fe_2O_3 content in a series of CFS slag melts with 60 mol% SiO_2, as shown in **Fig. 3.8**. The composition dependence of MV in the CFS series seems to be classified into two regions as (1) $0 \leq x \leq 7.5$ and (2) $7.5 \leq x \leq 14$ due to discontinuous change. MVs of CFS slag melts are in the range of 23–24.8 cm^3/mol **(Table 3.3)**. MV reaches almost constant values at ~7.5 mol% Fe_2O_3.

MV tends to increase by adding Al_2O_3 and Fe_2O_3 in the $CaO–SiO_2$ slag melts. Hence, MV of CAS slag melts monotonically increases **(Fig. 3.7)**, however, MV of CFS slag melts has the discontinuous change at the boundary between the regions (1) and (2) **(Fig. 3.8)**. This change suggests that the structural change of CFS slag melts occurred at ≥ 7.5 mol% Fe_2O_3.

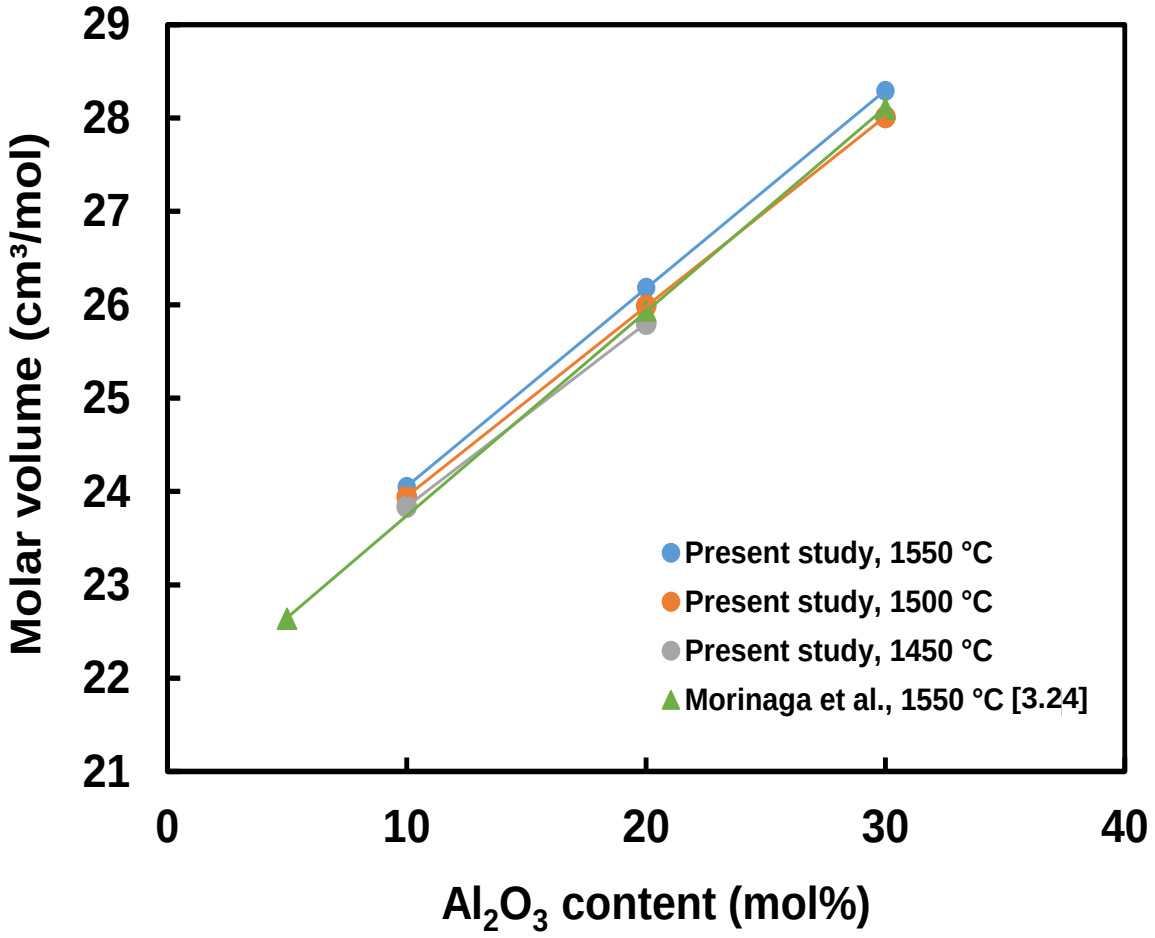

Fig. 3.7. Variations of molar volume with Al_2O_3 content in a series (60-x)CaO−xAl_2O_3−40SiO_2 slag melts (**Table 3.2**). Solid triangles (green) are reported values by Morinaga et al. [3.24]. The lines are the same as those in **Fig. 3.4.**

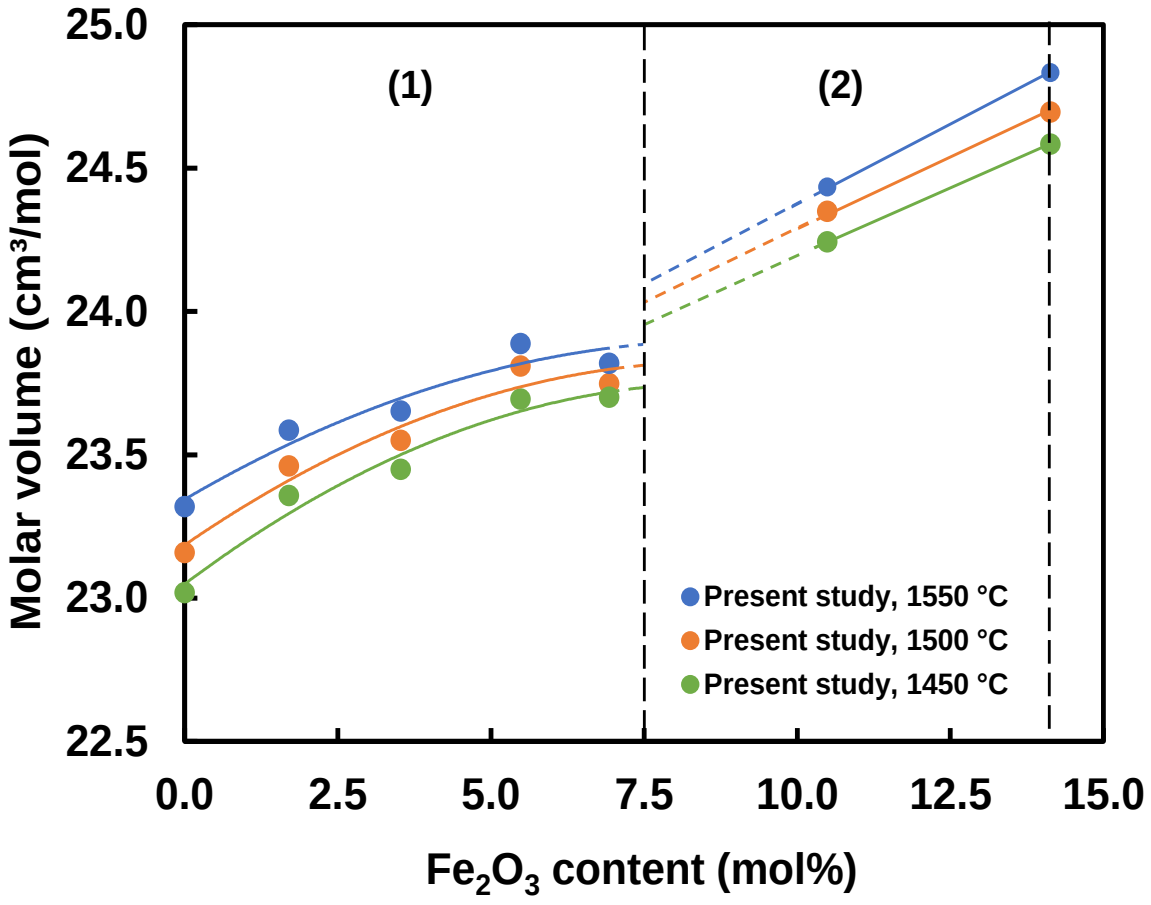

Fig. 3.8. Variations of molar volume with Fe_2O_3 content in a series of (40-x)CaO−xFe_2O_3−60SiO_2 slag melts (**Table 3.2**). Solid and dashed lines represent the experimental results and the guide lines to eyes at the boundary between regions (1) and (2), respectively. The molar volume using polynomial fits reaches constant values at ~7.5 mol% Fe_2O_3 in the region (1). The molar volume using least square fits exhibits discontinuously change between the regions (1) and (2).

3.3.4. Coefficient of volume expansion

Fig. 3.9 shows the relationship between the coefficient of volume expansion (CVE) and Al_2O_3 content for CAS slag melts. CVE increases monotonically with increasing Al_2O_3 content. **Fig. 3.10** shows the variation of CVE with Fe_2O_3 content for CFS slag melts. CVE of slag melts exhibits in the range of 7.4–13.5 × 10^{-5}/K **(Table 3.3)**. CVE is also classified into the two regions (1) and (2). CVE decreased with Fe_2O_3 addition exhibiting a minimum value at ~7 mol% and increased in region (2) of $x \geq 7.5$. The trend of CVE corresponds to that of the molar volume **(Fig. 3.9)**.

The CVE is calculated from the measured densities at two different temperatures. The CVE corresponds to the extent of change (slope) in the MV with increasing temperature. The minimum of CVE suggests that the temperature-induced structural change of the CFS slag melts occurs at ~7 mol% Fe_2O_3.

The density of CAS melt samples with ≥ 10 mol% Al_2O_3 has not been measured because of high temperature for homogenous melting, e.g., the CA00.40 at 1625 °C [3.36]. The good density results were obtained without solid components in the CAS slag melts.

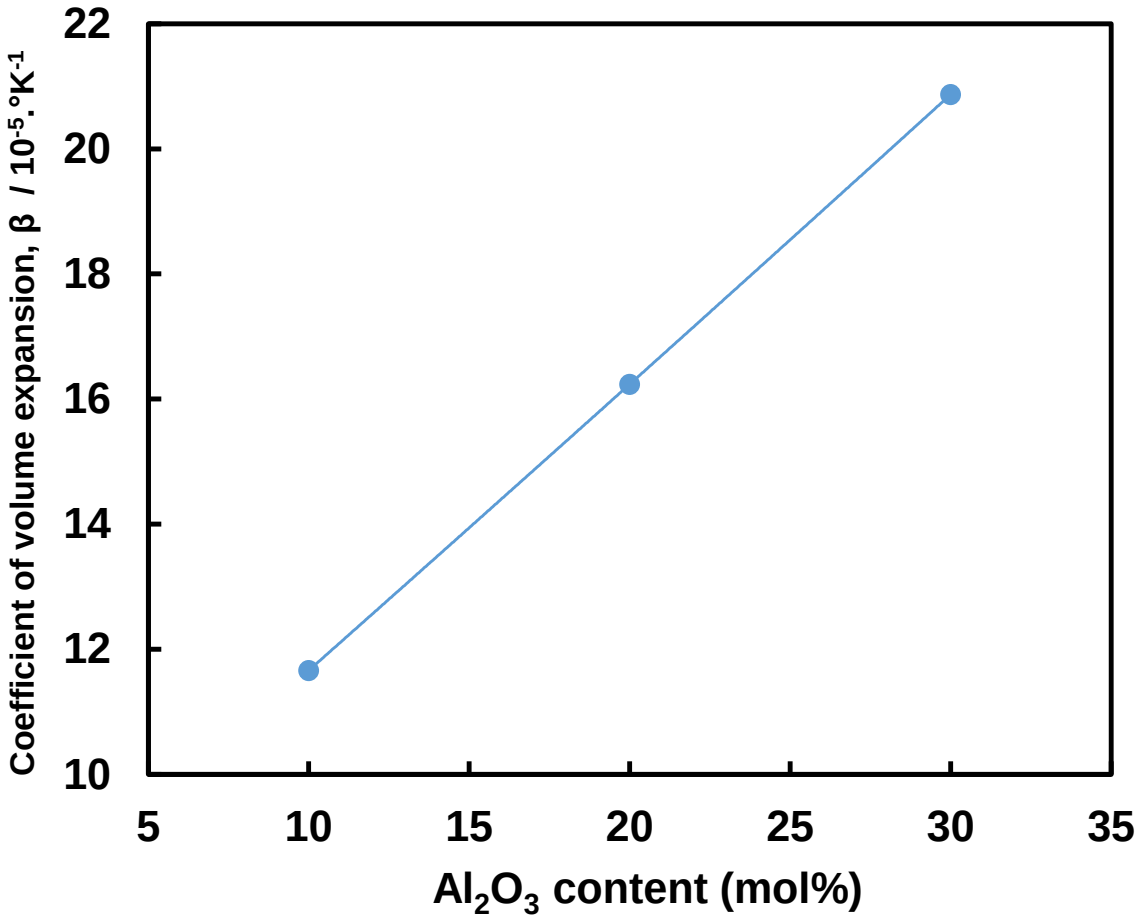

Fig. 3.9. Variation of the coefficient of volume expansion with Al_2O_3 content in a series of (60-x) $CaO–xAl_2O_3–40SiO_2$ slag melts (**Table 3.2**). The line is the same as those in **Fig. 3.4**.

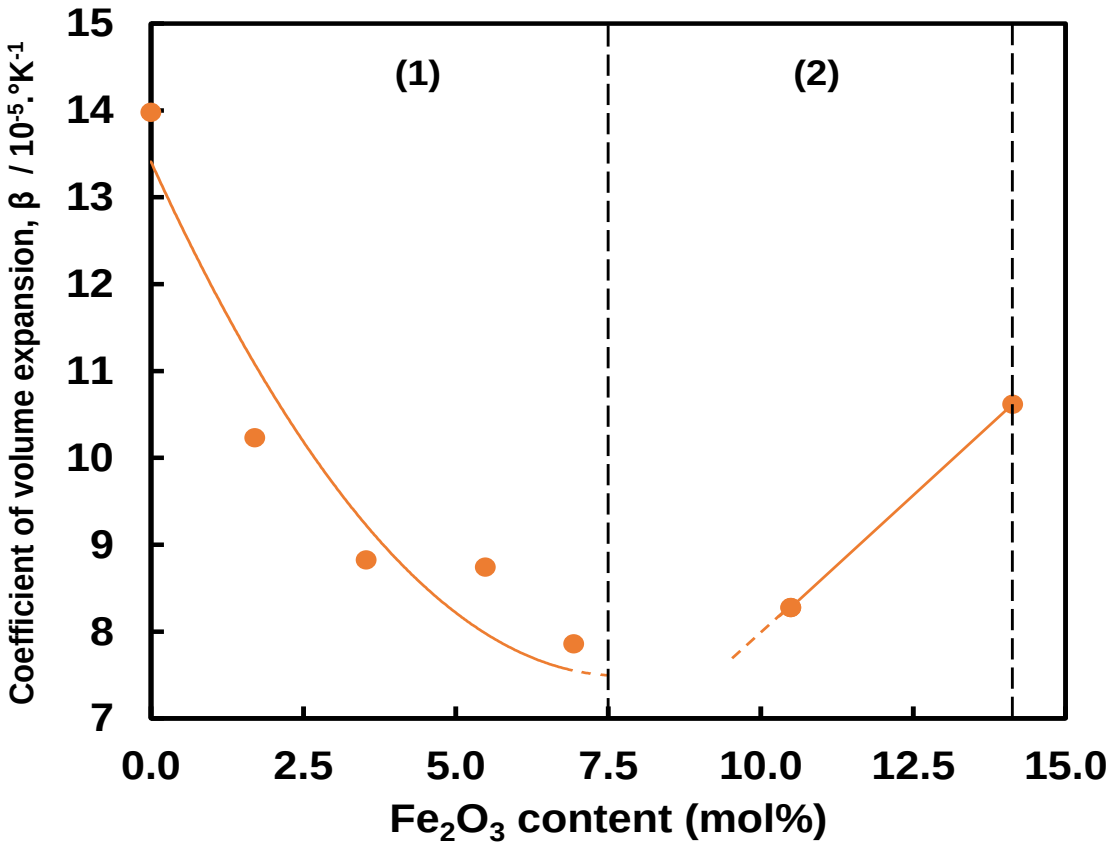

Fig. 3.10. Variation of the coefficient of volume expansion with Fe_2O_3 content in a series of $(40-x)CaO-xFe_2O_3-60SiO_2$ slag melts (**Table 3.2**). The solid and dashed lines are the same as those in **Fig. 3.8**.

3.3.5. The influence of Al_2O_3 and Fe_2O_3 on density

It is well known that Al_2O_3 and Fe_2O_3 are amphoteric oxides and their influence depends on the type and content of NWM as the basicity of slag melts [3.5, 3.20, 3.24]. The addition of CaO results in breaking of the structure of silicate network and the decrease of melt viscosity substantially. Influence of Al_2O_3 addition depends on $[Al_2O_3]/[R_2O, R'O]$ in molar ratio due to simple stoichiometric consideration. In the case of the molar ratio $[Al_2O_3]/[RO] < 1$, Al_2O_3 behaves NWF as described in previous studies of alumino-slicate melts and glasses [3.20, 3.24, 3.30]. Several authors reported that viscosity increased with increasing the polymerization degree of network structure by Al_2O_3 addition [3.24, 3.40]. In other words, Al^{3+} ideally plays the role of NWF for AlO_4 formation in order to link and share the corner between AlO_4 tetrahedra when charge compensating cation such as CaO exists enough for Al at $[Al_2O_3]/[CaO] \leq 1$ [3.5, 3.23, 3.30]. Moreover, the addition of Al_2O_3 to CaO-SiO_2 melts due to the formation of AlO_4 tetrahedral corresponds to the increases of MV and CVE [3.24].

The influences of CaO, MgO, and FeO contents as basic oxide (NWM) on density of synthesized slag melts are shown in **Fig. 3.5 and Table 3.3.** The influence of CaO on density in CAS and CFS systems depends on molar ratio of $[Al_2O_3]/[CaO]$ and $[Fe_2O_3]/[CaO]$. Density of CAS system decreases with increasing molar ratio of $[Al_2O_3]/[CaO]$ for 40 mol% SiO_2, as shown in **Tables 3.2 and 3.3**. On the contrary, the density increases with increasing molar ratio of $[Fe_2O_3]/[CaO]$ for ~60 mol% SiO_2 in CFS system. Similarly, the influence of FeO on density in CFS system increases with increasing FeO content, as shown in **Table 3.3**. Meanwhile, the influence of MgO on density of slag melts was investigated by substituting of CaO in CA10.60 sample by MgO (MA10.60). The result shows that MgO has little effect

on density of slag melts, as shown in **Fig. 3.5**. This result corresponds well with previous studies [3.27, 3.41].

In order to obtain the influence of Fe_2O_3 on the structure of slag melts, the molar volume (MV) and the coefficient of volume expansion (CVE) are used to support our discussion, as shown in **Figs. 3.8 and 3.10.** MV exhibits the discontinuous change at ~7.5 mol% Fe_2O_3 (x). This boundary corresponds well to the two regions of CVE with $0 \leq x \leq 7.5$ and $7.5 \leq x \leq 14$ mol% Fe_2O_3.

In the region (1) of CFS slag melts, MV tends to increase by adding Fe_2O_3 and reaches constant values at ~7.5 mol% Fe_2O_3. These results correspond to the decrease of CVE in the region (1), and it passes through a minimum at ~7 mol% Fe_2O_3, and then increases again in the region (2). Previous study [3.25] reported that the oxygen coordination number of Fe^{3+} ions can be determined by the ratio $[Fe_2O_3]/[R_2O, R'O]$. In the similar compositions of CFS quenched slag samples, Fe^{3+} as NWF and NWM are favored at $Fe_2O_3 \leq 10$ mol% and 10–20 mol%, respectively [3.25, 3.42]. It is suggested that the larger Fe_2O_3 content of > 10 mol% may form inhomogeneous melt structure including small crystals even in melt state. Further studies are necessary in order to understand the structure of silicate melts including large amounts of Fe_2O_3 (> 10 mol%).

3.3.6. Composition parameter

The contribution of main components of SiO_2, Al_2O_3, CaO, MgO, FeO and Fe_2O_3 on density was investigated for coal and synthesized slag melts. It was found experimentally that main components have different contributions on the density and molar volume of slag

melts. Based on measured density data of slag melts, a composition parameter is proposed to predict densities from the corresponding components determined by **Eq**. **(3-5)**:

$$P_\rho = 2.18 \cdot f_{SiO_2} + 2.73 \cdot f_{Al_2O_3} + 2.96 \cdot f_{CaO} + 2.92 \cdot f_{MgO} + 4.88 \cdot f_{FeO} + 5.00 \cdot f_{Fe_2O_3} \quad (3\text{-}5)$$

where P_ρ is the composition parameter of density, and f is the fraction of each component expressed by mol%.

Fig. 3.11 shows the relationship between density and the composition parameter for the density values measured at 1550°C. It compares with experimental and calculated results using the composition parameter for all density data. The average error Δ of all calculated values can be evaluated by using **Eqs. (3-6) and (3-7)**:

$$\delta_n = (\rho_n)_{cal} - (\rho_n)_{mea}/(\rho_n)_{mea} \cdot 100\ (\%) \quad (3\text{-}6)$$

$$\Delta = \frac{1}{N}\sum_{n=1}^{N}|\delta_n|\ (\%) \quad (3\text{-}7)$$

where δ_n is the percentage difference between the calculated $(\rho_n)_{cal}$ and measured $(\rho_n)_{mea}$ density values, and Δ is calculated by taking the summation sign ∑ of all absolute values of δ_n and divided by the total number of data.

The calculated value of the average error is 0.69%, which indicates a strong positive correlation between measured density and composition parameter for gasified and synthesized slag melts. This new model has the capability to predict the density of slag melts based on mole percentage.

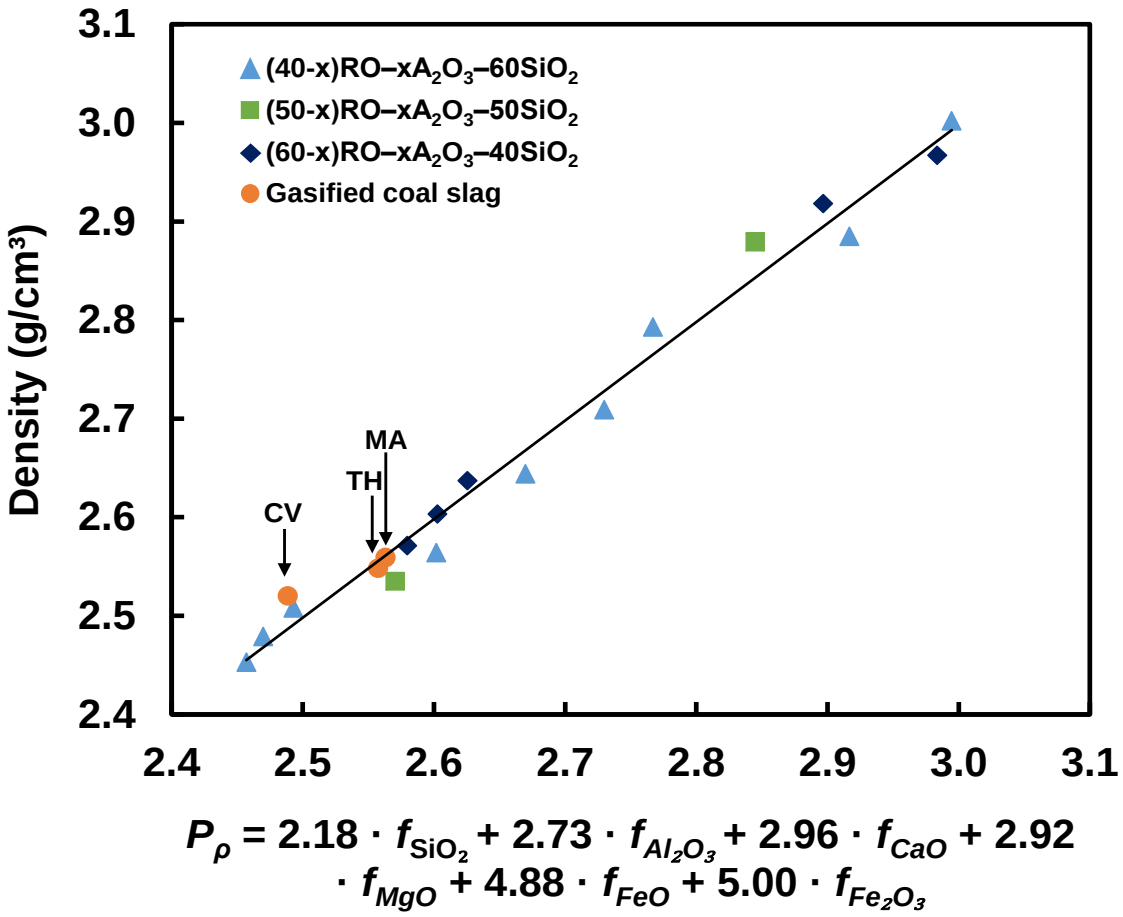

Fig. 3.11. Variation of density with the composition parameter based on mole percentage for synthesized and coal slag melts at 1550 °C.

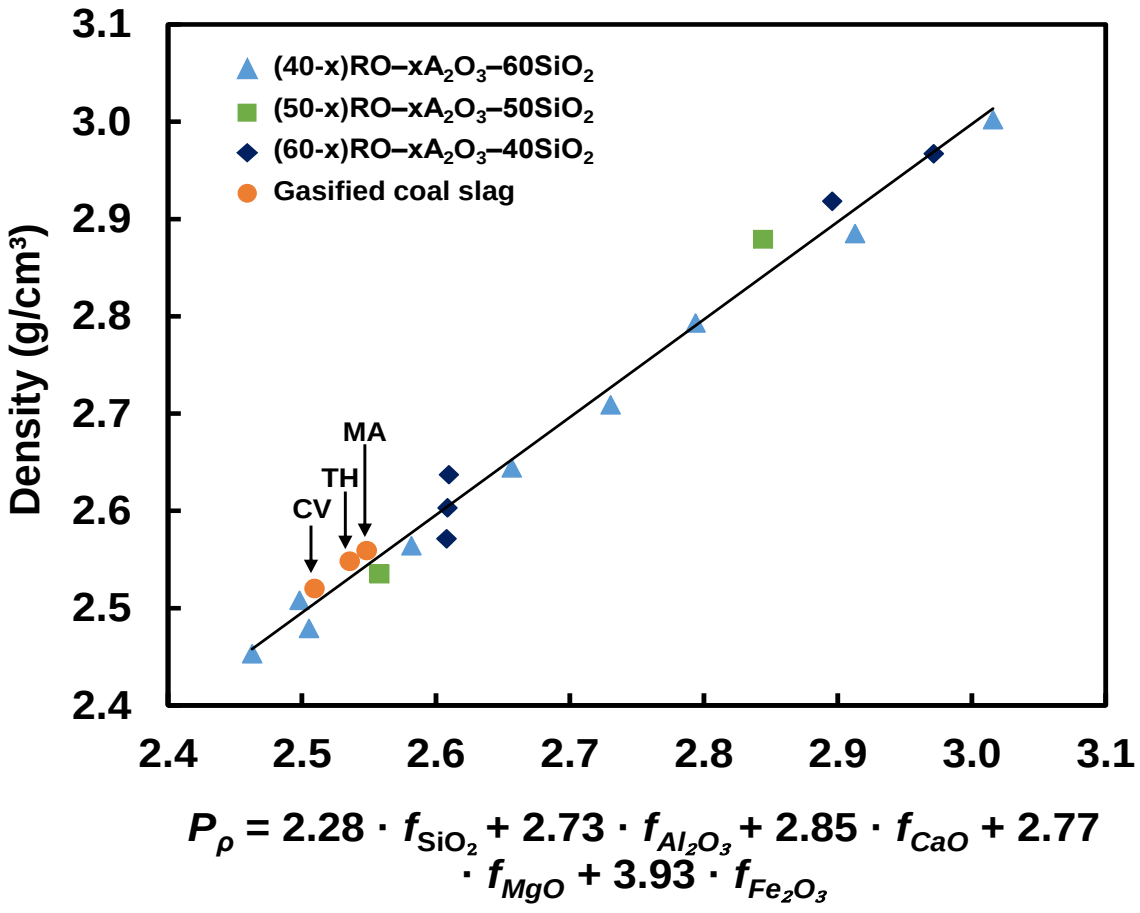

Fig. 3.12. Variation of density with the composition parameter based on mass percentage for synthesized and coal slag melts at 1550 °C without considering valence state of iron.

For engineering application, the composition parameter is used for predictions of the densities using mass percentage of synthesized coal slags as shown in **Fig. 3.12**. Because of generally low contents of FeO (≤10 mol%) in the investigated valence states of iron oxides, the contributions of the densities due to FeO were neglected and assumed that all of Fe component was Fe_2O_3. Based on these considerations, the second composition parameter as shown in **Eq**. **(3-8)** is used,

$$P_\rho = 2.28 \cdot f_{SiO_2} + 2.73 \cdot f_{Al_2O_3} + 2.85 \cdot f_{CaO} + 2.77 \cdot f_{MgO} + 3.93 \cdot f_{Fe_2O_3} \quad (3\text{-}8).$$

The second composition parameter can be used to estimate the densities of gasified coal slag melts as a function of composition mass % and confirmed that the calculated value of the average error was 0.66%. Furthermore, the empirical composition parameter can be beneficially used to predict density of gasified coal slag melts by the analysis of their chemical compositions without density measurements.

3.4. Conclusions

Density of gasified coals and slag melts decreased linearly with increasing temperature. Densities of gasified coal slag melts were found to increase in the order of CV < TH < MA. The density decreased with increasing Al_2O_3 and SiO_2 contents, on the contrary, it increased with increasing FeO and Fe_2O_3 contents.

Two types of amphoteric oxide in slag melts brought about different effects on the density: the density decreased with increasing Al_2O_3 content, on the contrary, it increased with increasing Fe_2O_3 content.

The MV and the CVE monotonically increased with increasing Al_2O_3 content for CaO–Al_2O_3–SiO_2 slag melts. On the basis of the MV and CVE, their composition variations with Fe_2O_3 content were classified into two regions: (1) low concentration ($0 \leq x \leq 7.5$) and (2) high concentration ($7.5 \leq x \leq 14$). The MV increases with increasing Fe_2O_3 content with the discontinuous change between the boundary of the two regions (x~7.5 mol%). The trend of the CVE corresponds to the MV. The CVE decreased with Fe_2O_3 addition showing a minimum value at ~7 mol% Fe_2O_3 and increased in $7.5 \leq x \leq 14$ mol% Fe_2O_3.

An empirical composition parameter was proposed to predict the density from the corresponding chemical composition of gasified coal slag melts for the next-generation IGCC.

References

[3.1] Strezov V, Lucas J a., Wall TF. Effect of pressure on the swelling of density separated coal particles. Fuel 2005;84:1238–45. doi:10.1016/j.fuel.2004.06.035.

[3.2] Aineto M, Acosta A, Rincon J, Romero M. Thermal expansion of slag and fly ash from coal gasification in IGCC power plant. Fuel 2006;85:2352–8. doi:10.1016/j.fuel.2006.05.015.

[3.3] Shannon GN, Matsuura H, Rozelle P, Fruehan RJ, Pisupati S, Sridhar S. Effect of size and density on the thermodynamic predictions of coal particle phase formation during coal gasification. Fuel Process Technol 2009;90:1114–21. doi:10.1016/j.fuproc.2009.05.002.

[3.4] Lin X, Ideta K, Miyawaki J, Takebe H, Wang Y, Yoon S, Mochida I. Study on structural and compositional transitions of coal ash by using NMR. J Coal Sci Eng 2012;18:80–7.

[3.5] Mills KC, Yuan L, Jones RT. Estimating the physical properties of slags. J South African Inst Min Metall 2011;111:649–58.

[3.6] Kong L, Bai J, Li W, Wen X, Liu X, Li X, Bai Z, Guo Z, Li H. The internal and external factor on coal ash slag viscosity at high temperatures, Part 2: Effect of residual carbon on slag viscosity. Fuel 2015;158:976–82. doi:10.1016/j.fuel.2015.06.055.

[3.7] Mills KC, Jeffrey M. Rhine. The measurement and estimation of the physical properties of slags formed during coal gasification: 1. Properties relevant to fluid flow. Fuel 1989;68:193–200. doi:10.1017/CBO9781107415324.004.

[3.8] Hsieh PY, Kwong KS, Bennett J. Correlation between the critical viscosity and ash fusion temperatures of coal gasifier ashes. Fuel Process Technol 2016;142:13–26.

doi:10.1016/j.fuproc.2015.09.019.

[3.9] Mysen BO, Virgo D, Seifert FA. The structure of silicate melts: Implications for chemical and physical properties of natural magma. Rev Geophys Sp Phys 1982;20:353–83. doi:10.1029/RG020i003p00353.

[3.10] Mills KC. Estimation of physicochemical properties of coal slag and ashes. Miner Mater Ash Coal, Am Chem Soc Washinton, DC 1986;301:195–214. doi:10.1021/bk-1986-0301.ch015.

[3.11] Hwang C, Fujino S, Morinaga K. Density of Bi_2O_3–B_2O_3 binary melts. J Am Ceram Soc 2004;87:1677–82. doi:10.1111/j.1551-2916.2004.01677.x.

[3.12] Kuromitsu Y, Yoshida H, Takebe H, Morinaga K. Interaction between alumina and binary glasses. J Am Ceram Soc 1997;80 (6):1583–7. doi:10.1111/j.1151-2916.1997.tb03020.x.

[3.13] Toyoda S, Fujino S, Morinaga K. Density, viscosity and surface tension of 50RO–$50P_2O_5$ (R: Mg, Ca, Sr, Ba, and Zn) glass melts. J Non Cryst Solids 2003;321:169–74. doi:10.1016/S0022-3093(03)00174-1.

[3.14] Shartsis L, Spinner S, Capps W. Density, expansivity, and viscosity of molten alkali silicates. J Am Ceram Soc 1952;35:155–60. doi:10.1111/j.1151-2916.1952.tb13090.x.

[3.15] Dingwell DB, Brearley M, Dickinson JE. Melt densities in the Na_2O–FeO–Fe_2O_3–SiO_2 system and the partial molar volume of tetrahedrally-coordinated ferric iron in silicate melts. Geochim Cosmochim Acta 1988;52:2467–75. doi:10.1016/0016-7037(88)90305-5.

[3.16] Muhmood L, Seetharaman S. Density measurements of low silica CaO–SiO_2–Al_2O_3

slags. Metall Mater Trans B 2010;41:833–40. doi:10.1007/s11663-010-9385-1.

[3.17] Lee J, Hoai LT, Choe J, Park JH. Density measurements of CaO–MnO–SiO_2 slags. ISIJ Int 2012;52:2145–8. doi:10.2355/isijinternational.52.2145.

[3.18] Sugawara T, Katsuki J, Shiono T, Yoshida S, Matsuoka J, Minami K, Ochi E. High-temperature heat capacity and density of simulated high-level waste glass. J Nucl Mater 2014;454:298–307. doi:10.1016/j.jnucmat.2014.07.055.

[3.19] Linard Y, Nonnet H, Advocat T. Physicochemical model for predicting molten glass density. J Non Cryst Solids 2008;354:4917–26. doi:10.1016/j.jnoncrysol.2008.07.013.

[3.20] Takebe H, Tsuruda A, Okada A, Ueda K. Viscosity characteristic of molten Slag for next-generation IGCC. J Japan Inst Energy 2015;94 (5):450–4.

[3.21] Kondratiev A, Jak E. Predicting coal ash slag flow characteristics (viscosity model for the Al_2O_3–CaO–"FeO"–SiO_2 system). Fuel 2001;80:1989–2000. doi:10.1016/S0016-2361(01)00083-7.

[3.22] Xuan W, Whitty KJ, Guan Q, Bi D, Zhan Z, Zhang J. Influence of SiO_2/Al_2O_3 on crystallization characteristics of synthetic coal slags. Fuel 2015;144:103–10. doi:10.1016/j.fuel.2014.11.091.

[3.23] Aksay I, Pask J, Davis R. Densities of SiO_2–Al_2O_3 Melts. J Am Ceram Soc 1973;62 (7-8):332–6. doi:10.1111/j.1151-2916.1979.tb19071.x.

[3.24] Morinaga K, Suginohara Y, Yanagase T. Density of CaO–SiO_2–Fe_2O_3, –Al_2O_3 melts. Tech Rep Kyushu Univ 1975;48 (6):859–65.

[3.25] Morinaga K, Suginohara Y, Yanagase T. Oxygen coordination number of Fe ions in CaO–SiO_2 and Na_2O–SiO_2 systems. J Japan Ints Met 1976;40 (05):480–6.

[3.26] Dingwell DB, Brearley M. Melt densities in the CaO–FeO–Fe_2O_3–SiO_2 system and the compositional dependence of the partial molar volume of ferric iron in silicate melts. Geochim Cosmochim Acta 1988;52:2815–25. doi:10.1016/0016-7037(88)90149-4.

[3.27] Courtial P, Dingwell DB. Nonlinear composition dependence of molar volume of melts in the CaO–Al_2O_3–SiO_2 system. Geochim Cosmochim Acta 1995;59 (18):3685–95. doi:10.1016/0016-7037(95)00272-2.

[3.28] Neuville DR, Cormier L, Massiot D. Al coordination and speciation in calcium aluminosilicate glasses: Effects of composition determined by ^{27}Al MQ-MAS NMR and Raman spectroscopy. Chem Geol 2006;229:173–85. doi:10.1016/j.chemgeo.2006.01.019.

[3.29] Chevrel MO, Giordano D, Potuzak M, Courtial P, Dingwell DB. Physical properties of $CaAl_2Si_2O_8$–$CaMgSi_2O_6$–FeO–Fe_2O_3 melts: analogues for extra-terrestrial basalt. Chem Geol 2013;346:93–105. doi:10.1016/j.chemgeo.2012.09.004.

[3.30] Takahashi S, Neuville DR, Takebe H. Thermal properties, density and structure of percalcic and peraluminus CaO–Al_2O_3–SiO_2 glasses. J Non Cryst Solids 2015;411:5–12. doi:10.1016/j.jnoncrysol.2014.12.019.

[3.31] Nakashima K, Saito N, Sukenaga S. Viscosity of iron oxide containing slag. J MMIJ 2011;127:111–6. doi:10.2473/journalofmmij.127.111.

[3.32] Takeshita R, Yoshida I, Ueno K. Adsorption behaviour of phosphate ion on the iron (III) compleks of a chelating Resin. Bul Chem Soc Japan 1979;52 (9):2577–80. doi:doi.org/10.1246/bcsj.52.2577.

[3.33] Bockris JO, Tomlinson JW, White JL. The structure of the liquid silicates: partial

molar volumes and expansivities. Trans Faraday Soc 1956;52:299. doi:10.1039/tf9565200299.

[3.34] Sukenaga S, Haruki S, Nomoto Y, Saito N, Nakashima K. Density and surface tension of $CaO–SiO_2–Al_2O_3–R_2O$ (R=Li , Na , K) melts. ISIJ Int 2011;51 (8):1285–9. doi:10.2355/isijinternational.51.1285.

[3.35] Ohta Y, Morinaga K, Yanagase T. Aplication of hot-thermocouple to high temperature chemistry. Bull Japan Inst Met 1980;19 (4):239–45. doi:10.11311/jscta1974.13.90.

[3.36] www.factsage.com.

[3.37] Waseda Y, Hirata K, Ohtani M. High-temperature thermal expansion of platinum, tantalum, molybdenum, and tungsten measured by x-ray diffraction. High Temp - High Press 1975;7 (2):221–6.

[3.38] Shiraishi Y, Ikeda K, Tamura A, Saito T. On the viscosity and density of the molten $FeO–SiO_2$ system. Mater Trans JIM 1978;19 (5):264–74. doi:10.2320/matertrans1960.19.264.

[3.39] Laboratories BE. General purpose silicone fluids, 2010, p. 1–6.

[3.40] Riebling EF. Structural similarities between a glass and its melt. J Am Ceram Soc 1968;51:143–9. doi:10.1111/j.1151-2916.1968.tb11857.x.

[3.41] Courtial P, Dingwell DB. Densities of melts in the $CaO-MgO–Al_2O_3–SiO_2$ system. Am Mineral 1999;84:465–76. doi:10.2138/am-1999-0401.

[3.42] Sumita S, Morinaga K, Yanagase T. Physical properties and structure of binary ferrite melts. Trans Japan Inst Met 1983;24 (1):35–41. doi:10.2320/matertrans1960.24.35.

Chapter 4

Surface Tension Measurements of Synthesized Coal Slag Melts

4.1. Introduction

Physical properties of coal slag melts play an important role in the integrated gasification combined cycle (IGCC) [4.1–4.3]. Several previous studies have been reported the essential effect of viscosity, density, and surface tension of coal slag melts in the IGCC [4.4–4.6]. The surface tension related with multicomponent slag melts is one of the most important parameters for controlling the various interfacial phenomena in the gasifier [4.7, 4.8]. The surface tension is defined as the energy required to increase the surface area of a liquid due to intermolecular forces. It is an essential property of coal slag melts since its relevant to fluid flow of slags in the gasifier operating of IGCC [4.9].

The surface tension plays a great role in controlling the homogeneity, wettability, and shape of slag melts [4.7, 4.10, 4.11]. Surface tension is relevant to fluid flow of coal slags, and slag melts interactions (wetting) for the successful design of gasifier in the IGCC power plant. However, the surface tension data of coal slag in the published literature are limited.

A previous study measured a surface tension of 0.320 N/m for a coal ash slag (54.6 SiO_2–18.3Al_2O_3–8.7Fe_2O_3–6.4CaO–4.3MgO–4.3SO_3–3.4Na_2O–2.4K_2O mol%) in the temperature interval from 1300 to 1400 °C. [4.12]. The other previous study reported

[4.13] used vitreous carbon as the substrate material when measuring the surface tension of a gasifier slag by a sessile drop method and found a value of 0.430 N/m for a temperature of 1350 °C. The other previous studies [4.14, 4.15] also used the sessile drop method found the data of surface tension data ranging from 0.190 to 0.960 N/m for different temperature intervals and gas atmospheres to study coal slag and model for glass melts.

The slags formed during the coal gasification process mainly contain SiO_2, Al_2O_3, CaO, MgO, FeO, and Fe_2O_3, with small amounts of Na_2O, K_2O, TiO_2, P_2O_5, SrO, MnO, and other compounds [4.6, 4.16, 4.17]. The basic slag systems of gasified coal slags are CaO–Al_2O_3–SiO_2 (CAS) and CaO–Fe_2O_3–SiO_2 (CFS). The simplified silicate systems of CAS, CFS, and CAFS slag melts have been prepared here to understand the behavior of SiO_2, Al_2O_3, CaO, FeO, and Fe_2O_3 and on surface tension. The roles of Al_2O_3 and Fe_2O_3 on surface tension as amphoteric oxides were mainly explored.

The surface tension data for synthesized slags presented in this study can be used for the validation of property prediction derived from measurements of real coal slags. The prediction of surface tension data of synthesized coal slag may use for the corresponding coal slags in the gasification process. Temperature and composition dependence of surface tension of synthesized coal slags have been measured and predicted for understanding the coal slag melts used in the IGCC process.

According to these scientific and engineering backgrounds, the objectives of this research are (i) to establish a maximum bubble pressure method to measure surface tension of silicate oxide systems (ii) to measure the surface tension of CAS, CFS, and CAFS system as synthesized coal slags melts (iii) to discuss the temperature and compositional dependence of surface tension (iv) to discuss the influence of major

component of coal on the surface tension, and (iv) to propose a composition parameter to predict the surface tension based on chemical composition.

4.2. Materials and Methods

4.2.1. Sample preparation of synthesized slags

Table 4.1 shows that the batches of synthesized slag samples were divided into three series of (60-x)CaO–xA_2O_3–40SiO_2, (50-x)CaO–xA_2O_3–50SiO_2, and (40-x)CaO–xA_2O_3–60SiO_2 in the molar ratio, A is Al and Fe without considering the valence state of iron oxide. There are compositions containing 40, 50 and 60% SiO_2 (nominal concentration) with various contents of CaO, Al_2O_3 and Fe_2O_3. The composition series of synthesized slags were systematically varied by considering those of gasified coal slags that had been determined in our previous study [4.18]. The surface tension of previous studies of CAS [4.19], CFS [4.20], and CAFS [4.21] slag melts in similar composition are also appeared for comparison data in this study as shown in **Table 4.1**. They are labelled RCA, RCF, and RCAF, where R is denoted as reference of CAS, CFS and CAFS slag melts, respectively.

4.2.2. Surface tension measurements of slag melts

The available experimental results of surface tension of CAS and CFS slag melts were obtained several researches using the maximum bubble pressure method, sessile drop method, pendant drop method, ring method, and dipping-cylinder method [4.22–4.25]. In the present study, the maximum bubble pressure method was used to measure surface tension. This method was selected because the ability to give accurate results at high temperatures [4.26, 4.27]. The apparatus used for the maximum bubble pressure method described frequently in the previous studies [4.3, 4.28–4.31].

Table 4.1 Chemical composition of synthesized coal slag samples.

Series	Samples	mol% (mass %)										Molar ratio		
		SiO_2		Al_2O_3		CaO		FeO[a]		Fe_2O_3[a]		$\sum[A_2O_3]/\sum[RO]$ [b]	$[Al_2O_3]/\sum[RO]$ [c]	$[Fe_2O_3]/\sum[RO]$ [d]
(60-x)RO−xA_2O_3−40SiO_2	CA10.40	40.0	(38.6)	10.0	(16.4)	50.0	(45.0)	0.0	(0.0)	0.0	(0.0)	0.00	0.20	0.00
	CA20.40	40.0	(35.9)	20.0	(30.5)	40.0	(33.6)	0.0	(0.0)	0.0	(0.0)	0.00	0.50	0.00
	CA25.40	40.0	(34.8)	25.0	(36.9)	35.0	(28.4)	0.0	(0.0)	0.0	(0.0)	0.00	0.71	0.00
	CA30.40	40.0	(33.6)	30.0	(42.8)	30.0	(23.5)	0.0	(0.0)	0.0	(0.0)	0.00	1.00	0.00
	CF08.39	39.2	(35.5)	0.0	(0.0)	49.0	(41.4)	4.0	(4.3)	7.8	(18.8)	0.00	0.00	0.16
	CAF15.11.39	38.6	(30.2)	14.5	(19.3)	29.0	(21.2)	6.9	(6.5)	11.0	(22.9)	0.88	0.50	0.38
(50-x)RO−xA_2O_3−50SiO_2	CA10.50	50.0	(47.9)	10.0	(16.3)	40.0	(35.8)	0.0	(0.0)	0.0	(0.0)	0.00	0.25	0.00
	CF07.49	48.5	(44.2)	0.0	(0.0)	38.8	(33.0)	6.1	(6.6)	6.7	(16.2)	0.00	0.00	0.17
(40-x)RO−xA_2O_3−60SiO_2	CA10.60	60.0	(57.2)	10.0	(16.2)	30.0	(26.7)	0.0	(0.0)	0.0	(0.0)	0.00	0.33	0.00
	CF07.58	58.3	(52.7)	0.0	(0.0)	29.2	(24.6)	5.6	(6.1)	6.9	(16.6)	0.00	0.00	0.24
Mukai and Ishikawa [19]	RCA10.43[e]	43.1	(0.0)	10.0	(0.0)	46.6	(0.0)	0.0	(0.0)	0.0	(0.0)	0.00	0.21	0.00
	RCA20.44	44.4	(0.0)	20.0	(0.0)	35.6	(0.0)	0.0	(0.0)	0.0	(0.0)	0.00	0.56	0.00
	RCA29.41	41.0	(0.0)	29.0	(0.0)	30.0	(0.0)	0.0	(0.0)	0.0	(0.0)	0.00	0.97	0.00
	RCA15.46	45.7	(0.0)	15.1	(0.0)	39.2	(0.0)	0.0	(0.0)	0.0	(0.0)	0.00	0.39	0.00
	RCA11.57	57.0	(0.0)	10.8	(0.0)	32.2	(0.0)	0.0	(0.0)	0.0	(0.0)	0.00	0.30	0.00
Slag atlas, 2nd edition [21]	RCAF10.34.56	56.2	(0.0)	9.8	(0.0)	29.7	(0.0)	0.0	(0.0)	34.0	(0.0)	1.47	0.33	1.14
Skupien and Gaskell [20]	RCF16.58[f]	58.3	(0.0)	0.0	(0.0)	41.7	(0.0)	0.0	(0.0)	15.7	(0.0)	0.00	0.00	0.38
	RCF16.49	48.5	(0.0)	0.0	(0.0)	51.7	(0.0)	0.0	(0.0)	15.6	(0.0)	0.00	0.00	0.30
	RCF16.43	42.6	(0.0)	0.0	(0.0)	57.4	(0.0)	0.0	(0.0)	15.5	(0.0)	0.00	0.00	0.27

[a] The FeO and Fe_2O_3 were determined experimentally using chelate titration method in the quenched samples.
[b] $\sum[A_2O_3]$ / $\sum[RO]$: molar ratio of total contents of amphoteric and bivalent metal oxides.
[c] $[Al_2O_3]$ / $\sum[RO]$: molar ratio of Al_2O_3 and total content of bivalent metal oxides.
[d] $[Fe_2O_3]$ / $\sum[RO]$: molar ratio of Fe_2O_3 and total content of bivalent metal oxides.
[e] RCA: R is denoted as reference of CAS slag melts.
[e] RCF: R is denoted as reference of CFS slag melts.

The principle of this method is to measure surface tension using a capillary tube of known radius, *r* immersed into liquid slag to a known immersed depth, *d*. The bubble is produced at the tip of the capillary by progressively increasing the gas pressure, *P* in the tube until to form an independent bubble which detached from the orifice. The measuring temperature was selected for homogeneous melting state. The temperature for homogeneous melting was confirmed by hot thermocouple method [4.32] and FactSage data bank [4.33].

The measuring apparatus consists of three main parts: an electric furnace, a furnace controller and a one set of maximum bubble pressure devices as shown in **Fig. 4.1**. The latter consists of a capillary, precision jack, manometer, and transducer to connect the PC using WAVE LOGGER software. The capillary made of Pt−13%Rh alloy was used. The inner diameter of the capillary is 1.27 mm. The precision jack, fixed on the upper furnace lid, determined the position of the exact touch of the capillary in the liquid surface and showing the chosen immersion depth. The manometer was used for pressure measurement.

The cooled sample was crushed and then re-melted at the highest measuring temperature and was kept for 2 hours before surface tension measurements. After the temperature holding, a gas used to form the bubbles, a flowmeter, the narrow tube, the manometer with Teflon tube were connected to PC with using a transducer. Before surface tension measurements, the gas was slowly flowed through the capillary to avoid condensation about 20 minutes. Then, the capillary was lowered into the slag melt samples to set gas flow rate using the flowmeter. The capillary was raised above the melt samples until the displayed manometer of 0.00.

The measurements were performed after the established an electric furnace, furnace control, and devices of the maximum bubble pressure method. The capillary was lowered by precision jack until the tip touched the surface of slag melts. The tip capillary was lowered at five different depths

of immersion (0.005, 0.010, 0.015, 0.020 and 0.025 m). The Argon (Ar) gas flow was adjusted using a capillary. The rate of bubble formation was kept constant six bubbles per three minutes. The bubble pressure in the capillary at one depth of immersion was measured six times and the average value was used for the calculation of surface tension. The measured surface tension was made at the highest temperature and decreased to some lower temperature measurements depend on homogeneous melting state of samples.

The bubble pressure was measured by a digital and analog transducer connected from manometer to PC. The bubble pressure changes linearly with the immersion depth of the capillary in slag melts. For considering of ruptured bubbles is non spherical behaviour in the slag melts, surface tensions were calculated using the Schrodinger's approximation by **Eq. 4–1**,

$$\gamma = rP_0/2[1 - 2/3\,(r\rho g/P_0) - 1/6\,(r\rho g/P_0)^2] \quad (4\text{–}1)$$

where γ is the surface tension, r is the is the inner radius of capillary tube calculated at room temperature and the coefficient of thermal expansion platinum of Pt−13%Rh [4.33], P_0 is the maximum bubble pressure at the melt surface, ρ is the density of slag melts and g is the gravity acceleration. The reproducibility of the surface tension measurement was evaluated for the surface tension of pure water and a slag melt of 40CaO–20Al_2O_3–40SiO_2 (mol%) as standard samples.

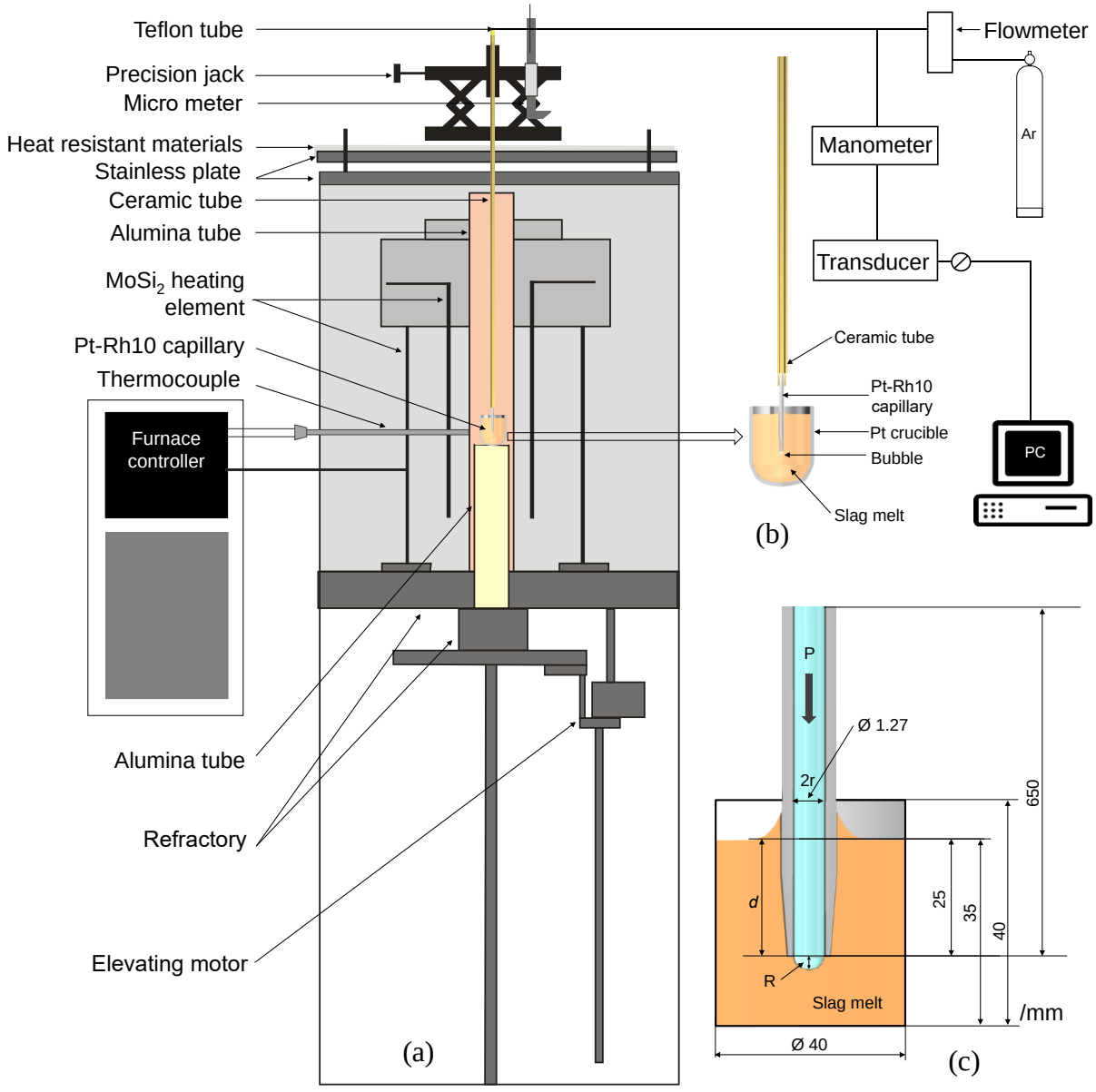

Fig. 4.1. Schematic apparatus for measuring surface tension of slag melts: **(a)** whole diagram, **(b)** experimental setup, and **(c)** the Pt crucible and Pt-Rh10 capillary of maximum bubble pressure method.

4.3. Results and Discussions

4.3.1. Error estimation

The maximum bubble curves were measured constant of six bubbles per three minutes each immersion depth. Immersion depths were measured nine times at every temperature measurement. The one maximum peak corresponds to one bubble. The pressure response with time is shown in **Fig. 4.2**. It shows the result of $40CaO–20Al_2O_3–50SiO_2$ slag melts at 1600°C using Ar gas as an example.

The maximum bubble pressure obtained when the ruptured bubbles were measured by a digital manometer. A computer interface was added to monitor and record the bubble pressure directly using analog transducer. The signal data has the line in the monitor correlation between output voltage with time at various immersion depths as shown in **Fig. 4.2**.

The density of the slag melts can be determined by a slope of the curve correlation between maximum bubble pressure and immersion depths. An example of the relationship between maximum bubble pressure and immersion depth is shown in **Fig. 4.3**. It shows results of measurements for $40CaO–20Al_2O_3–40SiO_2$ slag melts at 1600°C. The maximum bubble pressure was measured at various immersion depths. From these results, density was determined from the slope using a least square method. The surface tension was obtained from density and maximum bubble pressure at an immersion depth of zero as labelled P_0. Then, the surface tension can be calculated using the Schrodinger's approximation using **Eq. 4–1**.

A previous study reported that the major sources of experimental errors related to the measured surface tension using maximum bubble pressure are capillary radius, pressure measurement, determination of surface, temperature, and density [4.26]. The individual errors are summarized in **Table 4.1** for each measuring condition. The errors caused by viscosity and

inhomogeneity of the sample in surface tension measurements do not exceed do not exceed ± 0.3 × 10^{-2} N/m for CAS and ± 0.2 × 10^{-2} N/m for CFS slag melts. The error range was dependent on temperature in the slag melts. The average value of errors is 0.12% for all measured surface tension data.

The accuracy and reproducibility of surface tension measurements were determined in the following ways. Firstly, the surface tension of pure water was measured at 19 °C. The experimental result of surface tension of pure water was 0.0735 N/m with an error estimation of ± 0.0002. The measured surface tension of pure water has good agreement with the previous data 0.0728 N/m [4.35] with a precision of 0.08%. Secondly, the surface tension of 40CaO–20Al_2O_3–40SiO_2 (mol%) slag melt was measured at 1400–1600 °C. **Fig. 4.4** shows variation of surface tension with temperature 40CaO–20Al_2O_3–40SiO_2 (mol%) with the previously reported values of Mukai and Ishikawa [4.19] with a similar composition of 44.4CaO–20Al_2O_3–35.6SiO_2 (mol%). The comparison of present study and the previous studies shows the mean deviation of 1.87%. The deviation result is probably due to difference compositions. The previous study reported that the error of maximum bubble pressure method was estimated with an uncertainty 1.68% [4.26]. It confirms that the surface tension values measured in the present study are reasonable.

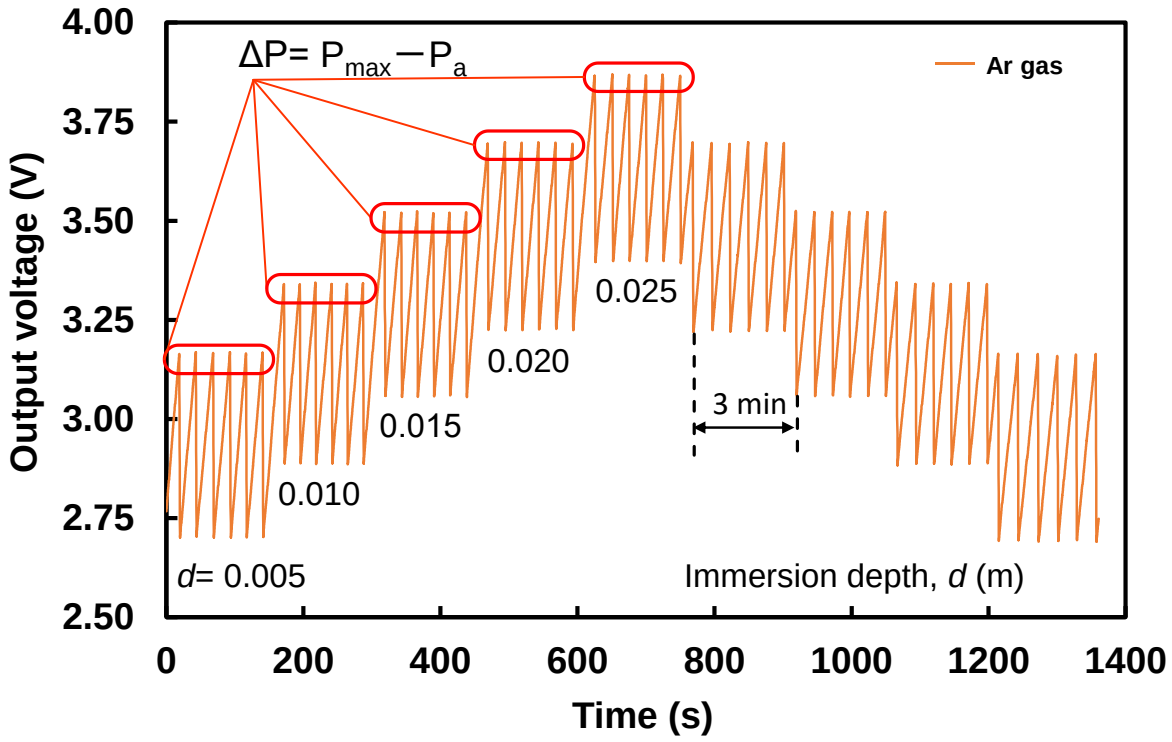

Fig. 4.2. Variations of output voltage with time as an example of measuring data of 40CaO–$20Al_2O_3$–$40SiO_2$ at 1600°C.

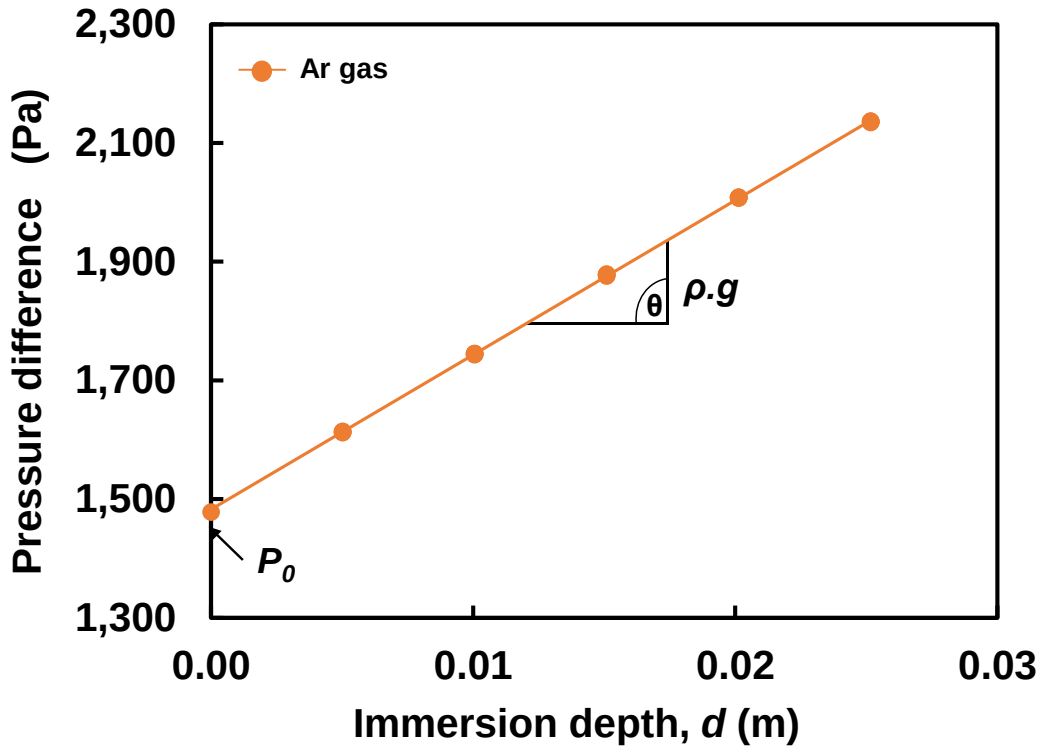

Fig. 4.3. Variations of pressure difference and immersion depth for $40CaO–20Al_2O_3–40SiO_2$ melts at 1600°C. The straight line is a least square fit to the data of the synthesized slag melts at immersion depths.

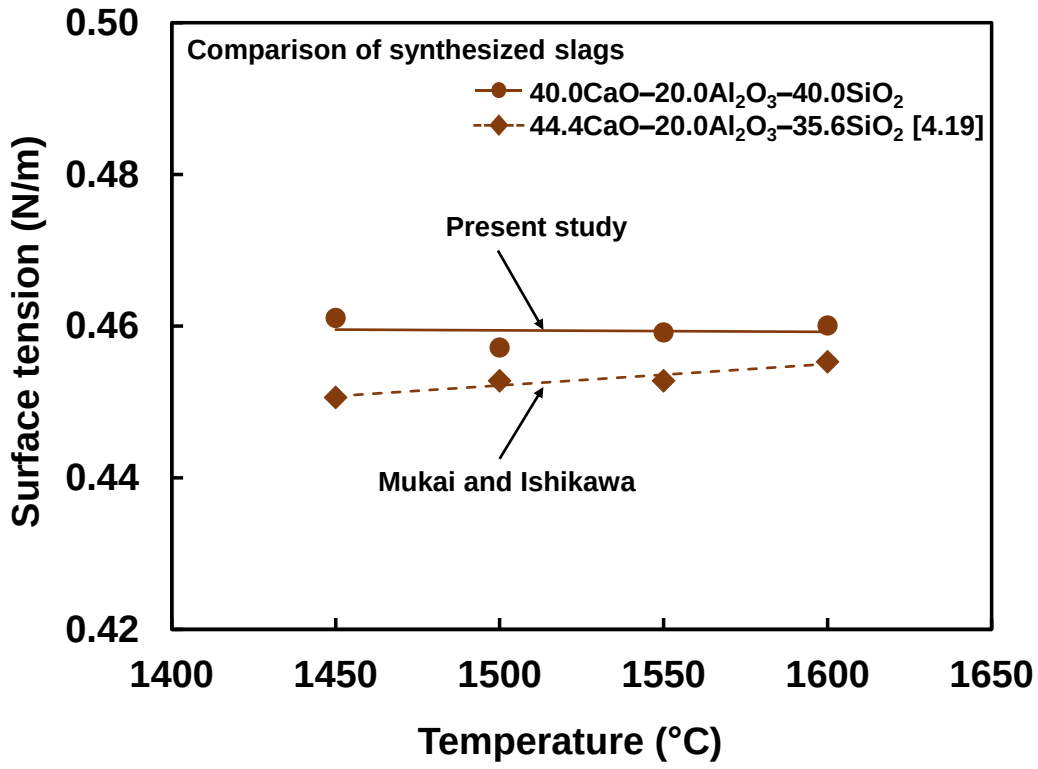

Fig. 4.4. Variations of surface tension with temperature for $40CaO–20Al_2O_3–40SiO_2$ melt (mol%) with the previously reported values of Mukai and Ishikawa [4.19] with a similar composition of $44.4CaO–20Al_2O_3–35.6SiO_2$ (mol%). The solid lines are a least square fit to the data of the synthesized slag melts at measuring temperatures.

4.3.2. Surface tension measurements

4.3.2.1. Temperature dependence

Table 4.2 summarizes measured results of surface tension in synthesized slag melts. **Figs. 4.5 and 4.6** show the temperature dependences of the viscosity of CAS, CFS, and CAFS slag melts in the temperature range 1300 to 1600 °C. **Fig. 4.5** shows the temperature dependences of viscosity in a series of $CaO-Al_2O_3-SiO_2$ slag melts with various Al_2O_3 contents at a fixed SiO_2 content of 40, 50, and 60 mol%. The surface tensions of CAS slag melts increase with increasing temperature. The surface tension varies from 0.433 to 0.524 N/m. Furthermore, **Fig. 4.5** also shows the comparison of surface tension of CAS system between this study and previous study [4.19]. A close agreement of surface tension with the previous study is found that the surface tension increases with increasing temperature at a higher SiO_2 content of 40 mol% [4.19].

Fig. 4.6 shows the temperature dependences of viscosity in a series of $CaO-Fe_2O_3-SiO_2$ and $CaO-Al_2O_3-Fe_2O_3-SiO_2$ slag melts with various SiO_2 approximate contents of 40, 50, and 60 mol%. The surface tensions of CFS and CAFS slag melts decrease with increasing temperature. A close agreement of surface tension with the previous studies [4.20, 4.21] is found that the surface tension decreases with increasing temperature with similar SiO_2 contents of 43−58 mol%.

The surface tension of CAS and CFS slag melts show different trends with respect to increase in temperature. The surface tension of CAS slag melts increases with increasing temperature, on the contrary, it decreases with increasing temperature of CFS slag melts.

Table 4.2 Surface tension measurements of synthesized slag melts.

Sample	Fe^{3+}/Fe_{tot}[e]	Surface tension (N/m) at temperature °C															
		1200		1300		1350		1400		1450		1500		1550		1600	
CA10.40	-	-	-	-	-	-	-	0.524	(0.001)[b]	-	-	0.521	(0.001)	-	-	0.512	(0.002)
CA20.40	-	-	-	-	-	-	-	-	-	0.461	(0.003)	0.457	(0.002)	0.459	(0.001)	0.460	(0.001)
CA25.40	-	-	-	-	-	-	-	-	-	0.459	(0.003)	0.458	(0.002)	0.457	(0.001)	0.455	(0.002)
CA30.40	-	-	-	-	-	-	-	-	-	-	-	0.442	(0.002)	0.4438	(0.0004)	0.444	(0.001)
CF08.39	0.80	0.484	(0.002)	-	-	-	-	0.484	(0.002)	-	-	0.4809	(0.0004)	-	-	0.479	(0.001)
CAF15.11.39	0.76	0.4669	(0.0005)	-	-	-	-	0.4669	(0.0005)	0.4660	(0.0004)	0.4661	(0.0003)	0.4660	(0.0003)	0.4651	(0.0004)
CA10.50	-	-	-	-	-	-	-	0.474	(0.001)	-	-	0.478	(0.001)	-	-	0.477	(0.001)
CF07.49	0.69	0.4323	(0.0004)	-	-	-	-	0.4323	(0.0004)	-	-	0.433	(0.001)	-	-	0.435	(0.001)
CA10.60	-	-	-	-	-	-	-	-	-	-	-	0.433	(0.002)	-	-	0.436	(0.001)
CF07.58	0.71	0.409	(0.001)	-	-	-	-	0.409	(0.001)	0.4064	(0.0004)	0.4074	(0.0004)	0.400	(0.001)	0.398	(0.002)
RCA10.43[c]	-	-	-	-	-	-	-	-	-	0.487	-	0.484	-	0.485	-	0.488	-
RCA20.44[c]	-	-	-	-	-	-	-	-	-	0.551	-	0.452	-	0.453	-	0.455	-
RCA29.41[c]	-	-	-	-	-	-	-	-	-	-	-	-	-	0.459	-	0.460	-
RCA15.46[c]	-	-	-	-	-	-	-	-	-	0.462	-	0.461	-	0.466	-	0.467	-
RCA11.57[c]	-	-	-	-	-	-	-	-	-	0.423	-	0.424	-	0.424	-	0.428	-
RCAF10.34.56[c]	-	0.437	-	0.432	-	0.428	-	-	-	0.425	-	-	-	-	-	-	-
RCF16.58[c]	-	-	-	0.460	-	0.450	-	0.447	-	0.442	-	-	-	-	-	-	-
RCF16.49[c]	-	-	-	0.502	-	0.500	-	0.504	-	0.495	-	-	-	-	-	-	-
RCF16.43[c]	-	-	-	-	-	0.520	-	0.517	-	0.516	-	-	-	-	-	-	-

[a]The fraction of Fe^{3+}/Fe_{tot} was analyzed two or three times for quenched samples.
[b]The number in brackets represent individual error's estimation for each temperature and composition.
[c] RCA, RCF, and RCAF are denoted as references (R) of CAS, CFS, and CAFS slag melts, respectively.

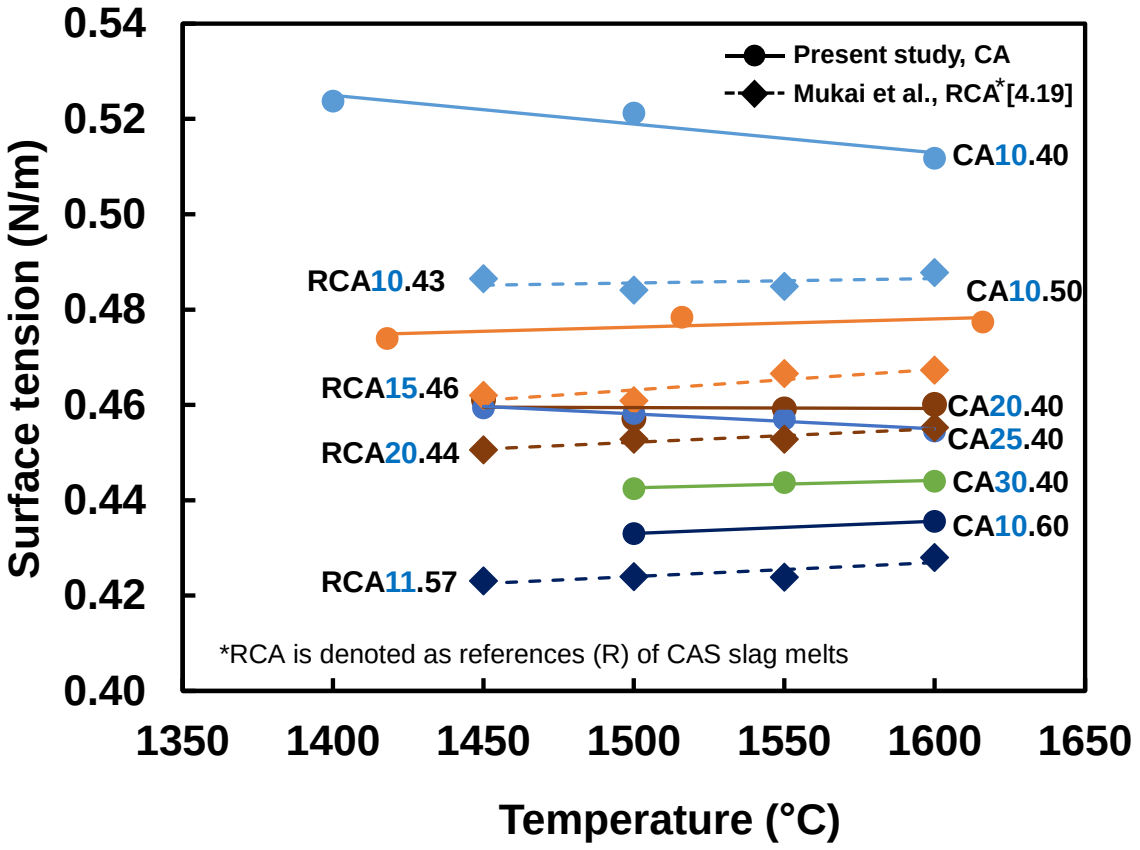

Fig. 4.5. Variations of surface tension with temperature in a series of (60-x)CaO−xAl_2O_3−40SiO_2, (50-x)CaO−xAl_2O_3−50SiO_2, and (40-x)CaO−xAl_2O_3−60SiO_2 slag melts with various Al_2O_3 and SiO_2 contents. Solid circles with solid lines and squares with dashed lines are surface tension values in this present study and previous study [4.19], respectively. The solid and dashed lines are least square fit to the data of the synthesized slag melts at measuring temperatures.

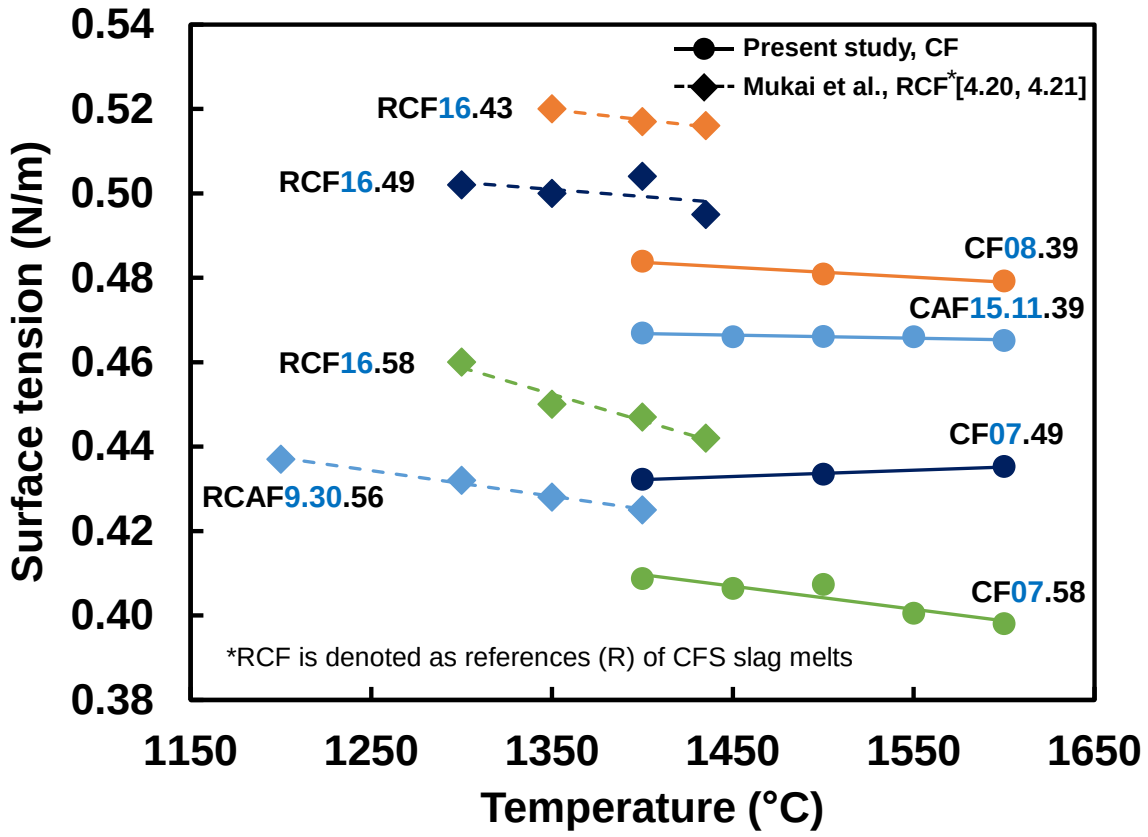

Fig. 4.6. Variations of surface tension with temperature in a series of (60-x)CaO−xA_2O_3−40SiO_2, (50-x)CaO−xFe_2O_3−50SiO_2, and (40-x)CaO−xFe_2O_3−60SiO_2 slag melts with various Fe_2O_3 and SiO_2 contents. The solid circles, squares, and the lines are the same as those in **Fig. 4.5.**

4.3.2.2. Composition dependence

Figs. 4.5 shows the surface tensions decrease as Al_2O_3 content increases in the range of 10 and 30 mol% (CA10.40>CA20.40>CA25.40>CA30.40). The influence of Al_2O_3 of surface tension can be seen obviously that the addition of Al_2O_3 decreases the surface tension of CAS slag melts. The surface tensions of CAS slag melts are also found to decrease monotonically with increasing SiO_2 content at fixed Al_2O_3 content of 10 mol% in order of CA10.40>CA15.50>CA10.60. The surface tensions in the previous study are in close agreement in the present study for similar compositions, as shown in **Tables 4.2 and Fig. 4.5.** The previous study [4.19] reported that the surface tension decreases with increasing Al_2O_3 and SiO_2 contents in $CaO-Al_2O_3-SiO_2$ slag melts. The contents of Al_2O_3 and SiO_2 were in the range of 10 to 20 and 43 to 57 mol% contents, respectively.

Figs. 4.6 shows the surface tension of synthesized slag melts gradually decreases with increasing SiO_2 content in a similar manner of CAS slag melts (**Fig. 4.5**). The surface tension decreases with increasing SiO_2 content in order of CF08.38>CF07.49>CF0758. Furthermore, **Fig. 4.6** also shows the surface tension of CFS and CAFS system and previous studies [4.20, 4.21]. The previous study reported that the surface tension of CFS slag melts decreases with increasing SiO_2 contents at constant Fe_2O_3 content of 16 mol%.

The surface tension monotonically decreases when Al_2O_3 is replaced by Fe_2O_3 for synthesized slag melts with constant SiO_2 contents (40, 50, and 60 mol%), as shown in **Table 4.2**. The surface tension increases monotonically when a part of Al_2O_3 is substituted by Fe_2O_3 for synthesized slag melts with a constant SiO_2 content of 40 mol% for CA30.40 and CAF15.11.39 slag samples. Furthermore, the surface tension of CAF15.11.39 is lower than

of CF8.39 even though FeO and Fe_2O_3 contents in CAF15.11.39 are larger than those in CF8.39. The higher surface tension of CF8.39, compared to that of CAF15.11.39, is probably related to the effect of Al_2O_3 addition. Further studies are necessary in order to understand the effect of Al_2O_3 and Fe_2O_3 on surface tension of coal slag and synthesized slag melts including large amounts of SiO_2 (> 40 mol%).

4.3.3. Composition parameter

The contribution of component of SiO_2, Al_2O_3, CaO, FeO and Fe_2O_3 on surface tension was investigated for synthesized slag melts. It was found experimentally that the components have different contributions on the surface tension of slag melts. Based on measured surface tension data of slag melts, a composition parameter is proposed to predict surface tension from the corresponding components determined by **Eq. 4–2**,

$$P_\gamma = A \cdot f_{SiO_2} + B \cdot f_{Al_2O_3} + C \cdot f_{CaO} + D \cdot f_{FeO} + E \cdot f_{Fe_2O_3} \quad (4–2)$$

where P_γ is the composition parameter of surface tension, A, B, C, D and E are the coefficients of components, and f is the fraction of expressed by mol% and mass%. **Table. 4.3** shows the equations of P_γ for temperature of 1400, 1500, and 1600°C. **Figs. 4.7 and 4.8** show the relationships between surface tension and the composition parameter P_γ. Fe valence state was not taken into account in the latter mass% based parameter. The mass% based parameter without considering Fe valency state may be much convenient for engineering applications.

Table 4.3 The equations for the composition parameter of molar and mass percentages basis at 1400, 1500, and 1600 °C.

Temperature (°C)	molar percentage		mass percentage	
	Equation	Δ^a	Equation	Δ^a
1400	$P_\gamma = 0.29 \cdot f_{SiO_2} + 0.68 \cdot f_{Al_2O_3} + 0.66 \cdot f_{CaO} - 0.08 \cdot f_{FeO} + 0.62 \cdot f_{Fe_2O_3}$	0.52	$P_\gamma = 0.25 \cdot f_{SiO_2} + 0.61 \cdot f_{Al_2O_3} + 0.72 \cdot f_{CaO} + 0.41 \cdot f_{Fe_2O_3}$	0.57
1500	$P_\gamma = 0.32 \cdot f_{SiO_2} + 0.42 \cdot f_{Al_2O_3} + 0.65 \cdot f_{CaO} - 0.71 \cdot f_{FeO} + 1.08 \cdot f_{Fe_2O_3}$	2.61	$P_\gamma = 0.28 \cdot f_{SiO_2} + 0.44 \cdot f_{Al_2O_3} + 0.71 \cdot f_{CaO} + 0.40 \cdot f_{Fe_2O_3}$	2.98
1600	$P_\gamma = 0.33 \cdot f_{SiO_2} + 0.43 \cdot f_{Al_2O_3} + 0.64 \cdot f_{CaO} - 0.74 \cdot f_{FeO} + 1.10 \cdot f_{Fe_2O_3}$	2.78	$P_\gamma = 0.28 \cdot f_{SiO_2} + 0.45 \cdot f_{Al_2O_3} + 0.70 \cdot f_{CaO} + 0.40 \cdot f_{Fe_2O_3}$	3.26

[a] Δ is the average error of all calculated values.

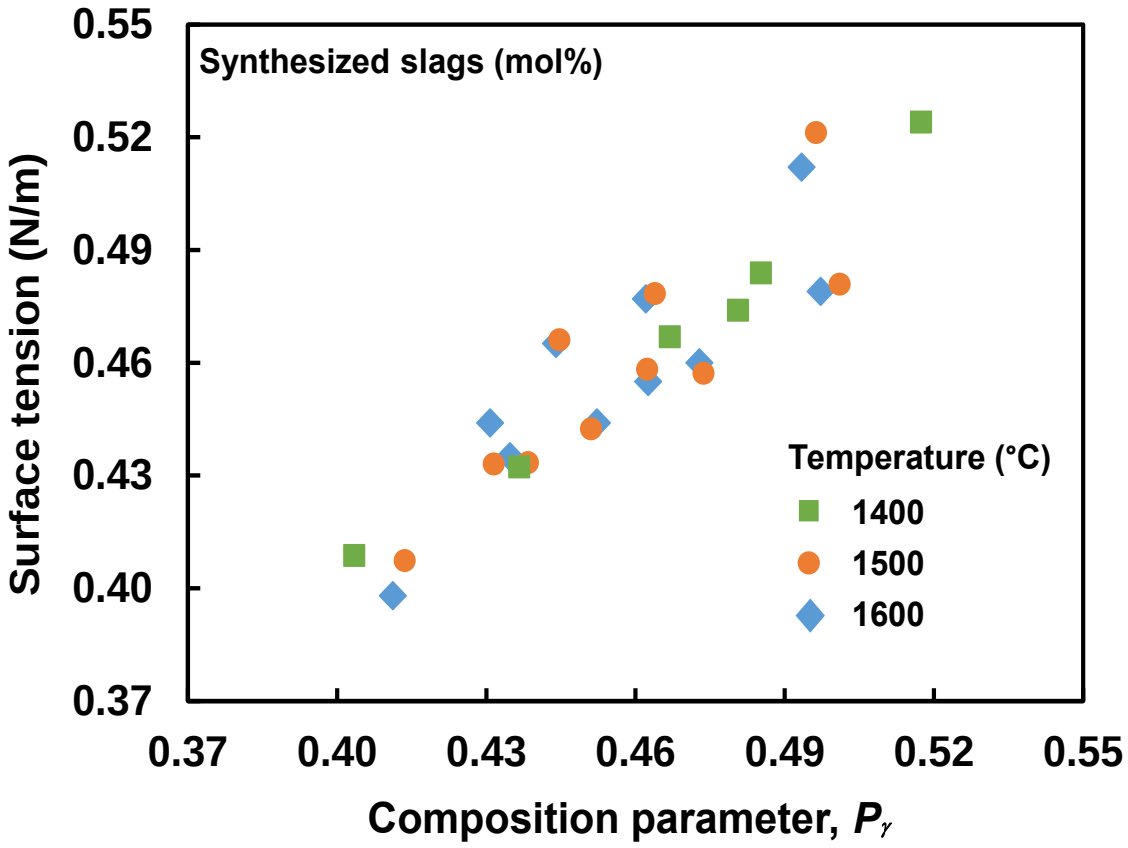

Fig. 4.7. Variations of surface tension with the parameter P_γ for synthesized slag melts series at 1400, 1500, and 1600°C. Solid circles and squares represent the measured and calculated data (**Table 4.3**) by the empirical composition parameter for the data with the molar percentage basis.

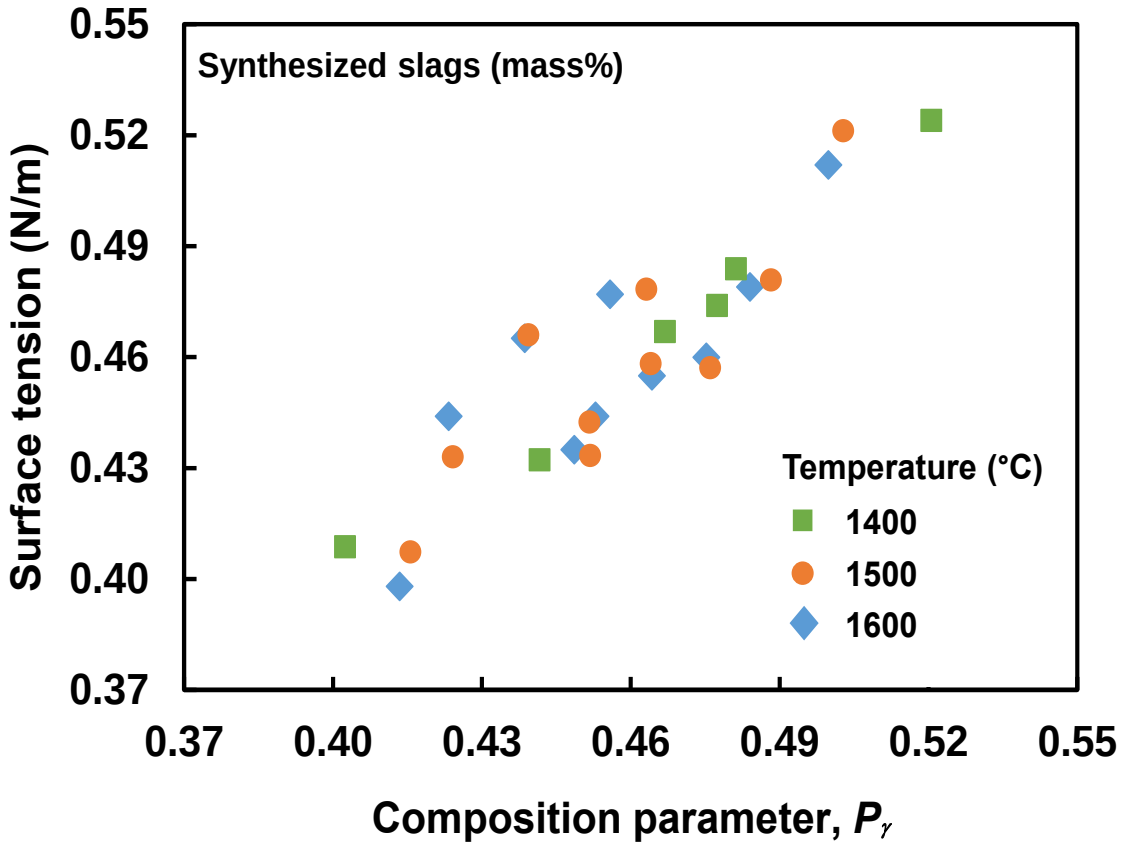

Fig. 4.8. Variations of surface tension with the parameter P_γ for synthesized slag melts series at 1400, 1500, and 1600°C with the mass percentage basis. It is postulated all iron oxide exists as Fe_2O_3. The solid circles and squares are the same as those of **Fig. 4.7.**

The average error Δ of experimental and composition parameter P_γ was calculated by using **Eqs. 4–3 and 4–4**,

$$\delta_n = (\gamma_n)_{cal} - (\gamma_n)_{mea}/(\gamma_n)_{mea} \cdot 100\ (\%) \quad (4\text{–}3)$$

$$\Delta = \frac{1}{N}\sum_{n=1}^{N}|\delta_n|\ (\%) \quad (4\text{–}4)$$

where δ_n is the percentage difference between the calculated $(\gamma_n)_{cal}$ and measured $(\gamma_n)_{mea}$ surface tension values, and Δ is calculated by taking the summation sign ∑ of all absolute values of δ_n and dividing by the total number of data.

The calculated value of the average error is 0.52–2.78% and 0.57–3.26% for mol% and mass%, respectively. In **Figs. 4.7 and 4.8**, the plots indicated have good correspondence to the calculated values using the composition parameter P_γ. Using the composition parameter represented by **Eq. 4-2** the surface tension of $CaO-Al_2O_3-Fe_2O_3-SiO_2$ slag melts was calculated for synthesized slag melts. The composition parameter as shown in **Table 4.3** has the capability to predict the surface tension of synthesized slag melts based on mole and mass percentages by the analysis of their chemical compositions without surface tension measurements. In future, an attempt will be made to develop a maximum bubble pressure method to measure surface tension of gasified coal slag melts.

4.4. Conclusions

The surface tension of $CaO-Al_2O_3-SiO_2$ (CAS) slag melts with SiO_2 content of 40, 50, and 60 mol% increases with increasing temperature, on the contrary, it decreases with increasing temperature of $CaO-Fe_2O_3-SiO_2$ (CFS) slag melts.

The surface tension decreases with addition of Al_2O_3 content of CAS slag melts at fixed SiO_2 content. The surface tension was also found to decrease with increasing SiO_2 content of CAS and CFS slag melts.

The surface tension monotonically decreases when Al_2O_3 is replaced by Fe_2O_3 for synthesized slag melts with constant SiO_2 contents (40, 50, and 60 mol%). The surface tension increases monotonically when a part of Al_2O_3 is substituted by Fe_2O_3 for synthesized slag melts with a constant SiO_2 content of 40 mol% for CA30.40 and CAF15.11.39 slag samples.

An empirical composition parameter at temperatures of 1400, 1500 and 1600 °C is proposed to predict the surface tension from the corresponding chemical composition of synthesized slag.

References

[4.1] Sun S, Zhang L, Jahanshahi S. From viscosity and surface tension to marangoni flow in melts. Metall Mater Trans B 2003;34:517–23. doi:10.1007/s11663-003-0019-8.

[4.2] Shannon GN, Rozelle PL, Pisupati S V., Sridhar S. Conditions for entrainment into a FeOx containing slag for a carbon-containing particle in an entrained coal gasifier. Fuel Process Technol 2008;89:1379–85. doi:10.1016/j.fuproc.2008.06.010.

[4.3] Inaba S, Kimura Y, Shibata H, Ohta H. Measurement of physical properties of slag formed around the raceway in the working blast furnace. ISIJ Int 2004;44:2120–6. doi:10.2355/isijinternational.44.2120.

[4.4] Van Dyk JC, Waanders FB, Benson SA, Laumb ML, Hack K. Viscosity predictions of the slag composition of gasified coal, utilizing FactSage equilibrium modelling. Fuel 2009;88:67–74. doi:10.1016/j.fuel.2008.07.034.

[4.5] Jiang Y, Lin X, Ideta K, Takebe H, Miyawaki J, Yoon SH, Mochida I. Microstructural transformations of two representative slags at high temperatures and effects on the viscosity. J Ind Eng Chem 2014;20:1338–45. doi:10.1016/j.jiec.2013.07.015.

[4.6] Takebe H, Tsuruda A, Okada A, Ueda K. Viscosity characteristic of molten Slag for next-generation IGCC. J Japan Inst Energy 2015;94 (5):450–4.

[4.7] Melchior T, Pütz G, Müller M. Surface tension measurements of coal ash slags under reducing conditions at atmospheric pressure. Energy & Fuels 2009;23:4540–6. doi:10.1021/ef900449v.

[4.8] Melchior T, Bläsing M, Pütz G, Müller M. Surface tension measurements of coal ash slags under reducing conditions at elevated pressures. Fuel 2011;90:280–7. doi:10.1016/j.fuel.2010.07.051.

[4.9] Miller S, Kalmanovitch D. Relation of slag viscosity and surface tension to sintering potential. Prepr Pap - Am Chem Soc Div Fuel Chem 1988;33:42–9.

[4.10] Kuromitsu Y, Yoshida H, Takebe H, Morinaga K. Interaction between alumina and binary glasses. J Am Ceram Soc 1997;80 (6):1583–7. doi:10.1111/j.1151-2916.1997.tb03020.x.

[4.11] Hsieh PY, Kwong KS, Bennett J. Correlation between the critical viscosity and ash fusion temperatures of coal gasifier ashes. Fuel Process Technol 2016;142:13–26. doi:10.1016/j.fuproc.2015.09.019.

[4.12] Raask E. Slag-coal interface phenomena. J Eng Power 1966;88:40–4. doi:10.1115/1.3678475.

[4.13] Mills KC, Jeffrey M. Rhine. The measurement and estimation of the physical properties of slags formed during coal gasification: 1. Properties relevant to fluid flow. Fuel 1989;68:193–200. doi:10.1017/CBO9781107415324.004.

[4.14] Nowok JW, Bieber JA, Benson SA, Jones ML. Physicochemical effects influencing the measurements of interfacial surface tension of coal ashes. Fuel 1991;70:951–6. doi:10.1016/0016-2361(91)90050-K.

[4.15] Nowok JW, Hurley JP, Bieber JA. The cause of surface tension increase with temperature in multicomponent aluminosilicates derived from coal-ash slags. J Mater Sci 1995;30:361–4. doi:10.1007/BF00354396.

[4.16] Mills KC. Estimation of physicochemical properties of coal slag and ashes. Miner Mater Ash Coal, Am Chem Soc Washinton, DC 1986;301:195–214. doi:10.1021/bk-1986-0301.ch015.

[4.17] Ilyushechkin AY, Hla SS. Viscosity of high-iron slags from Australian coals. Energy

and Fuels 2013;27:3736–42. doi:10.1021/ef400593k.

[4.18] Arman, Okada A, Takebe H. Density measurements of gasified coal and synthesized slag melts for next-generation IGCC. Fuel 2016;182:304–13. doi:10.1016/j.fuel.2016.05.117.

[4.19] Mukai K, Ishikawa T. Surface tension measurements on liquid slags in $CaO–SiO_2$, $CaO–Al_2O_3$ and $CaO–Al_2O_3–SiO_2$ system by a pendant drop method. J Japan Inst Met 1981;45:147–54.

[4.20] Skupien D, Gaskell DR. The surface tensions and foaming behavior of melts in the system $CaO\text{-}FeO\text{-}SiO_2$. Metall Mater Trans B Process Metall Mater Process Sci 2000;31:921–5. doi:10.1007/s11663-000-0068-1.

[4.21] Keene BJ. Slag atlas, 2nd Ed., Verlag Stahleisen GmbH, Dusseldorf, (1995), 456. 1995.

[4.22] Sumita S, Morinaga K, Yanagase T. Density and surface tension of binary ferrite melts. J Japan Ins Met 1983;47:127–13.

[4.23] Hara S, Yamamoto H, Tateishi S, Gaskell DR, Ogino K. Surface tension of melts in the $FeO-Fe_2O_3-CaO$ and $FeO-Fe_2O_3-2CaO.SiO_2$ system under air and and CO_2 atmosphere. Mater Trans JIM 1991;32:829–36.

[4.24] Choi JY, Lee HG. Thermodynamic evaluation of the surface tension of molten $CaO–SiO_2–Al_2O_3$ ternary slag. ISIJ Int 2002;42:221–8. doi:10.2355/isijinternational.42.221.

[4.25] Ikemiya N, Umemoto J, Hara S, Ogino K. Surface tensions and densities of molten Al_2O_3, Ti_2O_3, V_2O_5 and Nb_2O_5. ISIJ Int 1993;33:156–65. doi:10.2355/isijinternational.33.156.

[4.26] Vadász P, Havlík M, Daněk V. Density and surface tension of the systems CaO–FeO–

Fe_2O_3–MgO, CaO–FeO–Fe_2O_3–ZnO and CaO–Fe_2O_3–Cu_2O. Open Chem 2006;4. doi:10.1007/s11532-005-0014-9.

[4.27] Mysels K. Improvements in the maximum bubble pressure method of measuring surface tension. Langmuir 1986:428–32. doi:10.1021/la00070a009.

[4.28] Kihm KD, Deignan P. Dynamic surface tension of coal-water slurry fuels. Fuel 1995;74:295–300. doi:10.1016/0016-2361(95)92669-W.

[4.29] Moser Z, Gasior W, Pstrus J, Ishihara S, Liu XJ, Ohnuma I, Kainuma R, Ishida K. Surface tension and density measurements of Sn–Ag–Sb liquid alloys and phase diagram calculations of the Sn–Ag–Sb ternary system. Mater Trans 2004;45:652–60. doi:10.2320/matertrans.45.652.

[4.30] Fainerman VB, Mys VD, Makievski AV, Miller R. Application of the maximum bubble pressure technique for dynamic surface tension studies of surfactant solutions using the Sugden two-capillary method. J Colloid Interface Sci 2006;304:222–5. doi:10.1016/j.jcis.2006.08.023.

[4.31] Ohta Y, Morinaga K, Yanagase T. Aplication of hot-thermocouple to high temperature chemistry. Bull Japan Inst Met 1980;19 (4):239–45. doi:10.11311/jscta1974.13.90.

[4.32] www.factsage.com.

[4.33] Barter BB, Darling AS. Thermal expansion of rhodium-platinum alloys. Platin Met Rev 1960;4:138–40.

[4.34] Vargaftik NB, Volkov BN, Voljak LD. International tables of the surface tension of water. J Phys Chem 1983;12:817–20. doi:10.1063/1.555688.

Chapter 5

General Conclusion and Future Work

5.1. General Conclusion

In spite of experimental difficulties arising from the high melting temperatures, viscosity (chapter 2), density (chapter 3), and surface tension (chapter 4) of gasified coal and synthesized slag melts were measured in air at 1300 and 1650 ^{o}C depending on their homogenous melting temperatures. The gasified coal slags of multi component minerals encompass oxides of silicon, aluminum, calcium, magnesium, and iron used in IGCC process. The compositional and temperature dependences of viscosity, density, and surface tension data of gasified coal and synthesized slag melts have been positioned on the results and discussion.

The contribution of main components of oxides of silicon, aluminum, calcium, magnesium, and iron on viscosity, density, and surface tension was investigated for gasified coal and synthesized slag melts. Based on measured data of slag melts, various composition parameters are proposed to predict viscosity, density, and surface tension from the corresponding components. The empirical composition parameters can be beneficially used to predict viscosity and density for gasified coal slag melts and and surface tension for synthesized slag melts by the analysis of their chemical compositions without density measurements.

The findings can be summarized as follows:

Apparatuses of rotation cylinder, Archimedean double-bob, and maximum bubble pressure methods have been successfully established to measure viscosity, density, and surface tension of gasified coal and synthesized slag melts, respectively. The accuracy and reproducibility of the measurements were evaluated using silicone fluids and pure water at room temperatures and synthesized slag melts as standard samples at high temperatures.

The viscometer was calibrated with different speeds of rotation cylinder and the measured deviation from the mean was within 1.04% at room temperature of 25 °C. The reproducibility of the measurement at 1550–1650 °C was also evaluated for the viscosities of synthesized slag melt as a standard sample. The comparison between present study and the previous study confirmed that the measured viscosities were close agreement with previously reported values within the deviation of 1.5 %. Another previous study reported that the error of rotational cylinder method was estimated with an uncertainty of ≤ 10%.

The measured densities have good agreement with the data of silicone fluid standards with a precision of 0.16% at room temperature of 25 °C. In the high temperature of 1350 – 1500 °C, the density values of synthesized slag melts as standard samples are good agreement with previously reported values within a deviation of 0.10%. Another previous study reported that precision of density measurement of 0.14–0.33% using Archimedean method depending on the sample viscosity.

The measured surface tension of pure water has good agreement with the previous data with a precision of 0.08% at room temperature 19 °C. The surface tension of slag melt as standard sample was measured at 1400–1600 °C. The comparison between present study and the previous studies shows the deviation of 1.87%. Another previous study reported that the error of maximum bubble pressure method was estimated with an uncertainty of

1.68%. It confirms that the surface tension values measured in the present study are needed to improve accuracy of the maximum bubble pressure method.

The gasified coal slag samples were rapidly cooled at room temperature to evaluate their chemical compositions after measurements. The chemical compositions of the coal slag samples determined by X-Ray fluorescence (XRF) analysis. The valence state of iron oxide was evaluated using chelate titration method in the quenched samples. The major components in the coal slags are confirmed as SiO_2, Al_2O_3, CaO, MgO, FeO, and Fe_2O_3. The main components are in good agreement with the previous studies of 130 gasified coal slags from China, Australia, Indonesia, USA, and Russia used in the IGCC process. The synthesized slag melts containing the main components with systematic composition variations have been prepared here to understand the effects of the main components on viscosity, density, and surface tension. The behavior of Al_2O_3 and Fe_2O_3 on as amphoteric oxides were mainly explored.

The experimental results of the viscosity measurements showed that the viscosity exponentially increases with decreasing temperature for gasified coal and synthesized slag melts. While the viscosity of AD coal slag melt exhibits the rapid increase at 1300 ℃. The viscosity of AD coal slag melts with relatively-high Fe_2O_3 (~8 mol%) and low SiO_2 (~40 mol%) contents rapidly increased with decreasing temperature from 2 Pa·s at 1350 °C to ~10 Pa·s at 1300 °C presumably due to crystallization. The viscosity of gasified coal slag melts increased with increasing contents of Al_2O_3 and SiO_2 and decreased with increasing contents of CaO, MgO, FeO, and Fe_2O_3. The roles of these main components on melt viscosity are classified into network former (NWF) and modifier (NWM). Two types of amphoteric oxides: Al_2O_3 and Fe_2O_3 play different respective roles of NWF and

NWM on viscosity for gasified and synthesized slag melts in $CaO–MgO–Al_2O_3–FeO–Fe_2O_3–SiO_2$ system.

The experimental results of the density measurements showed that the density of gasified and synthesized coal slag melts was found to decrease linearly with increasing Al_2O_3 and SiO_2 contents and to increase with increasing Fe_2O_3 and FeO contents. The molar volume and the coefficient of volume expansion, which were calculated from measured density values, increased monotonically with increasing Al_2O_3 content for $CaO–Al_2O_3–SiO_2$ (CAS) synthesized samples with 40 mol% SiO_2. The molar volume for $CaO–FeO–Fe_2O_3–SiO_2$ (CFS) synthesized samples with 60 mol% SiO_2 increased with Fe_2O_3 addition and exhibited discontinuous change at ~7.5 mol% Fe_2O_3. The coefficient of volume expansion in the same CFS series decreased with increasing Fe_2O_3 content also showed a minimum value at ~7 mol% Fe_2O_3 and increased in higher Fe_2O_3 content.

The experimental results of the surface tension measurements showed that the surface tension of synthesized slag melts of CAS and CFS exhibits different trends with respect to increase in temperature. The surface tension of CAS slag melts increases with increasing temperature, on the contrary, it decreases with increasing temperature of CFS slag melts. The surface tension decreases with addition of Al_2O_3 content of CAS slag melts at fixed SiO_2 content. The surface tension is also found to decrease with increasing SiO_2 content in CAS and CFS slag melts at constant Al_2O_3 and Fe_2O_3 content. The surface tension monotonically decreases when Al_2O_3 is replaced by Fe_2O_3 for synthesized slag melts with constant SiO_2 contents (40, 50, and 60 mol%).

Based on measured data of slag melts, a new empirical composition parameter can be beneficially used to predict viscosity and density of gasified coal slag melts for the next-generation IGCC by the analysis of their chemical compositions without measurements.

And also the empirical composition parameter calculated from chemical composition was proposed to predict the surface tension of synthesized slag melts.

In practical gasification operation, depending on the gasifier type, the limiting requirements for coal slag viscosity and temperature can vary from 5 to 25 Pa·s and from 1200–1600 °C, respectively. The required of gasified coal slag melts is a need to predict viscosity and the temperature of critical viscosity. The viscosity of coal slag melts at the tapping temperature should be 5–20 Pa·s (moderate) for entrained flow gasifier. The viscosity of coal slag is above 20 Pa·s (hard), it will cause viscous. The viscosity is below 5 Pa·s (soft), it will result in rapid refractory wear of the gasifier. Therefore, it is essential to understand and to predict the composition and temperature dependences of coal slag viscosity of 5–20 Pa·s at operation temperatures.

A composition parameter P_η and basicity parameter B_p are also proposed to predict viscosity based on the studied compositions and the roles of their main components of gasified coal slag melts. It was found experimentally that the roles of the main components on melt viscosity are classified into two types of network former (NWF) for SiO_2 and Al_2O_3 and network modifier (NWM) for CaO, MgO, FeO, and Fe_2O_3. The composition parameter P_η calculated from the sum of molar for NWF and NWM in gasified and synthesized slag melts. Based on measured viscosity data, a factor 2 for MgO, FeO, and Fe_2O_3 is proposed to account for the sum of molar ratios for NWM. The basicity parameter B_p calculated from the sum of molar ratios for basic oxides (CaO, MgO) and acidic oxides (SiO_2, Al_2O_3) in gasified coal and synthesized slag melts. The basicity parameter B_p without considering Fe_2O_3 into account because Fe_2O_3 in silicate melts plays the role of amphoteric oxide and its behavior depends on the addition of R_2O and RO as basicity of slag melts.

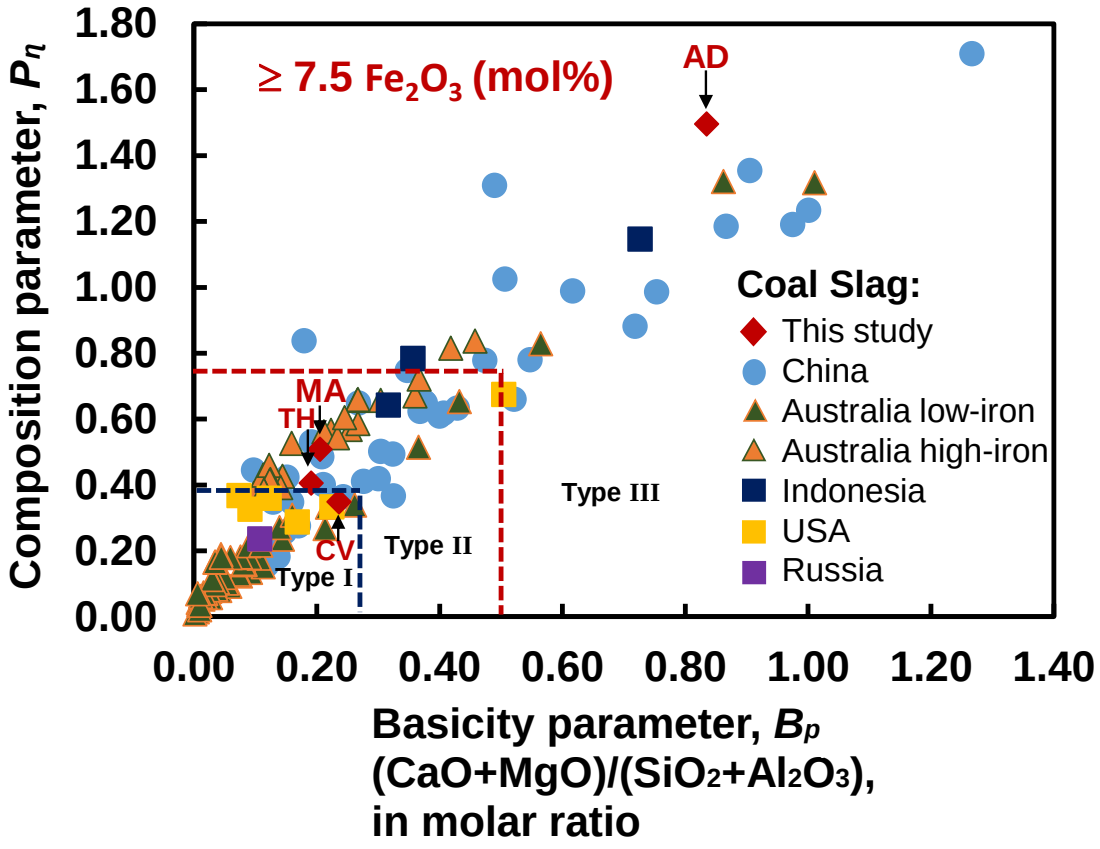

Fig. 5.1. Variations of composition parameter, P_η with basicity parameter, B_p of molar basis of 130 gasified coals from China, Australia, Indonesia, USA, Russia and measured this study. The dashed lines are the guide to eyes for classification of slag flow at 1550 °C of type I (hard type, ≥ 15 Pa·s), type II (moderate type, 5 – 15 Pa·s), and type III (soft type, ≤ 5 Pa·s).

The top 10 of coal producing countries:

- China
- USA
- India
- Australia
- Indonesia
- Russia
- South Africa
- Germany
- Poland
- Kazakhstan

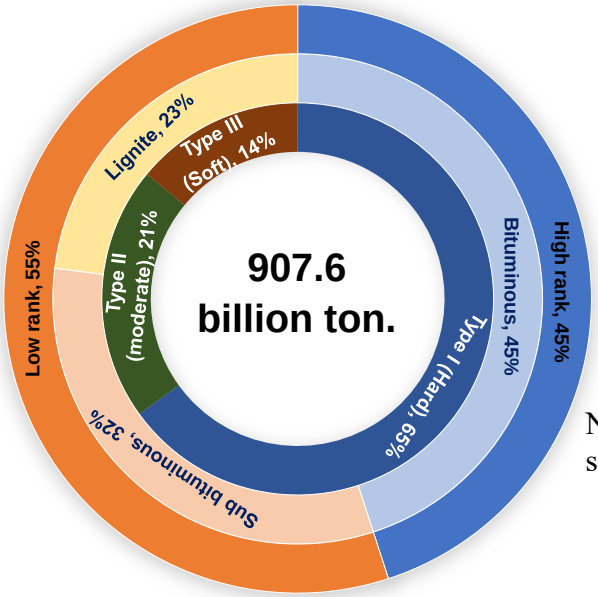

130 coal used for IGCC process:

- China
- USA
- Australia
- Indonesia
- Russia

New classification based on slag flow at 1550°C:

- Type I (≥ 15 Pa·s)
- Type II (5 – 15 Pa·s)
- Type III (≤ 5 Pa·s)

Fig 5.2. The coal classification of bituminous (high rank), sub-bituminous and lignite (low rank) in the world by percentage. And the new classification of coal slag melts based on the slag flow at 1550 °C.

Fig. 5.1 shows the relationship between composition parameter, P_η and basicity parameter, B_P values at 1550°C. There are good relationships between the P_η and B_P for 130 gasified coals from some countries and measured this study. P_η increases with increasing B_P values. **Fig. 5.1** is also classified into the three types of slag flows at 1550 °C. P_η gives a prediction that the hard flow (type I) of slag melts with ≥15 Pa·s, moderate flow (type II) with 5 ≤ x ≤ 15 Pa·s and soft flow with ≤ 5 Pa·s (type III) at 1550 °C.

The viscosity of coal slag melts with ≤ 5 Pa·s (type III) have a soft flow in the gasifier. However, the coal slag melts tapped from the gasifier are perhaps homogenous liquid slags or heterogeneous liquid slags containing crystallized particles. Therefore, it is important to describe not only the viscosity of fully liquid phase but also the viscosity of the liquid phase containing the partly crystallized in coal slag melts. Moreover, coal slag melts with low viscosities of < 1 Pa·s and with higher P_η values of >1.1, including relatively-high FeO and Fe_2O_3 contents > 8 mol%, may have a possibility existing the critical temperature of T_{cv} (1345°C) with rapid viscosity increase in a similar manner of AD coal slag melts. The result is in good agreement with the molar volume (MV) and the coefficient of volume expansion (CVE) calculated from measured density values of synthesized slag melts exhibited discontinuous change at ~7.5 mol% Fe_2O_3. The CVE corresponds to the extent of change (slope) in the MV with increasing temperature. The minimum of CVE suggests that the temperature-induced structural change of the CFS slag melts occurs at ~7.5 mol% Fe_2O_3. It is suggested that the larger Fe_2O_3 content of > 7.5 mol% may form inhomogeneous melt structure including small crystals even in melt state. Further studies are necessary in order to understand the structure of silicate melts including large amounts of Fe_2O_3 (> 7.5 mol%).

The new classification of coal melts also was proposed based on slag flow at 1550 °C as shown in **Fig. 5.2**. Most classification schemes for coal were developed for geological and commercial reasons. A widely used and convenient term is the highest rank for bituminous followed by lowest rank of sub-bituminous and lignite. Furthermore, the new classification of gasified coal slag flow of hard, moderate, and soft types can be added and beneficially used for selecting the coal suitable for IGCC applications.

5.2. Future work

In future, an attempt will be made to measure surface tension of gasified coal slag melts.

1) There is a host factor of properties of coal slag melts and maximum bubble pressure apparatus that are intricately related to the surface tension. Factors such as varying compositions e.g. gasified coal slag melts in high viscosity, increasing detachment time of maximum bubble pressure as the relate to the surface of properties slag melts can measure in future with the same setup of this study.
2) A continuing measurements of gasified coal slag melts is important for understanding their properties surface tension and calculating a new empirical composition parameter based on measured data.

The measured data and empirical composition parameter of viscosity, density, and surface tension of gasified coal slag melts can be used as a processing optimization method in order to have a boarder understanding of the slag melts behavior in a gasifier for IGCC process.